DEVELOPMENT OF A COMPUTER-AIDED ACCELERATED DURABILITY TESTING METHOD FOR GROUND VEHICLE COMPONENTS

By

A. K. M. Shafiullah

A Thesis Submitted to the Faculty of Graduate Studies of

The University of Manitoba

In partial fulfilment of the requirements of the degree of

MASTER OF SCIENCE

Department of Mechanical and Manufacturing Engineering

University of Manitoba

Winnipeg, Manitoba

Copyright © 2012 by A. K. M. Shafiullah

Abstract

Presently in ground vehicle industries, conducting durability tests with a high acceleration factor have become increasingly demanding for the less time and cost involvement. In the previous work, to accelerate the field test, the standard 'test tailoring' approach has been modified due to the requirement of high acceleration factors and the limitations of testing implementation. In this study, a computer-aided testing method is developed for the validation of this modified approach. Hence, a new test-piece has been designed by a conjugative approach involving the finite element technique and fatigue analysis. Afterwards, the accelerated durability loading profiles synthesized via the modified approach have been applied on the designed test-piece and the fatigue life has been simulated to verify the effectiveness of those loading profiles. Simulation results show that loading profiles with an acceleration factor up to 330 can be successfully generated with an accuracy of 95% by this modified approach.

Acknowledgements

I would like to express my sincere gratitude to my advisor, Dr. Christine Q. Wu for the guidance to carry out this work. I deeply appreciate for her valuable time, patience and insight throughout the course of this work. This thesis would not have been possible without the help and support she has given towards me. Thank you Dr. Wu.

Along with my advisor I would like to thank Dr. Olanrewaju Ojo and Dr. Dagmar Svecova for serving my committee. I would like to express my appreciation for their valuable suggestions to improve this work. I also like to thank Dr. Neil Popplewell for providing me the fundamental background knowledge of vibration and make me interested to work better in this field.

I am also thankful to Mr. Brad Lamothe from the 'Motor Coach Industries', Mr. Steve Swiddle and Mr. Ken Carmichael from the 'WESTEST' for their technical support in this work. I would also like to thank my colleagues Ms. Ke Xu, Mr. Sushil Doranga, and Mr. Ehsan Jalayeri for their help in preparing the materials for the tests.

Last but not the least I would like to thank my friends and family for their enormous support. Specially, I would like to thank my wife for her inspiration, without which I could not have achieved my goals.

Dedication

I would like to show my heartiest gratitude to my parents for the sacrifices they made for me and for always believing in me.

Table of Contents

Abstract i

Acknowledgements ii

Dedication iii

Table of Contents iv

List of Figures vi

List of Tables ix

Nomenclature xi

1. Introduction 01

1.1. Accelerated Durability (AD) Tests 01

1.2. Literature Survey 03

1.3. Problem Statement 08

1.4. Objective and Problem Formulation 09

1.5. Organization 11

2. Computer-Aided Accelerated Durability Test- Methodology 12

2.1. Synthesizing AD Testing Loading Profiles 12

2.2. Development of the CAM With Specific Dynamic Features and Fatigue Life 19

2.2.1. Numerical Vibration and Stress Analysis of the Specimen 19

2.2.2. Experiments for Vibration and Stress Analysis 21

2.3. FE Based Numerical Fatigue Analysis and the Verification of the Synthesized AD Loading Profiles 25

3. Results and Discussion 32

3.1. Synthesized Highly AD Profiles, FDS And ERS Comparison 32

3.2. Design of the Test-Piece and Its Validation 36

3.2.1. Features of the Designed Test-piece 36

3.2.2. Determination of the Dynamic Parameters of the System 39

3.2.3. Comparison between Numerical and Experimental Result 41

3.2.4. Dynamics and Stress Analysis of the CAM 44

3.2.5. Stress Relation with the Fatigue Life 52

3.3. Verification of the AF of the developed AD Tests 55

3.3.1. Numerical Fatigue test and Validation 55

3.3.2. Experimental Durability Tests and Fractography 57

3.3.3. Effect of Plasticity and S-N Curve Slope in Durability Test Life 61

4. Conclusions and Future Works 69

References 71

Appendix A- Details of the all Considered Test-Piece and their Comparison with the Selected One 77

Appendix B- Other Fatigue Results 85

Appendix C- Miscellaneous Findings While Generating the AD Test 88

List of Figures

Title	Page No
Figure 1: Pennsylvania Testing Facility	02
Figure 2: Shaker Machines Used in Durability Tests	03
Figure 3: The Process Flow Of Generating AD Profiles From nCode GlyphWorks	16
Figure 4: (a) Road Test Acceleration Data (Z-Vertical Direction) and (b) Geometry of the Seven Events	18
Figure 5: Meshed CAD with Solid Elements with a Finer Mesh around the Critical Notches	21
Figure 6: The Experimental Setup: (a) Hydraulic Shaker with the Mounted Specimens (b) The Data Acquisition System	23
Figure 7: Beams with Attached (a) Strain Gauges and (b) Accelerometer and Tip Mass	24
Figure 8: Attached Strain Gauges and their Locations in the Designed Specimen Used for the Test with the 24 Hours Accelerated PSD	24
Figure 9: S-N Curve Formulation for Aluminum 6061 T651 Alloy	28
Figure 10: Vibration Fatigue Process Flow in DesignLife	30
Figure 11: Process Flow of AD Testing Methodology	31
Figure 12: Generated AD Tests of Different Duration for Constant a FDS	33
Figure 13: Response Spectra for Different AD Tests for Constant a FDS	34
Figure 14: Damage Spectra for Different AD Tests for Constant a FDS	35
Figure 15: Notch Orientations of the Designed Specimen (Top-View)	37
Figure 16: (a) The Physical Test-Piece (b) The Test-Piece with Sensors, for the Experimental Comparisons	38
Figure 17: Linearity Approximation around the Resonance	40
Figure 18: Sample Vibration Time History From the Test-Piece	41

Figure 19: First Four Vibration Modes of the Specimen 45
Figure 20: Experimental Sine Sweep FRF Spectra 46
Figure 21: Von Mises Strains at First Four Natural Frequencies of the Specimen 47
Figure 22: Von Mises Stress Distribution Over the Model 48
Figure 23: Stress/Strain Distributions for the 4 Hours PSD Over the Critical Region 50
Figure 24: The Stress PSD Determined From the FEA 51
Figure 25: Relation between the Absolute Maximum Principal Stress and the Durability Life 53
Figure 26: Effect of the Notch Orientations to the Different Stress Transfer Functions 54
Figure 27: Effect of the End Masses to the Different Stress Transfer Functions 54
Figure 28: Fatigue Life Distribution over the CAM for 20 Hours PSD 56
Figure 29: Fatigue Life Distributions over the CAM for Different Accelerated PSD 57
Figure 30: Failure of the Designed Test-Piece (Experimental) 58
Figure 31:(a) Fracture Surfaces of the Failed Test-Pieces 59
(b) Fracture Surfaces of the Failed Test-Pieces under Optical the Microscope 60
Figure 32: The Strain History of an Overly Compressed Durability Loading Profile 64
Figure 33: Comparison of the TC Ratio of Different AD Profiles With the Theoretical One 66
Figure 34: Deviation in the Determined Fatigue Life for Different TC Ratios 67

Appendix Section

Figure 1A: Comparison of the Natural Frequencies between the FE and the Experiment 81

Figure 2A: Attached Strain Gauges in Differently Designed Specimens 81
Figure 3A: Comparison of Strain Results between the FE and The Experiment 83
Figure 4A: Response Spectra of Different AD Tests for Constant FDS (*b*=6) 88
Figure 5A: Damage Spectrums of Different AD Tests for Constant FDS (*b*=6) 89
Figure 6A: Response Spectra for Different AD Tests (Full) for Constant ERS (*b*=6) 90
Figure 7A: FDS for Different AD Tests (Full) For Constant ERS (*b*=6) 91

List of Tables

Title	Page No
Table 1: Range of Values of 'b' for Different Materials	14
Table 2: The Natural Frequencies And the Damping Ratios for the First Two Vibration Modes for Different Specimens	39
Table 3: Comparison of the Natural Frequencies between the FE and the Experimental Model	42
Table 4: Comparison of Strains between the FE and the Experimental Model for the 24 Hours Loading Profile	42
Table 5: The Comparison of Maximum Tip Deflections between the FEA the Experiment	43
Table 6: Comparisons of the RMS Stresses (1-Sigma) Over the CAM	49
Table 7: Verification of the Synthesized AD Tests (b=6)	56
Table 8: Natural Frequencies and Damping Ratios for the First Two Bending Vibration Modes for the Different Specimens	61
Table 9: Comparison of Strains between the FE and the Experiments for Beam Set 2	62
Table 10: Verification of the Synthesized AD Tests (b=5.5)	65
Appendix Section	
Table 1A: Fatigue Lives of the Different Test-Pieces under the 24 Hours Loading	77
Table 2A: The Natural Frequencies and the Damping Ratios for the First Two Bending Modes for Different Specimens (Experimental)	78
Table 3A: Gain Ratios of the First Two Bending Modes (Experimental)	78
Table 4A: Strains Developed in the 24 Hours Durability Test in	79

the FE Models
Table 5A: Comparison of the Natural frequencies between the FE and the Experimental Model 80
Table 6A: Comparison of Strains between the FEA and the Experiment 82
Table 7A: Comparison of Strain Distributions between the FEA and the Experiments 84
Table 8A: Fatigue Lives in Different Locations of the Specimens Based on Experiments 85
Table 9A: Estimated Fatigue Life of the Four Selected Specimens Using Different Cycle Counting Algorithms in the Frequency Domain 86

Nomenclature

1. Acronyms

AD	Accelerated Durability
AF	Acceleration Factor
CAE	Computer-Aided Engineering
CAM/ CAD	Computer-Aided Model/Design
FEA	Finite Element Analysis
FDS	Fatigue Damage Spectrum
FRF	Frequecy Response Function
FE	Finite Element
FLR	Fatigue Life Ratio
LVDT	Linear Variable Differential Transformer
PSD	Power Spectral Density
RMS	Root Mean Square
S-N	Stress Life
SRS/ ERS	Shock/ Extreme Response Spectrum
SAST/MAST	Single/Multi Axis Simulation Table
SDOF	Single Degree Of Freedom

2. Definitions for Selected Acronyms

FLR	The ratio of the fatigue life of a specific specimen under the original load and the accelerated load.
LES	A system whose deformation under load is assumed to be linear elastic.
AF	AF is the ratio of the duration of the original (field) test and the duration of the accelerated test.

PSD	PSD describes how the power of a signal is distributed with frequency. In random vibration problems its unit is g^2/Hz.
FDS	FDS is obtained by plotting the variation of damage to a SDOF linear system versus its natural frequency for a given damping ratio and stress-life (S-N) curve exponent.
SRS/ ERS	ERS or SRS has been defined as a curve representing the maximum value of the response of a linear SDOF system to any vibration according to its natural frequency, for a given damping ratio. In the case of ERS the input is a PSD and for the SRS the input is a time-series. In random vibration problems its unit is g.
RMS	The RMS value of a set of values (or a time series) is the square root of the arithmetic mean of the squares of the original values (or the time series).
FRF	A FRF is a transfer function which expresses the structural response to an applied force as a function of frequency. The response may be given in terms of displacment, velocity or acceleration.
SAST/MAST	Machines for performing the vibration (durability) tests.
SDOF	Systems, whose motion can be explained with a single coordinate.
LVDT	A sensor, that is used for measuring linear displacement of a system.

Chapter 1

Introduction

1.1. Accelerated Durability (AD) Tests

Ground vehicles must pass the durability tests as a pre-launch requirement to meet the necessary standards for the safety, reliability, durability and comfort. These durability tests (field tests) are usually conducted in the proving grounds, which are designed to simulate the real road environments (events) during the tests. A map of a typical durability testing facility at *Pennsylvania Transportation Institute* has been presented in Figure 1 [1]. During the durability tests the ground vehicles need to be driven a certain amount of mileage without exhibiting any failure mechanism including any crack initiation in critical suspension, frame and cab systems to certify the marketability of the vehicle [2]. Hence, these durability assessments also possess the risk of nullifying the invested time and money, if any of the components of the driven vehicle fails during the test.

As an alternate, AD test can be designed for the laboratories to simulate the driving conditions of the field tests in a shorter period of time. An effective accelerated lab test not only helps avoid the unexpected failures during the field tests but also can be used to quantify the life span of ground vehicle components with less investment of time and money. Moreover, information regarding the determination of the warranty timeframe of

the vehicle components to minimize the product recalls and complaints after marketing can be obtained once the AD test is conducted [2]. The benefit of AD tests over the field test is that it can be better reproduced and observed, as the individual vehicle component can be tested under the controlled environment rather than the full vehicle prototype. However, the challenge exists as the loads to be used in the rig test (controlled environment) have to be derived based on the measurements performed either on the test tracks or in the public roads [3].

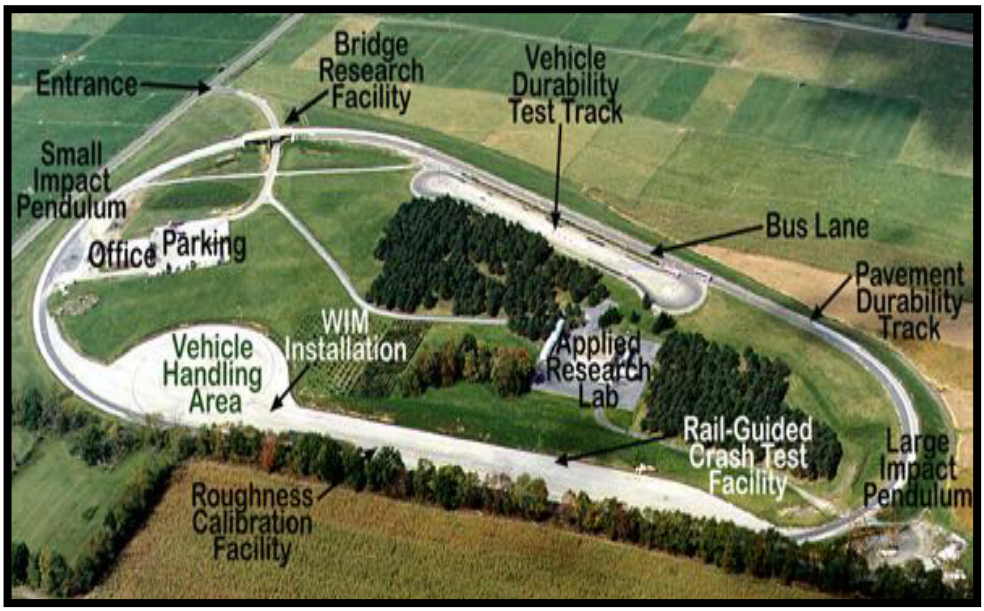

Figure 1: Pennsylvania Testing Facility [1]

A proficient AD test should satisfy the following two criteria [2]:

1. The AD test should produce the same failure mechanism as those observed in the real-world loading conditions, i.e., being representative of the real loading environments.

2. The AD test should be accelerated with no occurrence of the unrealistic high load which can possibly alter the response of the structure hence the failure mechanism.

The AD tests are carried out in the test rig (laboratory) by using the MAST or SAST. MAST is a mechanical system that works in a controlled laboratory environment by repeatedly replicating and analyzing 'in service' vibrations and motions of the testing components. The prototype of the MAST and SAST [4] that have been used for the sub-scaled AD test are shown in Figure 2. The MAST/SAST is initially driven through an iteration procedure via an input acceleration time series or PSD (derived from the field test data) signal. This iteration process is for generating the driving file for the durability test based on the allowed deviation of the input and the response of the test-piece. Therefore, the longer the input loading file, the longer will be this iteration process, hence the larger will be the time and cost involvement. Thus, in the rig tests the use of a shorter initial input is recommended.

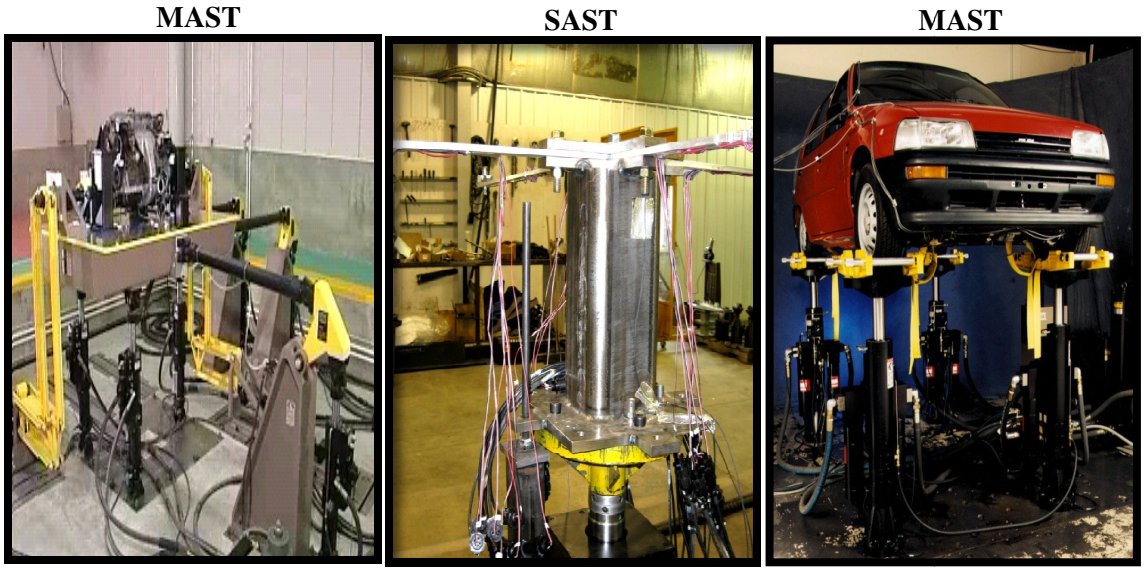

Figure 2: Shaker Machines Used in Durability Tests [2]

1.2. Literature Survey

Research has been ongoing on AD tests for decades, more accurately from 1990's when Nelson [5], Caruso *et al.* [6] and Meeker *et al.* [7] presented analytical models to perform

the accelerated tests. In 1992, Ashmore *et al.* [8] demonstrated a procedure to perform accelerated tests in the test course which can be treated as the first guideline to perform the AD test for ground vehicles. They explored the effect of critical test parameters (the test field roughness severity and the vehicle speed in the test course) on the AF and also verified their assumptions of the method to get valid results. More techniques have been introduced afterwards to accelerate the reliability or durability field tests. Briefly these techniques have been categorized as the *time-domain-based* or the *frequency-domain-based* approaches. Earlier techniques have been accelerating the durability tests mostly in the time domain.

Time-domain-based techniques include short-inverse-Fourier transform (SIFT) [9], time correlated fatigue damage (TCFD) [10], strain gauge editing technique (SGET) [11]-[13] and racetrack editing technique (RTET) [14]. All these techniques [9]-[14] are broadly termed as the '*fatigue damage editing',* which is a signal processing technique. In such a technique, the signal (the time-history of the strain, acceleration, and displacement) is collected from the field tests via sensors like strain gauges, accelerometers, LVDTs, etc and edited to retain the desired percentage of the damaging portion of the signal. In these techniques [9]-[14], non-damaging or less damaging parts (according to the S-N curve of the material) are removed from the signal hence accelerate the tests. To perform the test in the laboratory, the edited signal is correlated with the acceleration or the displacement of the shaker machines [12]. 'Mildly Non-Stationary Mission Synthesis' (MNMS) which is a *time-domain-based* signal processing technique, produces shorter mission signals from long records of experimental data [15]. In [15] the MNMS technique is demonstrated up to an AF of 10 and found to be efficient in low AF (1 to 3). Broadly, the

time-domain-based techniques are reliable as it deals with the real time data without any transformation. Moreover, the theories are well established and a lot of experimental data is also available in the *time-domain-based* techniques. However, the AF cannot be truly controlled in these techniques since the AF mostly depends upon the severity of the acceleration, displacement or strain data collected from the durability track [9]-[15]. Moreover, in [16] the experimental and numerical techniques (FE transient analysis) are blended together as an efficient and reliable means for performing the dynamic response and the durability analysis of heavy commercial vehicles. The transient analysis in time-domain becomes computationally expensive if the considered analysis time is large or the system is complex comparing to *frequency-domain-based* computational methods [17]. Hence, it can be also concluded that the *time-domain-based* techniques cost more computational time and machine memory than the *frequency-domain-based* techniques.

The earliest complete literature has been found practising the *frequency-domain-based* approach for fatigue life prediction of metallic structure in 1986 by Bishop [18]. This approach has been refined with computer-aided techniques, i.e. FE has been incorporated [19] [20] to perform the durability analysis of machine components in a more convenient way. For the random vibration problems, the methodology of performing the durability analysis of mechanical/electronic components in the frequency domain have been presented in [21]-[27]. The techniques used here have been tailored from [18] and [20]. In these works, durability assessments have been carried out using a combination of FE random vibration and numerical fatigue analysis. Furthermore, in [28] the spectral damage of a 'Linear Elastic System' (LES) has been predicted in the frequency domain using a novel approach of energy isoclines, whose function consists of both FRF and the

material fatigue properties of that system. Later, to reduce the testing time, *frequency-domain-based* durability tests have been accelerated using different techniques.

Literature that addressed accelerating the field test using the *frequency-domain-based* techniques can be found in [29]-[44]. In literature [29]-[33], to accelerate the test, the RMS values of the test PSD have been increased; hence higher stress levels have been developed in the structure to make it fail faster. In these cases, the RMS values have been found to be arbitrarily increased [29]-[32] or it has been increased by using the inverse power law [33]. In [29] the acceleration level (g) of the vibration test profiles has been elevated and applied to differently damped (coated) cantilever beams to determine the effect of damping on the AF of the considered vibration test profiles. In some cases the temperature loading profile also has been accelerated by elevating its RMS level to account the temperature effect along with the vibration loading while performing the bench test on a metallic component (the catalytic converter) [30]. In [31] and [32] the accelerated test has been performed in aluminum beams with elevated RMS level of the test PSD. In these works, the effect of the damping co-efficient [31] and the effect of different cycle counting algorithms (Dirlik, Narrowband, Steinberg, Lalanne etc) [32] on the fatigue lives of cantilever beams has been analysed. However, these techniques [29]-[33] have not been accounted for the impact failure or the failure mechanism alteration while accelerating the test. Some other techniques have also been proposed in the literature [34]-[36]. A 'step-stress accelerated random vibration life testing method' has been presented to accelerate the test in [34]. An analytical solution has been presented to calculate the fatigue damage for a linear elastic SDOF system which has been used as the specifications of the accelerated vibration tests [35]. Moreover literature have been found

which addressed the usage of inverse power laws in the accelerated fatigue testing under wide-band Gaussian random loading [36]. These techniques [34]-[36] are more on the theoretical side and not yet been exercised in the practical applications.

In 2006, Halfpenny [37] proposed a novel approach, the 'test tailoring approach' of accelerating the durability tests. In this technique, the AF can be controlled up to the theoretical limit defined by the **Condition 1**. This technique also contains the algorithm to avoid impact failures in high AF. The 'test tailoring approach' is consisting of two steps, (1) mission profiling and (2) test synthesis. Mission profiling involves determining the SRS and the FDS from the field test data by applying a SDOF transfer function to the input acceleration signal (field test acceleration data). The calculation is repeated over a range of natural frequencies to give histograms of maximum response and fatigue against the frequency. The 'test synthesis' process in the 'test tailoring approach' accelerates the field test using the information (FDS and SRS) of the mission profiling. The conditions of generating AD loading profiles through the 'test tailoring approach' can be briefly described as below,

Condition 1: ERS of the accelerated test must be below the SRS of the road/field test to avoid creating unrealistic load which may cause impact/shock failure.

Condition 2: FDS of the accelerated test must be same as the FDS of the road/field test to ensure the same failure mechanism.

So in this approach, accelerated test profiles are obtained by synthesizing a field test PSD with a same damage potential of FDS, while bounding the solution with SRS and ERS [38].

Halfpenny in 2008 [39], also embedded the 'test tailoring approach' with CAE, where the combination of generating the durability loading profiles and testing those in the test rig has been elaborated [39]. The 'test tailoring approach' has also been applied in the aviation applications [40]-[42], accelerating a 12000-hour field test to a 4-hour lab test to evaluate the durability of the helicopter components in uni-axial [41] and tri-axial directions [42]. In [40] the 'test tailoring approach' has been exercised to perform a numerical AD test of an automobile component. None of these works [40]-[42] validated the claimed AF of the generated loading profiles used in their durability analysis.

Xu *et al.* [43] and Cull *et al.* [44] also applied the 'test tailoring approach' to generate accelerated loading profiles for the durability tests of ground vehicle components. In [43] the damaging events of the field test acceleration data have been identified successfully for the 'mission profiling' process and later accelerated the field test via the 'test synthesis' technique. Prior to this work, the framework has been established in [44] for generating these successful AD loading profiles using the commercial software nCode GlyphWorks. This methodology has been refined and adopted in [43] to synthesise effective AD loading profiles in [44].

1.3. Problem Statement

Field test data of 330 hours, collected from Altoona test track [1] needs to be accelerated to perform a 24-hours equivalent (or less) lab test through any existing or new approach. The challenges of this works are described as follows:

1. To accelerate the concerned 330-hour test keeping all the dynamic features of the field test, where the conventional 'test tailoring approach' was exceeding the theoretical limit defined by **Condition 1**.

2. To generate an equivalent 60s acceleration time series from the 24-hours accelerated test PSD (of the 330-hour test) which can be repeated for 1440 times to get the desired FDS. This equivalent 60s time series must be produced for the rig tests to reduce the time and cost involved in the iteration process with the full period tests (e.g. 24-hour test).

Hence, to accelerate the field test, in [43] the standard 'test tailoring approach' has been modified' to obtain the desired AF (e.g. the AF of accelerating the 330 hours field test to 24 hours is 13.75) and to satisfy the **Condition 1** and **2** for implementation. To apply this new modified approach to industrial durability tests, it needs to be validated. Furthermore, in this modified approach some assumptions have been made on the important dynamic properties of the considered SDOF system [43], which should be verified to validate the framework adopted in [43].

1.4. Objective and Problem Formulation

This work is mainly focused on verifying the 'modified test tailoring approach' of generating the AD loading profiles for ground vehicle components presented in [43]. The significance of this work is to develop a tool which can potentially provide the guideline for the ground vehicle manufacturers to perform numerical AD tests complimentary to the expensive field or lab testing. The objectives of this work can be categorized in the following manner:

1. To synthesize AD loading profiles of higher AF (>13.75) from the considered 330-hours of field test through the 'modified test tailoring approach'. A different S-N curve slope and FDS generating algorithm than the previous work [43] have been chosen to accelerate the AD loading profiles of shorter duration in this work.

2. Designing a new test-piece having specific dynamic features and fatigue life to perform the numerical and experimental durability tests.
3. Validation of the AF of the synthesized AD loading profiles and the verification of consistent fatigue mechanism resulted for performing fatigue/durability assessment with those loading profiles. i.e., validation of the 'modified test tailoring approach'.
4. Presenting a guideline for performing a valid AD test both in the test-rig and in numerical techniques with the existing Altoona field [1] test data.

In this work, AD loading profile has been synthesized through 'modified test tailoring approach' via commercial software nCode GlyphWorks [45]. This approach consists of two distinguished techniques termed as 'Mission Profiling' and 'Test Synthesis'. Mission Profiling generates the reference SRS and FDS from the Altoona field [1] test acceleration data. In addition, via 'Test Synthesis' technique the AD loading profiles are obtained by synthesizing a field test PSD with a same damage potential of FDS, while bounding the solution with SRS and ERS. Furthermore, a new featured test-piece has been designed by a conjugative approach involving the FEA and the fatigue analysis (S-N analysis) for a specific fatigue or durability life. The design is validated afterwards to perform the durability tests and verify the AF of the applied durability test profiles. In this case, to perform the FEA, and the fatigue analysis, Education Version of ANSYS 13.0 [46] and nCode DesignLife 7.0 [47] has been used in this work. Ideally the durability or FLR should be same as the AF of the considered AD loading profiles. Hence, the FLR and the AF for every applied AD profiles have been compared to validate the effectiveness of the synthesized AD loading profiles. Experiments have also

been performed to validate failure mechanism of AD loading profiles to signify the numerical results.

1.5. Organization

In Chapter 2, the methodology computer-aided AD test has been discussed. In the first part of the computer-aided AD test, Section 2.1, the method and materials of the synthesized AD tests are presented, where the PSD of the AD loading profiles have been generated with the corresponding SRS and FDS satisfying the **Condition 1** and **2**, discussed in Section 1.2. In the second part of computer-aided AD test, Section 2.2, the design techniques of the test piece having a specific durability life of 24 hours are presented through FEA and the standard fatigue analysis. The 24-hour duration has been taken as a reference and it is the preferred applicable durability test, to simulate the 330 hour of the field test. Experiments which have been performed to validate the design are also presented in this section. In the third part of the computer-aided AD test, Section 2.3, the synthesized AD loading profiles have been applied to the CAM of the test-piece and the corresponding fatigue life has been determined. Later, the FLR and the AF for every AD profiles have been compared to validate the effectiveness of the synthesized AD loading profiles. Results and discussions are presented in Chapter 3. In this chapter the feature of the synthesized AD loading profiles (PSD, SRS and FDS) and the designed test-piece (material, geometry, boundary condition, dynamics and fatigue life) have been presented. The validations of the test-piece's design and the generated AD loading profiles have also been demonstrated in this chapter. Conclusions and the future works are presented in Chapter 4. References and appendices are appended afterwards.

Chapter 2

Computer- Aided Accelerated Durability Test-Methodology

This work has three major parts. They are synthesizing the AD loading profiles using the 'modified test tailoring approach', designing a specific dynamically featured test-piece or specimen with a certain fatigue life and testing the specimen under the generated AD profiles to verify their effectiveness. Such effectiveness has been defined as the consistency between the AF and the FLR, which is referred as the ratio of the fatigue life of a specific specimen under the original load and the accelerated load. The considered AD loading profiles have been synthesized from 330 hours of field test to 24, 20, 15, 10, 8, 6, 4, 2 and 1 hour via the modified approach with the identical data and the parameters presented in literature [43] using the commercial software nCode GlyphWorks. Nine (9) AD loading profiles have been synthesized in this work to provide enough information for the validation.

2.1. Synthesizing AD Testing Loading Profiles

The main objective of AD testing is to reduce the time of the conventional durability tests without altering failure mechanism. In *frequency-domain-based* techniques, the vibration test is usually accelerated by elevating the stress level [33]. In this process, the reference vibration loading profile, which needs to be accelerated, is in the form of a PSD. The relationship between the PSD levels and the test durations is given as [41],

$$(\frac{W_1}{W_2})^{B/n} = \frac{T_2}{T_1} \tag{1}$$

where, W_1 and W_2 are the field and accelerated laboratory test PSD amplitudes (g^2/Hz), respectively, T_1 and T_2 are the field and laboratory test durations in hours, respectively, B is the inverse slope of the Wohler curve (S-N curve) or the Basquin's exponent and n is the stress damping constant. In Eqn. (1) B and n are the material properties.

In this work the AD loading profile has been generated from the field test data through the 'modified test tailoring approach'. The 'test tailoring approach' has been developed based on a SDOF system. The first stage of the 'test tailoring approach' is the mission profiling, where the SRS and the FDS of the field test data is determined by the following formulations [39],

$$\mathrm{ERS}(f_n) = [\pi \cdot f_n \cdot Q \cdot \mathrm{PSD}(f_n) \cdot \ln(f_n \cdot T)]^{\frac{1}{2}} \tag{2}$$

$$\mathrm{FDS}(f_n) = f_n \cdot T \cdot \frac{K^b}{C} \cdot [\frac{Q \cdot \mathrm{PSD}(f_n)}{2(2\pi \cdot f_n)^3}]^{\frac{b}{2}} \cdot \Gamma(1 + \frac{b}{2}) \tag{3}$$

where, K is the spring stiffness of the SDOF system, f_n is the natural frequency of the SDOF system, T is the time period of the accelerated test, Q is the dynamic amplification factor, $PSD(f_n)$ is the power spectral density of the input acceleration, $\Gamma(g)$ is the Gamma function defined by $\Gamma(g) = \int_0^\infty x^{(g-1)} \cdot e^{-x} \cdot dx$, b and C are the slope and the intercept of the S-N curve respectively, where the S-N curve is defined by $C = N \cdot S^b$ where, N is the no of cycles to failure of cyclic stress amplitude S .

The second stage of the 'test tailoring approach' is the 'test synthesis', where the AD loading profiles (PSD) are generated using the following Eqn. (4) [39]. During the 'test

synthesis' process the **Condition 1** and **2** presented in Section 2.1 of the 'test tailoring approach' must be maintained. The generated loading profiles also follow the relation described in Eqn. (1).

$$PSD(f_n) = 2 \cdot \frac{(2\pi \cdot f_n)^3}{Q} [\frac{k_c \cdot \sum FDS(f_n) \cdot C}{K^b \cdot f_n \cdot T \cdot \Gamma(1 + \frac{b}{2})}]^{\frac{2}{b}} \quad (4)$$

where, k_c is the combined safety factor. Equation (4) can be rearranged as, $PSD \propto (\frac{1}{T})^{\frac{2}{b}}$ [43] which indicates the effects of the parameters, b and T, on the magnitude of the generated accelerated test PSD. In this study, the parameters of the SDOF system, the stiffness, $K=1$ in Eqn. (3, 4) and the dynamic amplification factor, $Q=10$, in Eqn. (2, 3), have been kept constant and S-N curve slope, b has been varied to observe its effect on the generated accelerated test PSD. A higher value of b results in a higher magnitude of the generated PSD when T is fixed. It allows involvement of higher AF while accelerating field test. The b values recommended for different materials are shown below [45].

Table 1: Range of Values of 'b' for Different Materials

Material	Value range
Brittle material	4 or less
Ductile material	4 to 8 or more

It has been suggested to use the inverse Basquin's exponent, b being specific to the material subjected to the vibration test via the synthesized AD loading profiles [48]. The limiting AF (maximum exaggeration factor) is determined as '2' (two) to conduct a valid

durability test in the test rigs [49]. The exaggeration factor is defined as the ratio of the PSD level of the accelerated test and the road test.

In this work, the 'modified test tailoring approach' [43] has been developed to generate the durability loading profiles to perform accelerated tests. In the modified approach, the acceleration time series of a duration of 60s is extracted using the inverse Fourier transformation (IFT) from the full period accelerated PSD, which is synthesized via the 'test synthesis' process of the standard 'test tailoring approach' [43]. This equivalent 60s loading profile (time series) is termed as the partial test loading profile and it must have the similar pattern and contain the same dynamic features of the field test. As the RMS value of the full period test is certain times (N_r) of the one of the partial test, the loading profile of the partial test is repeated for N_r times to obtain the desired FDS as the full period test. The number of recurrence (N_r) is calculated using Eqn. (5)

$$N_r = T_f / T_p \tag{5}$$

where, T_f and T_p are the durations of the full and partial periods of the accelerated durability tests respectively.

The other benefit of the partial testing is that it allows higher time compression than the full period AD loading profiles. Hence partial tests help in generating highly AD loading profiles for the industrial durability testing. The process-flow of generating the full period AD loading profiles and partial tests, using nCode GlyphWorks, has been presented in Figure 3.

For this work, the field test acceleration data has been collected via a tri-axial accelerometer from the front axle of the test vehicle driven in the Altoona proving ground [1]. This proving ground is designed to simulate the real road conditions during the

field/road test of the heavy ground vehicles. The collected 694 seconds acceleration data from the field test includes six laps and every lap contains seven different road events [2]. Figure 4 represents the field test acceleration data (sample) and the geometries of the seven road events of the durability track. In this case, the ground vehicles are required to drive 6250 miles without any failure in the main components [44].

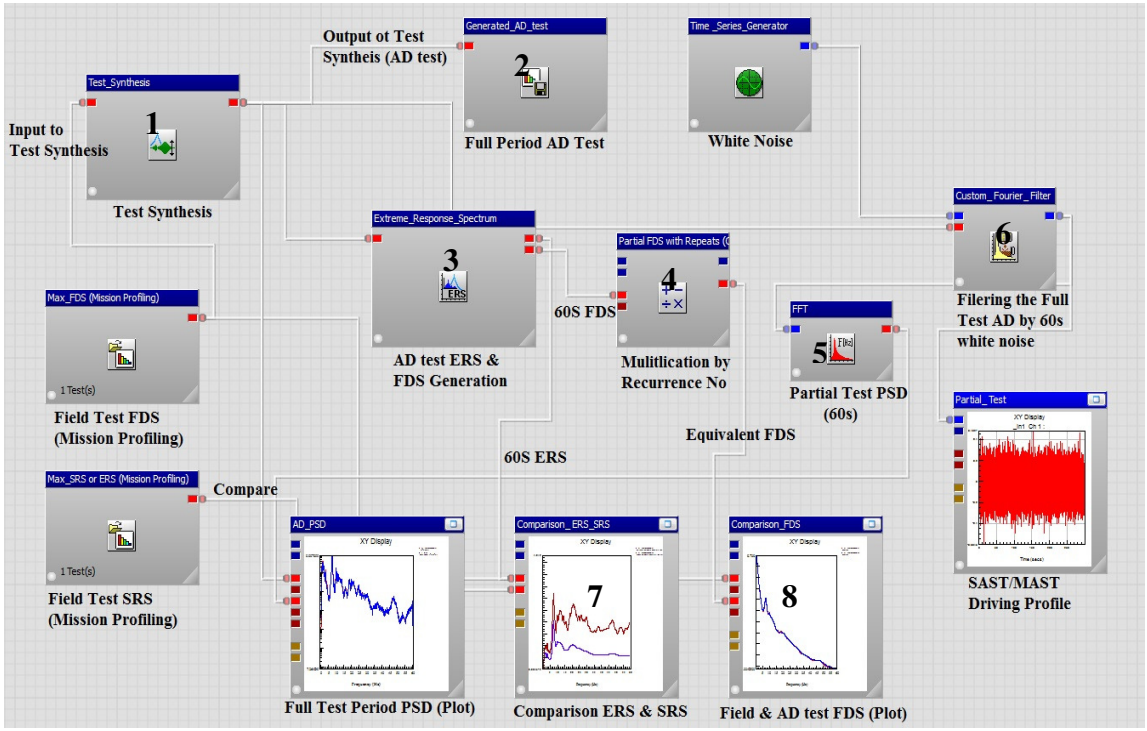

Figure 3: The Process Flow of Generating AD Profiles Using nCode GlyphWorks

As a first step of the modified approach, all of the seven (7) events have been successfully identified from the collected acceleration data [43]. Then using the acceleration data of each event, the SRS and the FDS of the field test have been developed through the 'mission profiling' technique. From this FDS of the field test data, the AD loading profiles of full duration period have been synthesized by the 'test

syntheses' technique. Later, the partial test has been obtained by filtering the full period test PSD by the white noise of duration of 60 seconds (60s). Later, the ERS and the equivalent FDS of the partial test have been determined and compared against the field test SRS and FDS to validate the synthesized partial tests. Here the equivalent FDS is determined by multiplying the recurrence number(N_r) with the FDS of the 60s partial test. To satisfy the **Condition 2**, presented in Chapter 1 the equivalent FDS determined from the accelerated partial tests have been kept the same as the FDS of the field test to ensure the same failure mechanism.

Moreover, the ERS of the partial test has been compared against the SRS of the field test. To satisfy the **Condition 1** mentioned in Chapter 1 the ERS of the synthesized partial tests have been kept lower than the field test SRS to avoid the alteration of the failure mechanism. As this work is based on the modified approach [43], the ERS of the partial test, instead of the ERS of the full period test has been compared with the SRS of the field test.

In GlyphWorks, the process starts with the 'Test Synthesis Glyph' (marked as '1') where the FDS of the field test determined via the mission profiling technique has been fed and the full test AD loading profile has been obtained as output ('Full Period AD Test', marked as '2') after the synthesis process. Afterwards, the full period AD test has been filtered (marked as '6') by white noise of 60s duration to get the partial test loading profile (MAST/SAST driving file). To confirm a valid AD test, the ERS and the equivalent FDS of the 'Partial Test PSD' (marked as '5') have been compared (marked as '7' and '8') with those of the field test. The equivalent FDS is found by multiplying (marked as '4') the FDS of the partial test (marked by '3') by the recurrence no.

(a)

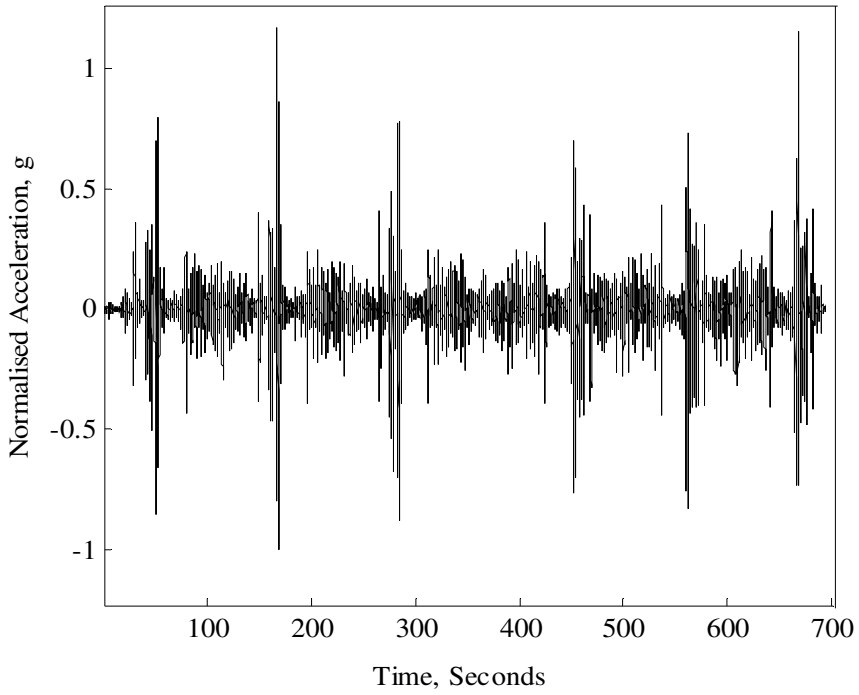

(b)

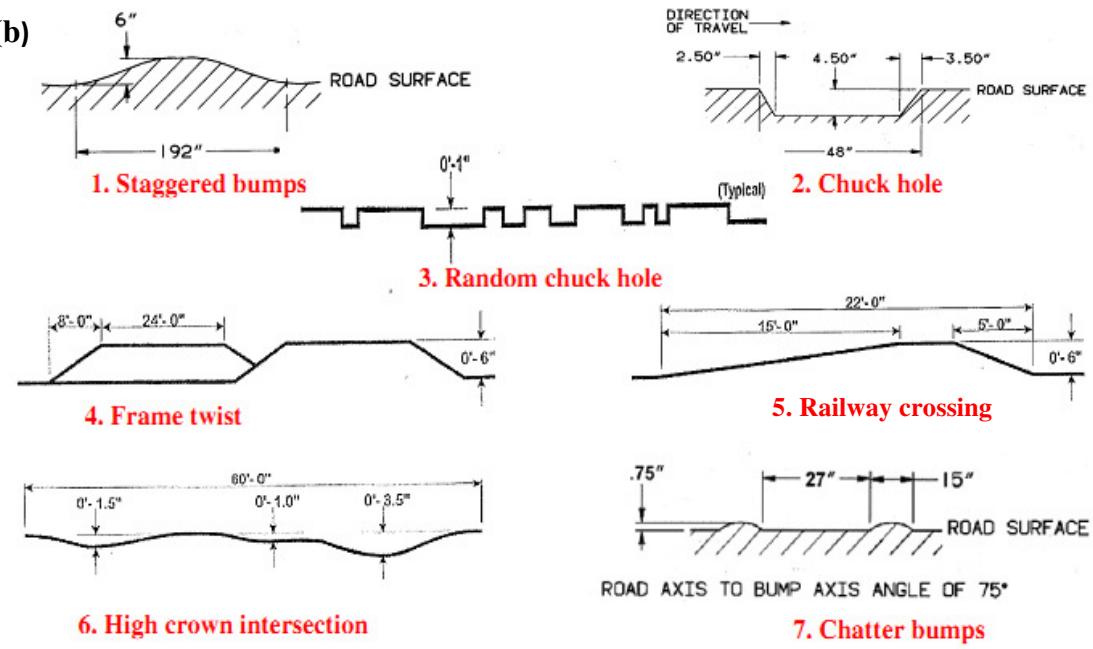

Figure 4: (a) Road Test Acceleration Data (Z-Vertical Direction) and (b) Geometry of the Seven Events

2.2. Development of the CAM with Specific Dynamic Features and Fatigue Life

A cantilever beam has been designed to demonstrate a computer-aided AD test and to validate the modified process of generating the highly compressed AD tests for the ground vehicle components. In this work, cantilever beams have been chosen for its well established mathematical model. The criteria of designing the test piece are as follows:

- The dominant vibration mode must be a bending mode and the natural frequency of this mode should be close to 7 Hz. It is crucial as it is the first natural frequency of the suspension system of the considered ground vehicles.
- The lateral vibration mode must be least dominant if it lies in the frequency bandwidth of 0-60 Hz. The specimen should have a very low tendency to vibrate in lateral directions because only the vertical excitation is applied.
- The fatigue life of the specimen should be 24 hours under the reference loading which is developed based on the modified procedure presented in [43].

The design process involves, (1) FEA along with a standard fatigue analysis (S-N) to obtain the specific durability life span of the cantilever beam and (2) experiments to verify the dynamic characteristics of the designed test-piece.

2.2.1. Numerical Vibration and Stress Analysis of the Specimen

The objective of the FEA is to analyze the dynamic response and the stresses of the test-piece. Firstly, the FE model has been developed in SOLIDWORKS. The geometry file is then imported to ANSYS. SOLID 95 elements have been used for meshing the SOLIDWORKS model. Approximately 150,000 elements have been used in the meshed model and it has been shown in Figure 5. The primary assumptions used in FEA are as follows:

- The model is linear and the material is homogeneous and linear elastic;
- The damping ratio is constant as 2%, temperature and humidity effects are negligible

Aluminum 6061-T651 alloy has been selected for the beam. Different notch orientations (cross section) and tip mass combinations have been analyzed to find the specimen with the desired frequencies and mode shapes. The modal analysis has been performed using software ANSYS through 'ANSYS Parametric Design Language'.

In this work, the cantilever beams have been placed horizontally and experienced the vertical acceleration to its fixed end. Hence, to achieve the structural responses (displacements and strains) both random vibration analysis and harmonic response analysis has been performed through ANSYS. The modal analysis is a pre-requisite to both of the above mentioned analyses, therefore the same boundary conditions, material properties, meshing, damping properties of modal analysis are applicable to both harmonic response analysis and random vibration analysis.

The random vibration analysis in ANSYS is capable of solving the base excitation problem using PSD as an input. Stress or displacement results are determined as a PSD in the probabilistic manner following the normal distribution through this analysis. On the other hand, as ANSYS is not capable of providing unit acceleration while performing harmonic response analysis, unit displacement have been used instead of the acceleration through coupled degree of freedom to excite the base. Considering a linear SDOF system, the stress response of the specimen can be obtained for different input. To determine the response PSD for a particular input PSD, the FRF results of the harmonic response analysis has been used as shown in Eqn. (6) [42]. This stress PSD has been used as the input for the fatigue analysis.

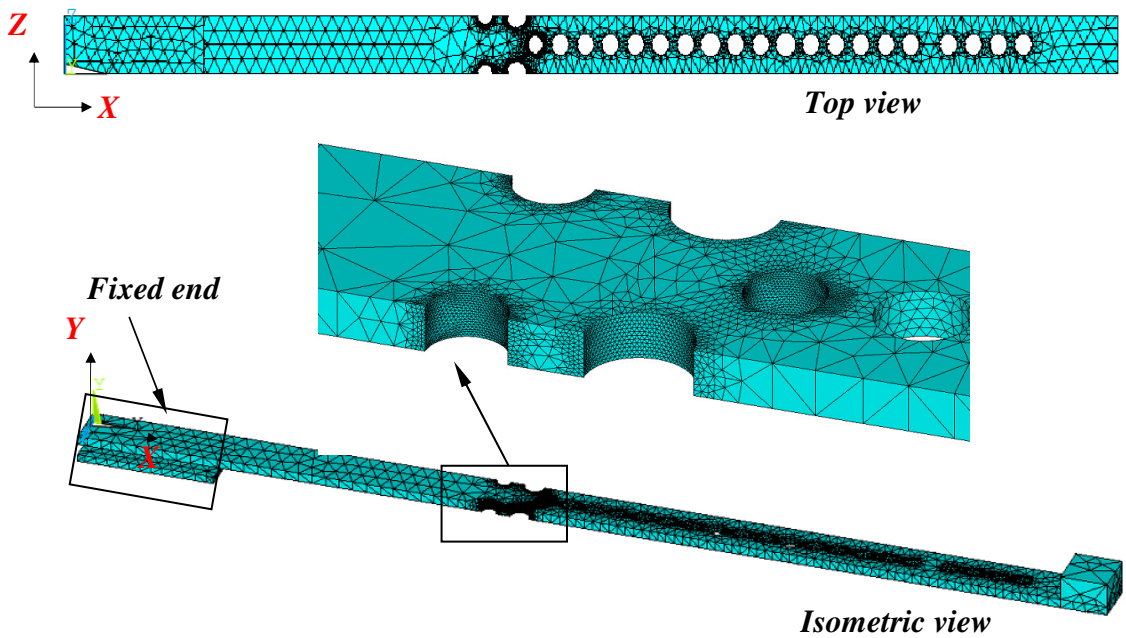

Figure 5: Meshed CAD with Solid Elements with a Finer Mesh around the Critical Notches

$$G_{yy}(f) = \sum_{i}^{q}\sum_{j}^{q} h_i(f) \cdot h_j^*(f) \cdot G_{ij}(f) \tag{6}$$

where, $G_{yy}(f)$ and $G_{ij}(f)$ are the output and input PSD to the system and $h(f)$ is the transfer function of the system. '*' is used to represent the complex conjugate of the transfer function [42]. The results from FEA are then passed to the commercial software nCode DesignLife for performing the fatigue analysis of the designed test-piece.

2.2.2. Experiments for Vibration and Stress Analysis

Performed FEA has been verified by the experiments as the CAM (FE model) needs to be used in the numerical fatigue analysis. Parameters, e.g., damping, linearity of the specimen and the response of the SAST to the input have also been obtained through experiments. The test procedure comprises of 'sine sweep tests' in three different

frequency ranges in the 3-65 Hz bandwidth and a 5-minute durability test with the partial tests extracted from the selected 24, 20, 4 and 1 hours accelerated PSD.

Here, The three sine sweep trials have been, 0.1g peak to peak at 0.5 octaves per minute in the range of 3-65 Hz (test-a), 0.2g peak to peak at 0.1 octaves per minute in the range of 3-8 Hz (test-b) and 0.2g peak to peak at 0.1 octaves per minute in the range of 45-65 Hz (test-c). The main objective of performing the sine sweep test is to determine the natural frequencies in the range of 0-60 Hz and the damping present in the system.

In the experiment, the specimens, placed horizontally, have been subjected to vertical vibration through the SAST [4]. This SAST is run by the hydraulic power by means of the MTS actuator series 206. This actuator has a moving mass of 16.8 kg. The fixture having a mass of 21.12 kg has been attached to the actuator which yields the total moving mass of the shaker to 37.92 kg without the specimens attached. While attaching the specimens (cantilever beams) to the fixture, an 88 N-m torque has been applied. Prior starting the test it has been verified through the iterative technique that the shaker table can implement the loading provided, with a very least amount of deviation, i.e. RMS deviation less than 4%.

One 4393 type piezoelectric uniaxial charge accelerometer has been attached at the tip of each attached beam to collect the acceleration response of the beam. This accelerometer is chosen for its very low weight (4 gm with magnet attached) and very high shock absorbing capacity (±25000g). An accelerometer of the same type is also attached to the fixture to get the response acceleration of the actuator or the base. Figure 6, shows the hydraulic shaker/SAST and all the four specimens mounted in the fixture (a) and the data acquisition system (Somat eDaq Plus) (b) to collect and store the data that was received

from the transducers.

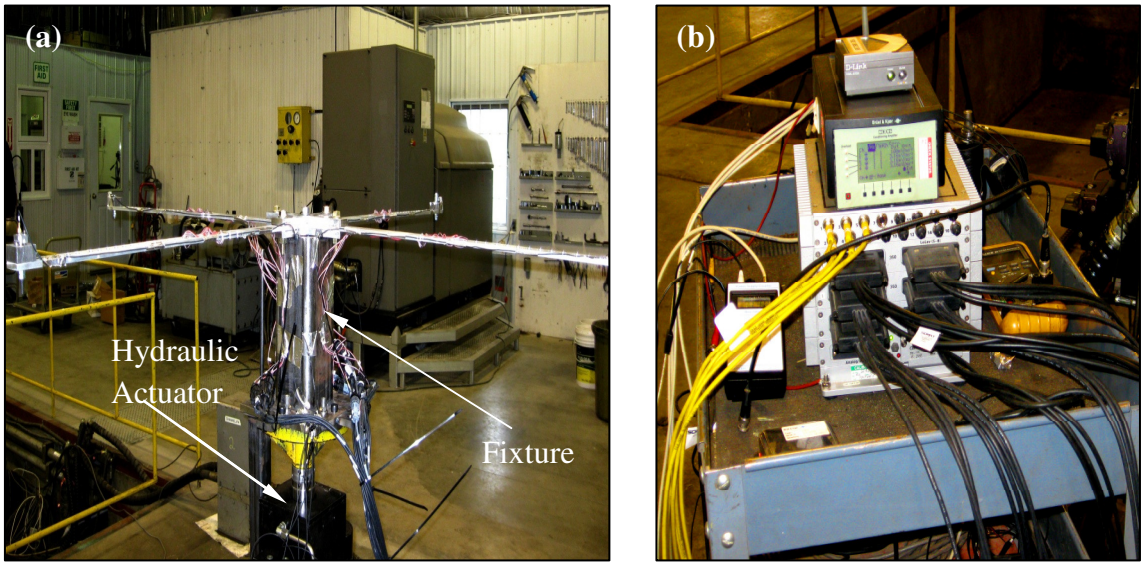

Figure 6: The Experimental Setup: (a) Hydraulic Shaker with the Mounted Specimens (b) The Data Acquisition system

Also six strain rosettes (CEA-13-062UR-350) and five axial strain gauges (two EA-031DE-350/E and three EA-062DN-350/E) have also been attached to different locations of the beams to collect the strain histories. Figure 7 shows the physical beam with the strain gauges, tip mass and accelerometer attached. Before starting the test, the accelerometers and the strain gauges have been calibrated to the required scale of the data acquisition system. After every trial the residual stresses have been recorded and calibrated to zero for the convenience of the analysis. The data acquisition system is capable of collecting data from 36 channels simultaneously. Data has been collected at a sampling rate of 2500 Hz which is around 39 times of the maximum frequency of the loading applied to the system. A 60s loading profile from the reference loading has been used to perform a 5-minute durability test. The profile has been repeated for five (5) times to generate more consistent strain data. 'Remote Parameter Control' (RPC)

software has been used to apply the loading to the SAST. As the iteration process becomes expensive using the full period AD loading profile, the representative 60s time series has been used.

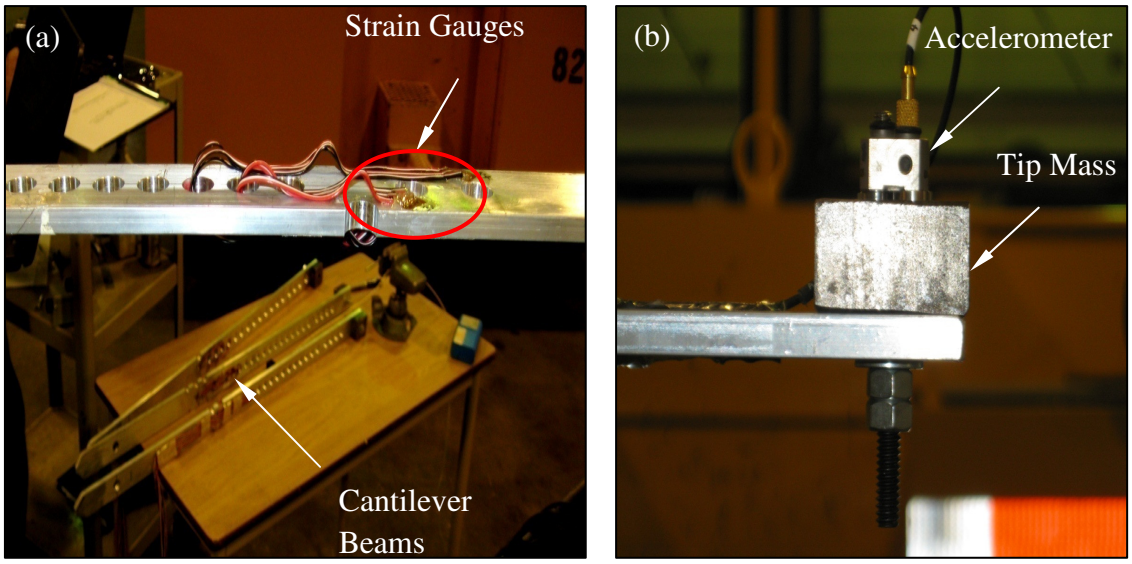

Figure 7: Beams with Attached (a) Strain Gauges and (b) Accelerometer and Tip Mass

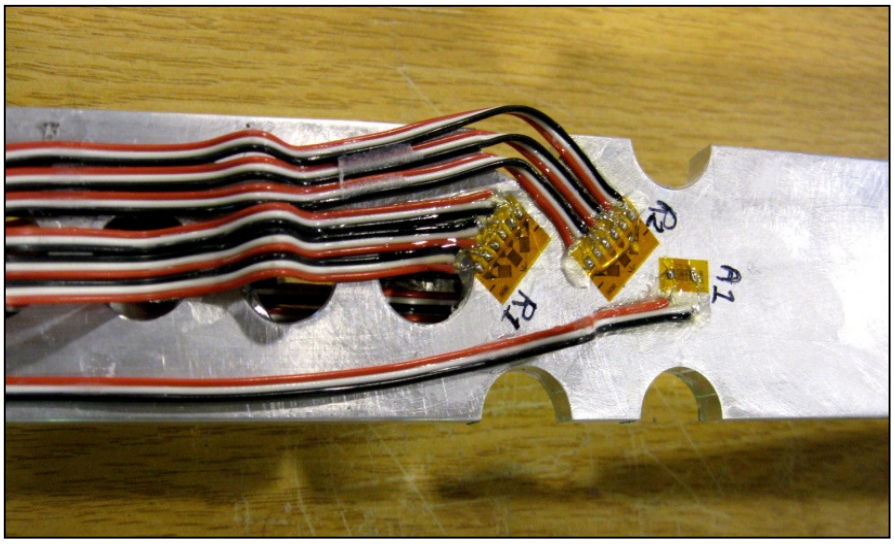

Figure 8: Attached Strain Gauges and their Locations in the Designed Specimen Used for the Test with the-24 Hours Accelerated PSD

Figure 8 presents the locations of the strain gauges attached to the designed beams. Strain

data has been collected during this 5-minute durability test to compare the experimental strains (maximum equivalent Von Mises) with the strain results found from the random vibration analysis performed on the FE model. The natural frequencies that were found from the sine sweep test will also be compared with those from the FE model. After verification, fatigue analysis is performed on the model based on the results of FEA. Furthermore, by double integrating the filtered (via a high pass filter, threshold is 3 Hz) tip response acceleration data, the displacement history of the tip of the beam has been obtained. Using the tip displacement history and the length of the beam the angular deviation history of the tip of the beam from the horizontal axis has been determined. Afterwards, the maximum angular deviation has been compared with that of the FEA to verify the soundness of the FE model. Linearity in the response of the beam has also been discussed from the angular deviation data.

2.3. FE Based Numerical Fatigue Analysis and the Verification of the Synthesized AD Loading Profiles

There are two distinct reasons for performing the numerical fatigue analysis. They are:

- To design a dynamically featured test-piece for approximately 24 hours of fatigue life (Significance level $\alpha \leq 0.05$).
- To determine the FLR of the designed test-piece for different AD loading profiles which are synthesized in this work and verify their effectiveness.

The FRF results (displacements, stresses and strains under the unit base excitation) of the CAM have been determined through the harmonic response analysis and transferred to nCode DesignLife for the fatigue analysis. In the case of heavy ground vehicles, the stress-life (S-N) method is very effective to be used in the determination of the durability

[50]. Hence, in this work, to determine the durability or the fatigue life of the test-piece, the S-N fatigue analysis has been performed in the frequency domain.

For the S-N method the stress information (stress-time histories or stress PSDs) needs to be separated to the stress ranges and the number of stress reversals. The Rainflow Cycle Counting Algorithm and 'Dirlik', 'Narrowband', 'Lalanne', 'Steinberg' algorithms can be used to perform this separation [51] in the *time-domain-based* and the *frequency-domain-based* S-N method, respectively. Afterwards, using the material's S-N data, the damage for each stress/strain reversal is determined and the accumulated damage is calculated according to Miner's law to find out the total damage. In the previous literature it has been found that Dirlik's algorithm is the most consistent with the 'Rainflow cycle algorithm' [17]. Hence, 'Dirlik's' algorithm has been widely used to perform the *frequency-domain-based* fatigue analysis. In this work, 'Dirlik's' algorithm has been used to design the final specimen as well. The mathematical model of the 'Dirlik's is as follows [39],

$$N(S) = E[p] \cdot T \cdot p(S) \tag{7}$$

where, $N(S)$ is the number of the stress cycles of range S (MPa) expected in time T (s), $E[p]$ is the expected number of peaks and probability density function of stress range S is as follows,

$$p(S) = \frac{\frac{D_1}{Q} \cdot e^{-\frac{Z}{Q}} + \frac{D_2 \cdot Z}{R^2} e^{-\frac{Z^2}{2R^2}} + D_3 \cdot Z \cdot e^{-\frac{Z^2}{2}}}{\sqrt{\lambda_0}} \tag{8}$$

Parameters $D_1, D_2, D_3, Z, \lambda_o$ and R can be determined from the respective mathematical formulations [28] prescribed by Dirlik. The Dirlik Eqn. (7 and 8) is based on the

weighted sum of the Rayleigh, Gaussian and exponential probability distributions [51]. Then the damage for each node of the FE model has been determined by the following Eqn. (9) [39],

$$D=\frac{E[p]\cdot T}{C}\sum_{i=0}^{i_{max}} S_i^b \cdot p(S_i)=\frac{E[p]\cdot T}{C}\int_{S=0}^{\infty} S^b \cdot p(S)dS \tag{9}$$

where, C and b are the intercept and the slope of S-N curve respectively.

Figure 9 represents the S-N curve of the test-piece material, Aluminum 6061 T651. The S-N-curves are usually determined empirically in an approximated way, from the ultimate tensile strength (σ_{UTS}) of the material and Basquin's exponent (B). However, the obtained curves must be corrected by modifying factors such as the temperature, surface roughness, size, thermal treatment, superficial hardness, and loading type [52].

Although metal fatigue is a complex subject that can be best treated using the principles of fracture mechanics, but in case of AD tests damage model can be approached using the simple 'S-N curve for the concerned material [48]. The following S-N curve has been formulated using the data for Aluminum 6061-T651 plate, stress-relieved material, thickness ≤ 90 mm [53]. Then the S-N curve slope, b and the Stress-Range Intercept *(SRI1)* has been determined using an exponential fit of the data used to generate the S-N curve. The high value of R^2 (0.9619) signifies the validity of the obtained approximation of the complex S-N curve from the discrete fatigue test data.

A relation has been developed between the stress under unit base excitation (displacement) and the estimated fatigue life for the specimen. Using the developed relation the specimen fatigue life is estimated to be 24 hours using a specific combination of the tip mass and the notch size. The specific combination has been determined through

the trial and error technique. While developing the relationship, the maximum absolute principal stress has been determined from a consistent location irrespective to the notch sizes/orientations and tip mass combinations. To determine the maximum absolute principal stress, the harmonic response analysis has been performed for the amplitude of 1 meter (unit displacement in the SI system) sinusoidal base excitation in the 0-60 Hz frequency bandwidth with a frequency step of 0.2 Hz. As this stress analysis has been performed for the unit excitation, it has been termed as the transfer function of stress transfer function (Pa/m).

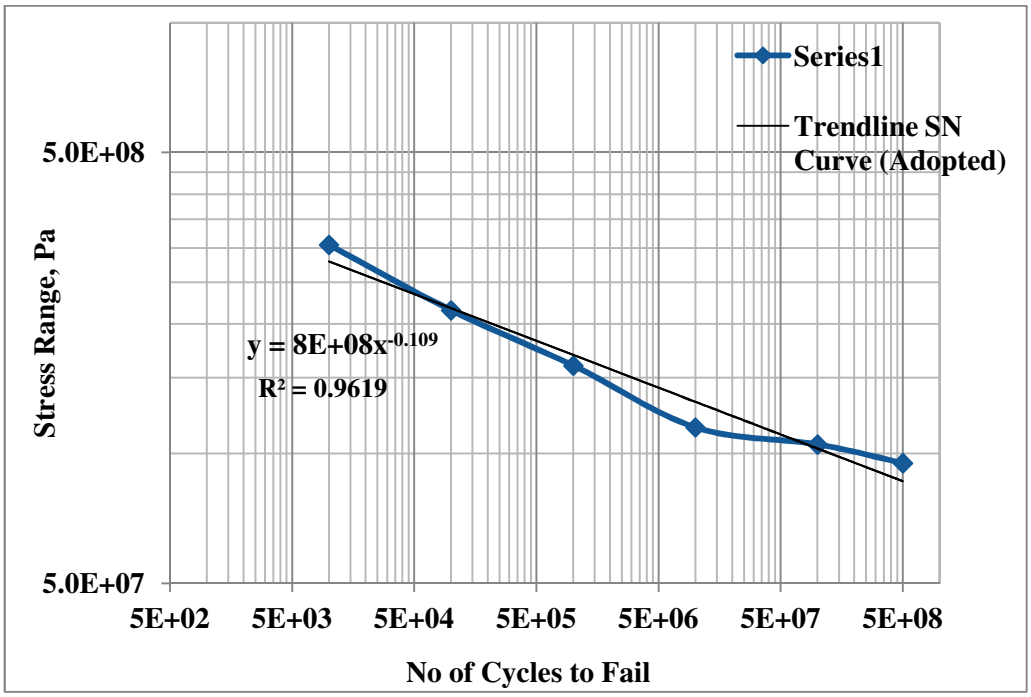

Figure 9: S-N Curve Formulation for Aluminum 6061 T651 Alloy

Validation of the 'modified test tailoring approach' presented in [43] has been performed by testing the designed specimen with the synthesized AD loading profiles. Theoretically, for a successful AD test the AF should be equal to the FLR of the specimen. To determine the fatigue life, the result file (.rst) of ANSYS containing the FRF results has

been imported to nCode DesignLife and the fatigue life has been determined for all synthesized AD loading profiles using *frequency-domain-based* S-N method. The absolute maximum principal stress has been used as the stress invariant as the mean bi-axiality ratio, 'r', which is in the range of $-1<r<0$ [54]. While determining the maximum absolute principal stress from the experimental strains, the transverse sensitivity of the gauges, 1, 2 and 3 of the rosettes have been taken as 0.012, 0.006 and 0.012 [55]. Dirlik algorithm [39] has been used to separate the absolute maximum principal stress PSD to the stress ranges, the number of stress reversals, and Goodman criteria has been used to correct the existing mean stress. As the level of AD loading profiles has a unit of 'g' and the stress transfer functions has an unit of 'Pa/m', to make the units consistent, the AD loading profiles have been integrated twice and converted to the displacement spectrum density before using it in the fatigue analysis [56]. Finally, the expected fatigue life and the estimated fatigue life of the developed model have been compared. The process flow of vibration fatigue analysis performed via nCode DesignLife has been presented below in Figure 10.

In this process it has been shown that the 'FE FRF Results Glyph' (marked as '1') and the displacement PSD ('FFT' (Fast Fourier Transform), marked as '2') of the 60s partial test has been used as the input to the 'Vibration CAE Glyph' ('Vibration Fatigue Analysis', marked as '3') for the fatigue analysis. Proper material, algorithms and the loading information have also been imported into this glyph for performing a standard S-N analysis to obtain the 'Fatigue Life Distribution Glyph' (marked as '4') in the model. The displacement PSD has been found by double integrating the acceleration signal of the partial test. Filtering has also been performed before the integration process to

remove the frequency content less than 3 Hz because the SAST/MAST cannot implement any frequency below this limit. Output of the process can be found in the 'Fatigue Life Distribution Glyph', and the 'Data Glyph' (marked as '5').

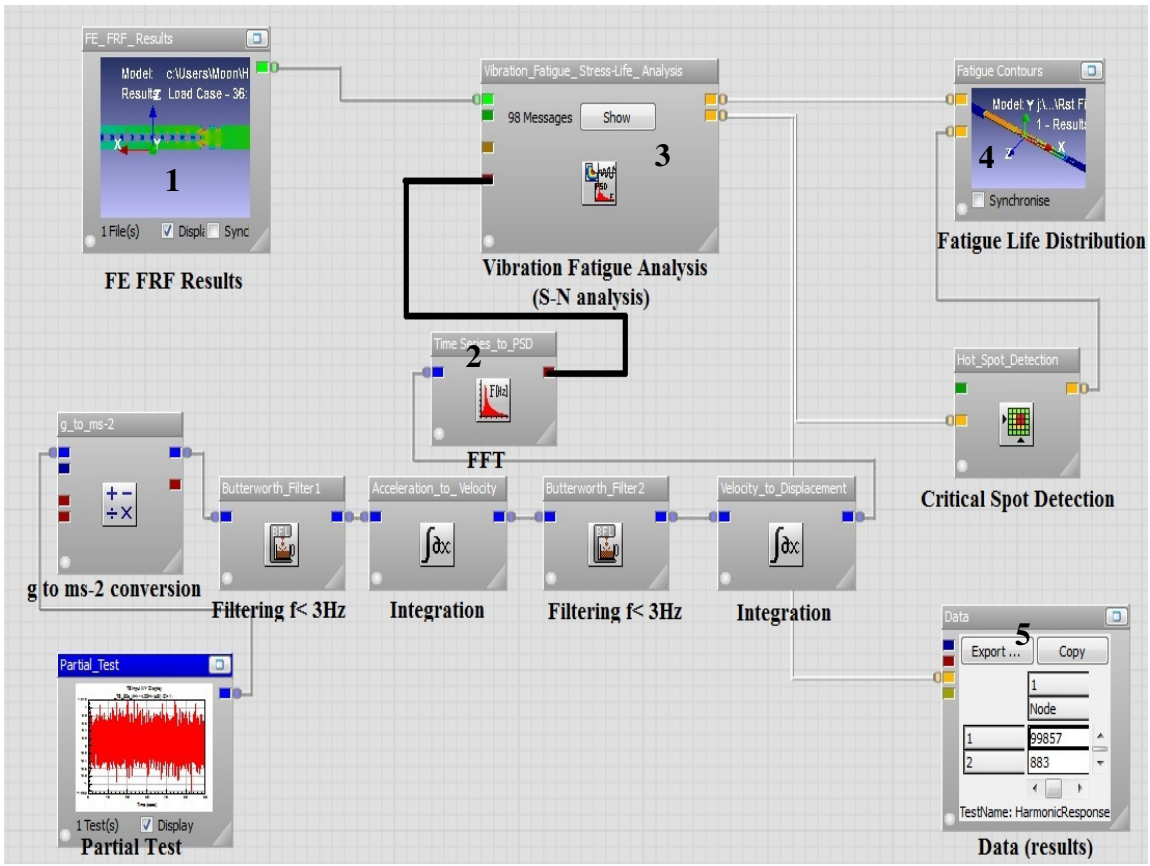

Figure 10: Vibration Fatigue Process Flow in DesignLife

In Figure 11, the design process of the test-piece has been described via a flow. It summarizes the techniques used in this chapter. The total flow divided into two analyses boxes for better understanding. They are 'AD Testing and FE Analysis' and the 'FE based Fatigue Analysis'. Detail of these two analyses can found within the boxes. Combining the results of these two analyses the test-piece has been designed via a trial and error method.

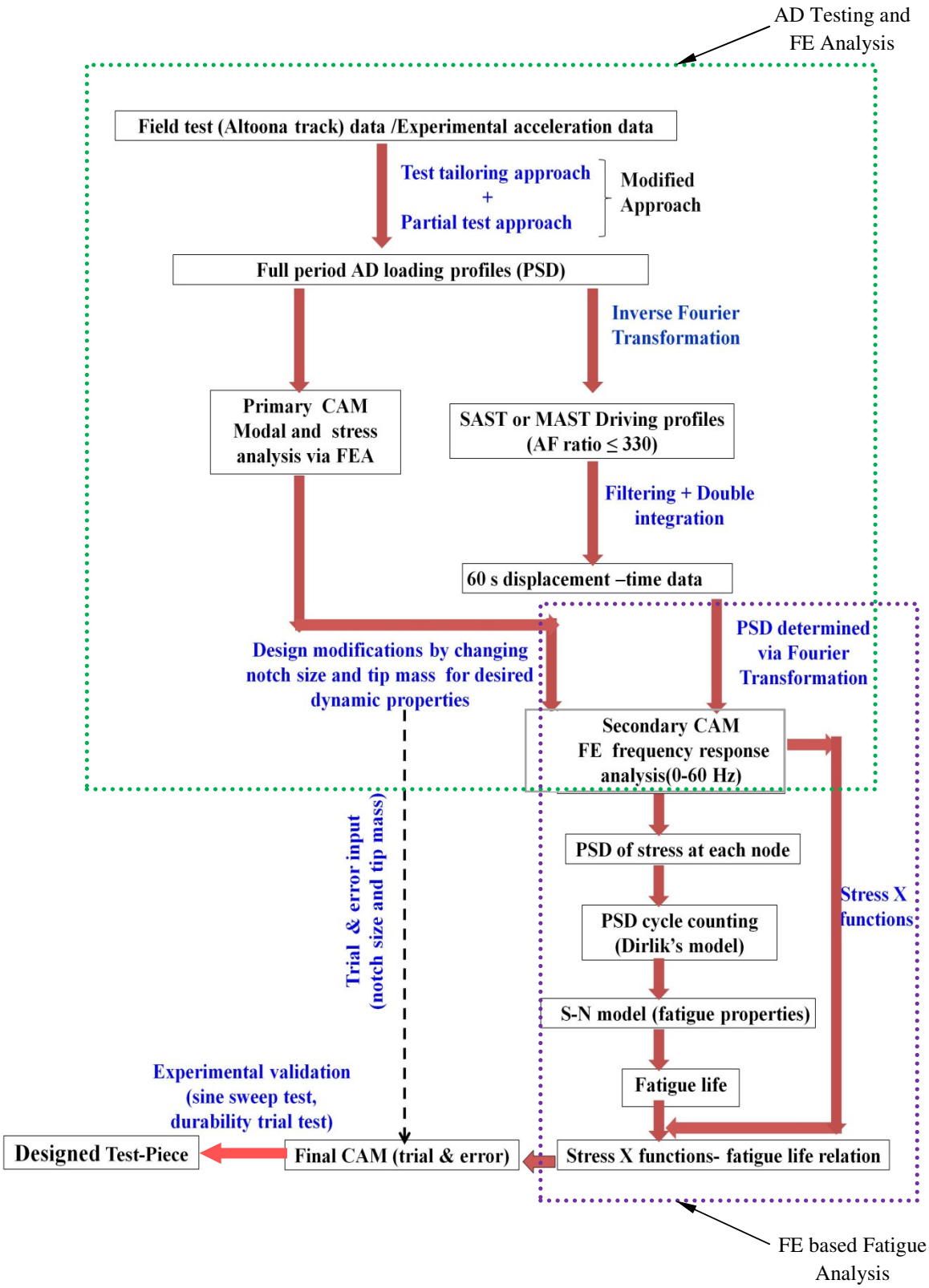

Figure 11: Process Flow of AD Testing Methodology

Chapter 3

Results and Discussion

This section consists of three subsections. In Section 3.1, results from the 'modified test tailoring approach' have been presented. In Section 3.2, the design of the test-piece has been presented with its featured results and experimental validation. Section 3.3 presents the numerical durability analysis results to validate the generated AD loading profiles hence the 'modified test tailoring approach'.

3.1. Synthesized Highly AD Profiles, FDS and ERS Comparison

Features of AD loading profiles generated via 'modified test tailoring approach' have been presented in this section. These loading profiles have been synthesised from 330 hours of field test data. In Figure 12, full period AD test profiles of different duration (1.5, 2, 4, 8, 10, 15, 20 and 24 hours) have been demonstrated. These AD loading profiles have been shown in a form of PSD against frequency in a bandwidth of 0-60 Hz. The amplitude of the PSD is expressed in 'g^2/Hz', where, 'g' is the gravitational acceleration. It is found that for all of the accelerated profiles, the level of the PSD gets higher when the duration of the test has been shortened. These loading profiles also keep the similar trends for the frequency components to ensure the same failure mechanism. Moreover, all of the PSD this figure show a peak around 7.25 Hz, which represents the natural frequency of the suspension systems of the vehicle under study.

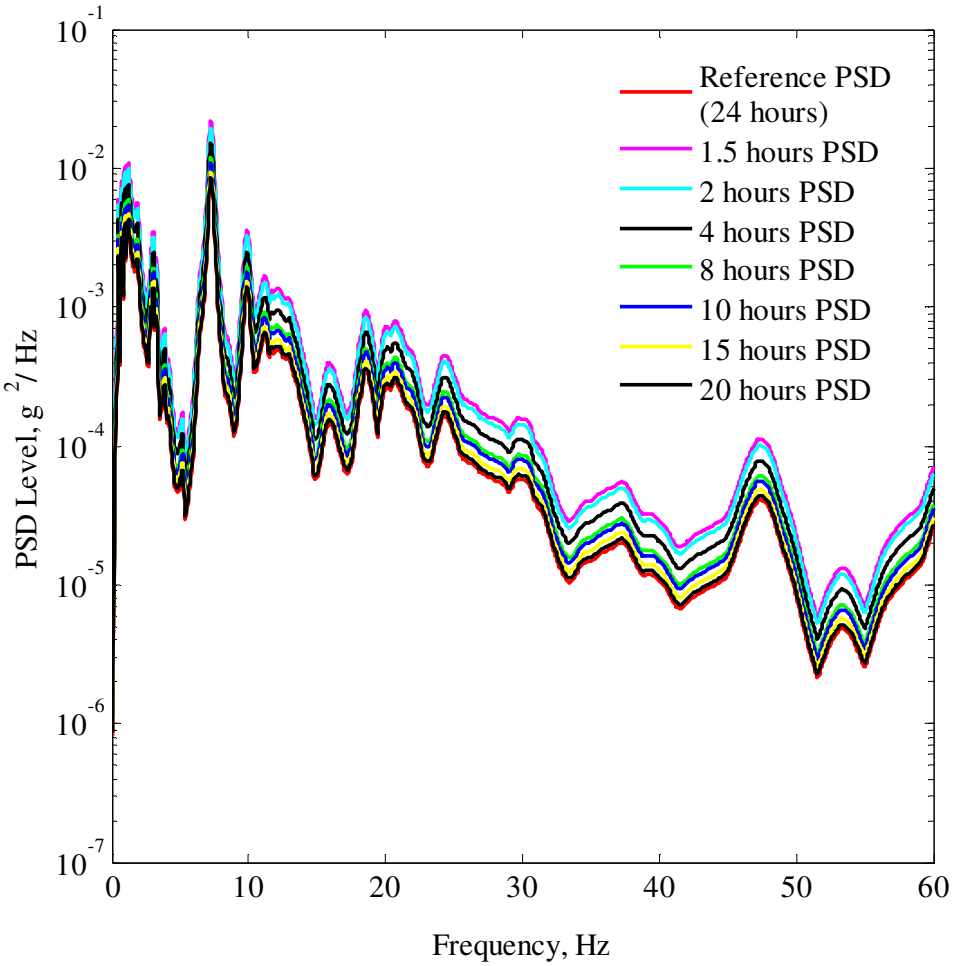

Figure 12: Generated AD Tests of Different Duration for a Constant FDS

These synthesized AD loading profiles can be used as the input to the SAST/MAST in two forms: 1) a PSD or equivalent time series of a full test period, and 2) an equivalent 60s time series. For implementation, the second method is recommended to save the cost and time involved in the iterative process of generating the driving files for the SAST/MAST [57]. Hence, the partial tests have been generated from the full period tests. As the partial tests are implemented in the durability tests, the ERS and equivalent FDS of the partial test has been compared with the SRS and FDS of the field test. The

equivalent FDS is determined by multiplying the recurrence number (N_r) (Eqn. 5) with the FDS of the 60s partial test.

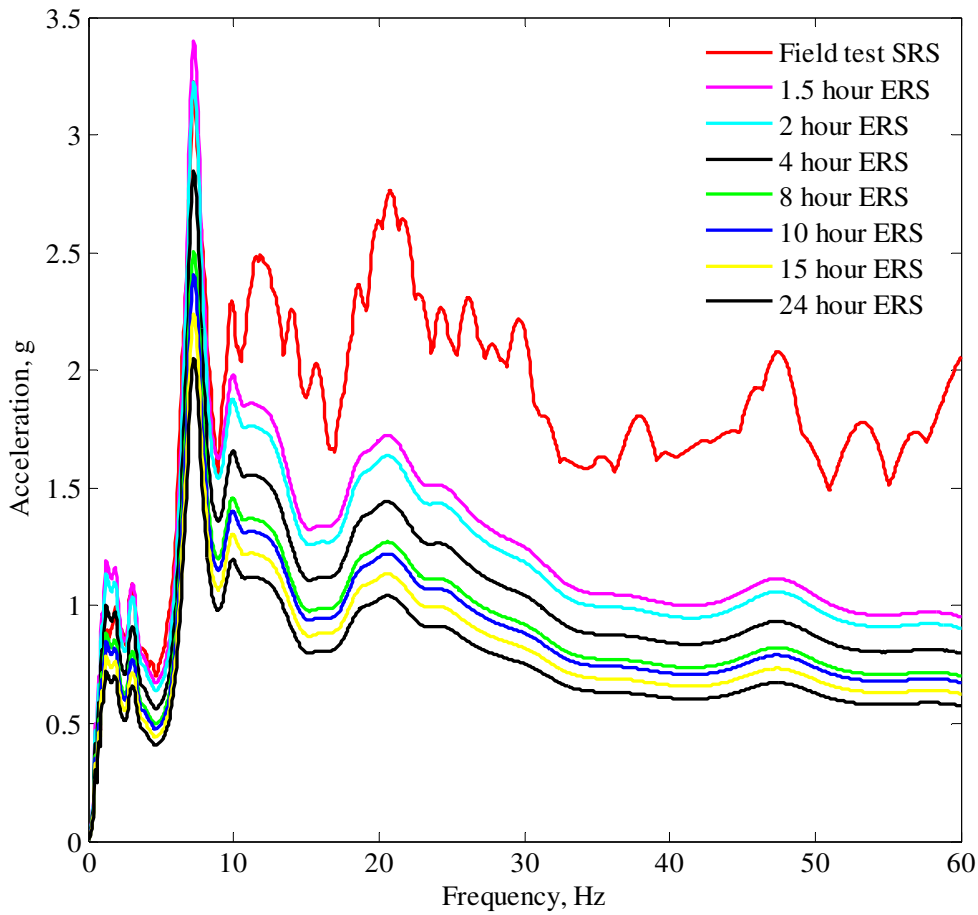

Figure 13: Response Spectra for Different AD Tests for a Constant FDS

Figure 13 represents the comparison of the ERS of the partial test profiles synthesized via modified approach with the SRS of the field test. The amplitude of the ERS is expressed in 'g', the gravitational acceleration. It has been shown that levels of all the ERS (g) are below the SRS of the field test. Therefore, the synthesized durability loading profiles have not caused any impact failure or alternation of the failure mechanism of the

structure. The bandwidth of 0-60 Hz has been chosen because after 60 Hz the response of the components of the ground vehicles is very low.

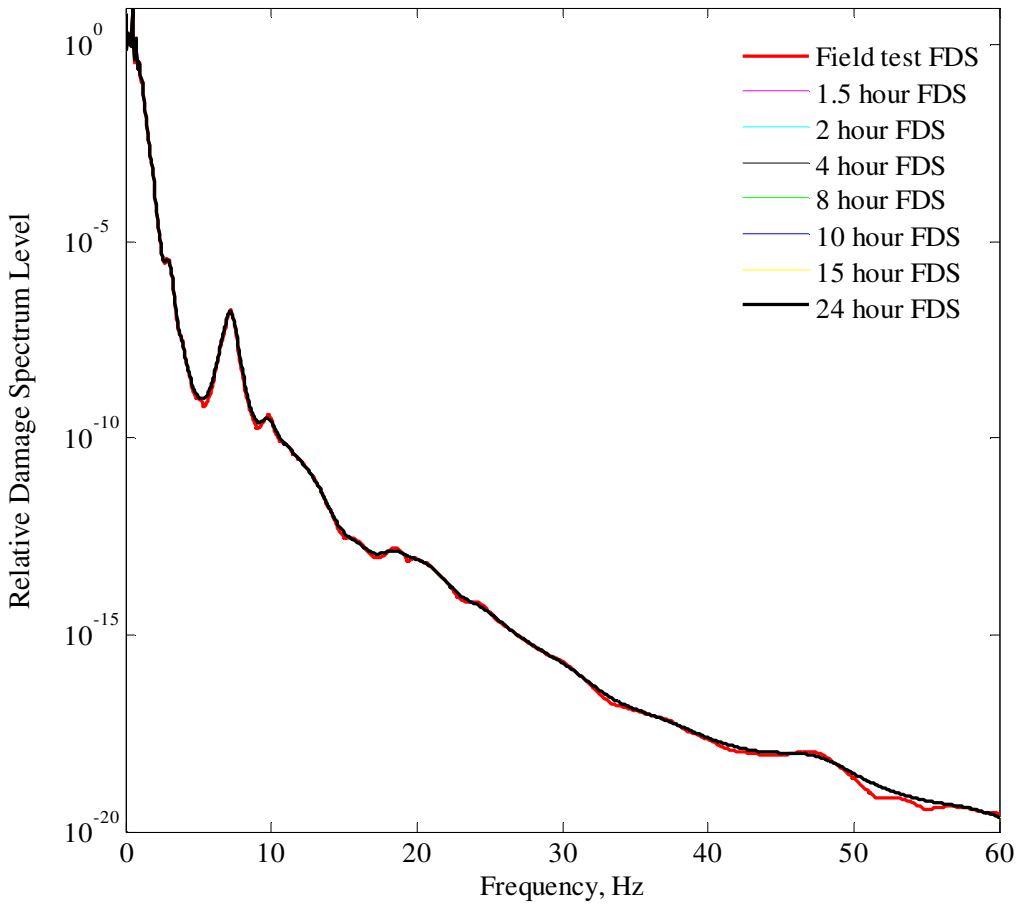

Figure 14: Damage Spectra for Different AD Tests for a Constant FDS

Equivalent FDS of the synthesized partial AD loading profiles via modified approach and the field test has been presented in Figure 14. Here, the partial tests (of 60s) have been repeated for 'N_r' times to cause the same damage as of the full period tests, i.e., to make the durations of the full period test and the partial test the same. Then the FDS of the field test and the equivalent FDS of the partial test have been compared. Figure 14 shows that the equivalent FDS of all of the partial accelerated profiles almost overlap with the FDS

of the field test. Thus the modified approach guarantees the consistence between the failure mechanisms for all the AD loading profiles, which is the most important feature of an accelerated test. In Figure 14, the damage is presented in log-scale along the Y axis as the damage is very low comparing to the linear scale. It has also been observed from Figure 12 and Figure 14 that in the frequency range of 25-60 Hz, the level of the accelerated PSD is low to cause any significant damage ($< 10^{-15}$) to the considered system. Some deviation on the FDS of the AD profiles with the field test has been observed between 50-55 Hz. This deviation has negligible effect on the durability process as the level of accelerated PSD (Figure 12) in this frequency range is low.

Hence, the field test may be accelerated to any durations within the upper-bound keeping the same damage mechanism using the 'modified test tailoring approach'. The Upper-bound is determined by the SRS of the field tests. Thus this approach eliminates the risk of high AF which can alter the failure mechanism. It can be concluded that the AF is much more controlled in this 'modified test tailoring approach' then other existing techniques. Importantly, the modified approach is valid up to linear elastic region of the considered system.

3.2. Design of the Test-Piece and Its Validation

The features of the designed test-piece, its experimental validation and the iterative technique of the design process have been presented in this section.

3.2.1. Features of the Designed Test-Piece

The features of the designed test-piece satisfying the criterion discussed in Section 2.2 has been summerized as follows with the notch orientations shown in Figure 15.

1.	Type of the structure	**Cantilever beam**
2.	Material	**Aluminum 6061 T651**
3.	Cantilever length	**73 cm**
4.	Cross section	**12.7 cm x 0.79 cm**
5.	Tip mass	**251 gm**
6.	Fatigue life under the reference loading	**23.8 hours(estimated)**

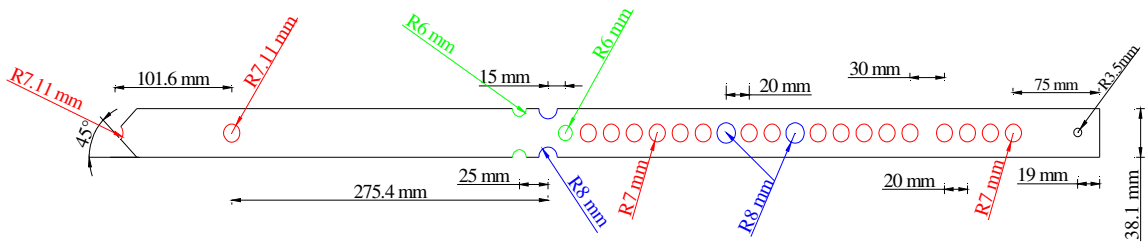

Figure 15: Notch Orientations of the Designed Specimen (Top-View)

Figure 16 shows (a) the physical test-piece attached to the fixture, (b) the same test-piece with the attached sensors for experimental strain collection. Two sets of beams of the same design configuration have been fabricated for the experimental validation.

These sets have beam fabricated in different places. First set (4 beams) of the beams have been manufactured earlier for the validation of the design and the second set (12 beams) has been fabricated later to perform the experimental durability tests to verify the AF of the synthesized AD loading profiles. The number of beams is a multiple integer of 4 (four) because the fixture has been built to hold maximum 4 specimens at a time. Test-pieces have been subjected to sine sweep tests and trial durability tests with 24, 20, 8 and 1 hour accelerated PSD. All the trial durability tests have been performed for 5 minutes.

To collect the strains, one rosette and two axial strain gauges have been attached in the location R_1, A_1 and A_2 respectively which are shown in Figure 16(a).

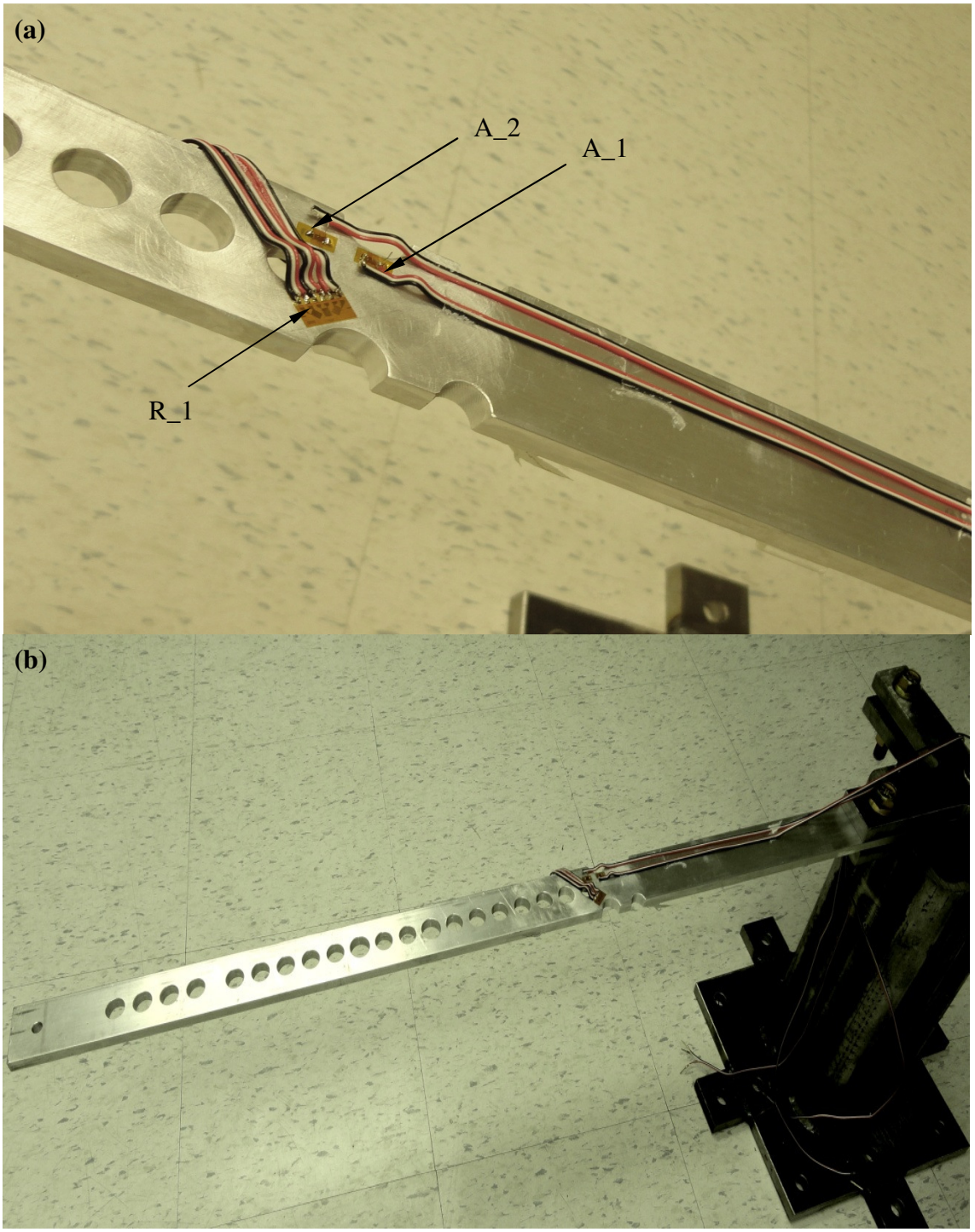

Figure 16: (a) The Physical Test-Piece (b) The Test-Piece with Sensors, for the Experimental Comparisons

3.2.2. Determination of the Dynamic Parameters of the System

In this section, important dynamic properties, i.e. the natural frequencies, damping coefficients and linear response behaviors of the designed test-piece have been experimentally determined. Table 1 summarizes the averaged results found from the three performed logarithmic-sine sweep tests presented in Section 2.2. From these test results, two vibration (bending) modes have been found within the frequency bandwidth of 0-60 Hz. As the acceleration data has been collected only for the vertical direction, no lateral vibration mode (second vibration mode) can be obtained from this experimental acceleration data. It is also observable from the experimental results that the first bending mode is, at an average, 3.5 times more dominant than the second one. Hence the damping ratio of the first mode is considered as the constant damping (0.2053%) throughout the FEA [25].

Table 2: The Natural Frequencies and the Damping Ratios for the First Two Vibration Modes for Different Specimens

Test Set	Natural Frequency of the 1st Mode (Hz)	Damping Ratio of the 1st Mode (%)	Natural Frequency of the 3rd Mode (Hz)	Damping Ratio of the 3rd Mode (%)	Gain Ratio of the 1st and 3rd Mode
1	7.114	0.2053	56.91	0.6857	3.190

Regarding the linearity approximation, around the vicinity of the natural frequencies of the first two bending modes, structural non-linear response has been observed. Beyond such vicinity, the specimen behaves closely to a linear system. This phenomenon can be observed in Figure 17. In this figure, gain ratios between two different base excitations have been plotted against the frequency. For the linear response of a system, the gain ratio for different excitation should be unity. In these cases the gain ratio violates this

criterion around 7.11 Hz and 56.9 Hz which are the first and third natural frequency of the specimen.

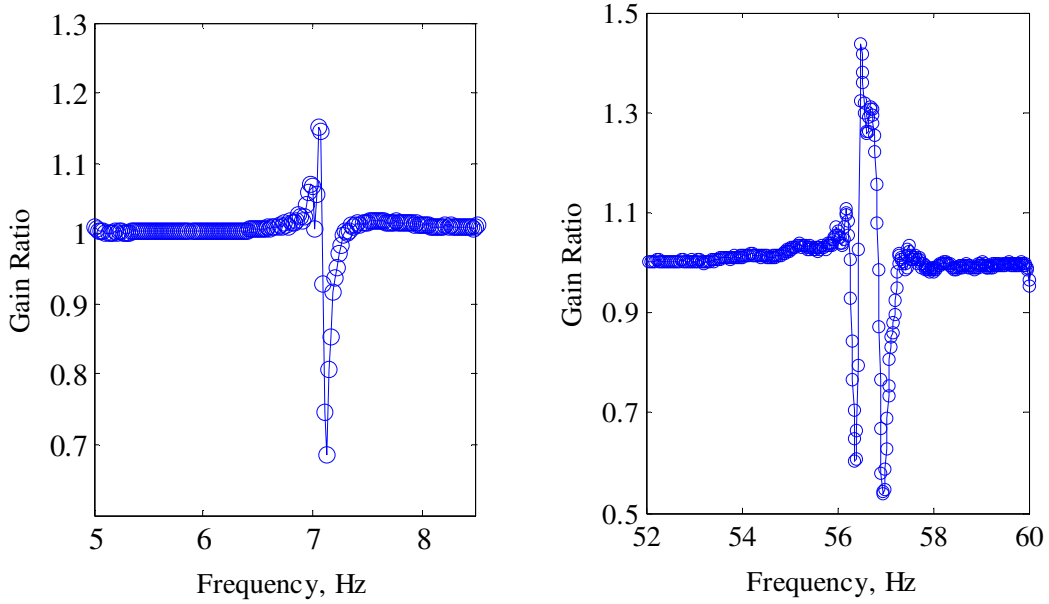

Figure 17: Linearity Approximation around the Resonance

However, the natural frequency and the damping ratio of the first mode can also be determined from the free vibration test using the *logarithmic decrement rule*. As the natural frequency and the damping ratio of the other vibration modes cannot be retrieved by this rule, sine sweep tests are necessary to determine the dynamics of the other modes. Figure 18 shows the free vibration history of the test piece along with the points considered for applying the *logarithmic decrement rule.* The exponential envelope (window) determined from the measured data has been presented in this figure shows how ideally the damping affects the vibration (response). Using the two points shown in Figure 18, the natural frequency and the damping ratio of the first mode can be determined using the fundamental relationships of a SDOF system. Importantly, the

results determined from the FRF of the sine sweep test and the free vibration test are close in both quantitative and qualitative sense.

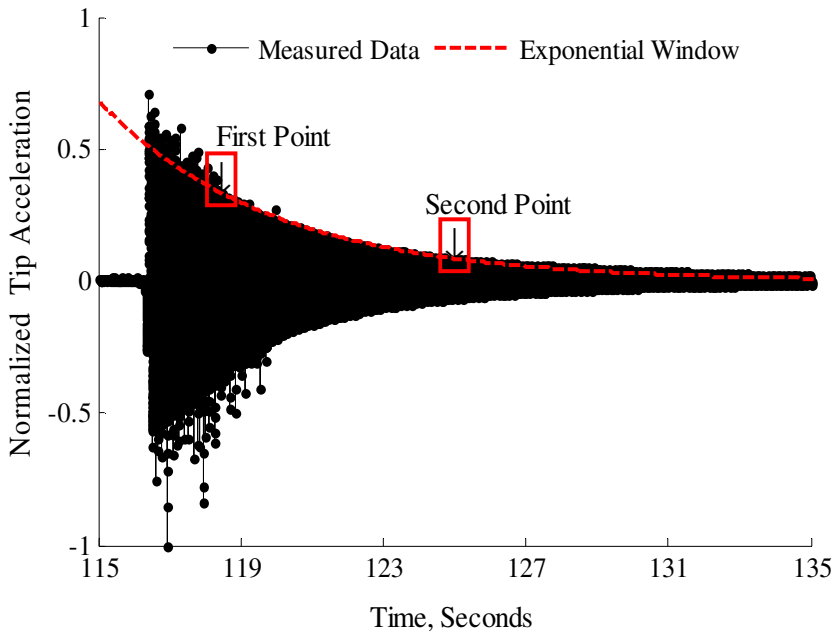

Figure 18: Sample Vibration Time History from the Test-Piece

3.2.3. Comparison between Numerical and Experimental Results

In this section, the FEA and the experimental results have been compared to validate the design. The damping ratio determined from the experiments has been updated in FEA to compare strains of FEA with those from the experiments. Table 2 presents a comparison of the averaged natural frequencies for the first four vibration modes of the test-pieces. It shows that the maximum deviation between the FEA and the experiments based on the natural frequency of the first mode is 2.162% and overall the maximum deviation is 5.091% in the fourth mode. Test has also been performed to ensure the convergence of the FEA results prior to the analysis.

Table 3: Comparison of the Natural Frequencies between the FE and the Experimental Model

Test Set	Vibration Modes	Analytical Natural Frequencies (FE) Hz	Experimental Natural Frequencies Hz	Percentage (%) of deviation
1	First (bending)	7.272	7.114	2.161
	Second(transverse)	33.82	N/A	-------
	Third (bending)	59.66	56.91	4.616
	Forth (bending)	174.7	165.8	5.091

Another comparison between the maximum equivalent Von Mises strains from the experiments and the FEA for the selected locations (Figure 5) is presented in Table 3. An axial strain gauge is attached at the location A1 and two of the strain rosettes are attached at locations R1, R2. The maximum deviation in the strain results is found as 2.610% at the location A1 and the minimum deviation is found as 0.390% at R2. While determining the maximum Von Mises strains from the FEA, $3-\sigma$ results are considered 99.73% of the results (data).

Table 4: Comparison of Strains between the FE and the Experimental Model for the 24 Hours Loading Profile

Test Set	Strain Gauges/ Rosettes	Area Averaged FE Strains (3-sigma) (με)	Experimental Strains (με)	Absolute Deviation in Strains (%)
1	A1	1416	1454	2.610
	R1	984.0	990.6	0.660
	R2	1266	1271	0.390

The maximum tip deflections of the cantilever beams (the test-piece) under different AD

loading profiles have been compared between the numerical and experimental techniques in Table 4. In the experiment 24, 4 and 1 hour loading profiles have been implemented. From these tests, the average deviation in maximum tip displacement has been found as 6.30%. It is observed from the results presented in Table 4, as the duration of the accelerated PSD gets lower, this deviation becomes higher. The 4 hour and the 1 hour loading profile have been implemented in a different set of beams (test set 2) which may have caused the relatively larger deviation in the tip displacements.

In Table 4 the experimental axial angular deviations from the fixed end in the first vibration mode have been presented. It shows that the maximum angular deviation is 7.42 degree which indicates the non-linearity in the structural response. The maximum angular deviation has been found to be increasing with the RMS of the accelerated profile. Analyzing the results from Section 3.2.3, it can be concluded that the CAM truly represents the physical test-piece as the deviations between the FEA and the experimental results are low.

Table 5: The Maximum Tip Deflection Comparison between the FEA and the Experiment

Test Sets	Duration of Accelerated PSD (Hours)	Numerical Maximum Tip Displacement (3-sigma) (cm)	Mean-corrected Experimental Maximum Tip Displacement (cm)	Percentage (%) of Deviation in the Results	Experimental Angular Deviation with the Fixed end (degree)
1	24	6.09	6.41	4.99%	5.01
2	04	8.48	7.42	12.5%	5.80
	01	10.6	9.12	13.9%	7.12

3.2.4. Dynamics and Stress Analysis of the Test-piece

In this section several dynamic features (the mode shapes, tip displacements and stress/strains) of the designed cantilever beam have been discussed. Firstly, Figure 19 presents the first four mode shapes of the developed CAM of the designed test-piece. The natural frequencies and the damping ratio of these vibration modes can be obtained through the sine sweep tests (Table 2). In Figure 20, the FRF results obtained from the sine sweep tests have been presented. These results (spectra), (a) input acceleration, (b) response acceleration, (c) coherence, (d) gain of the system, (e) cross spectrum, (f) inertance and (g) receptance has been plotted against the frequency. Receptance only describes the response of the system in terms of its displacement amplitudes under the unit excitation. Velocity and acceleration amplitude can also used as the FRFs which are known as the mobility and the inertance.

In Figure 20, the gain spectrum (Figure 20(d)) of the system, three distinguished peaks around 7 Hz, 59 Hz and 174 Hz have been observed. These peaks represent the three natural frequencies (bending modes) of the test-piece at the given frequency range (0-200 Hz). Furthermore, the coherence (Figure 20(c)) of the signal has been found significant (very close to unity) at the natural frequencies. In the inertance (Figure 20(d)) and receptance (Figure 20(d)) spectra the response of the second and third vibration mode have been insignificant which indicates the first mode of vibration is much more dominant than the other vibration modes.

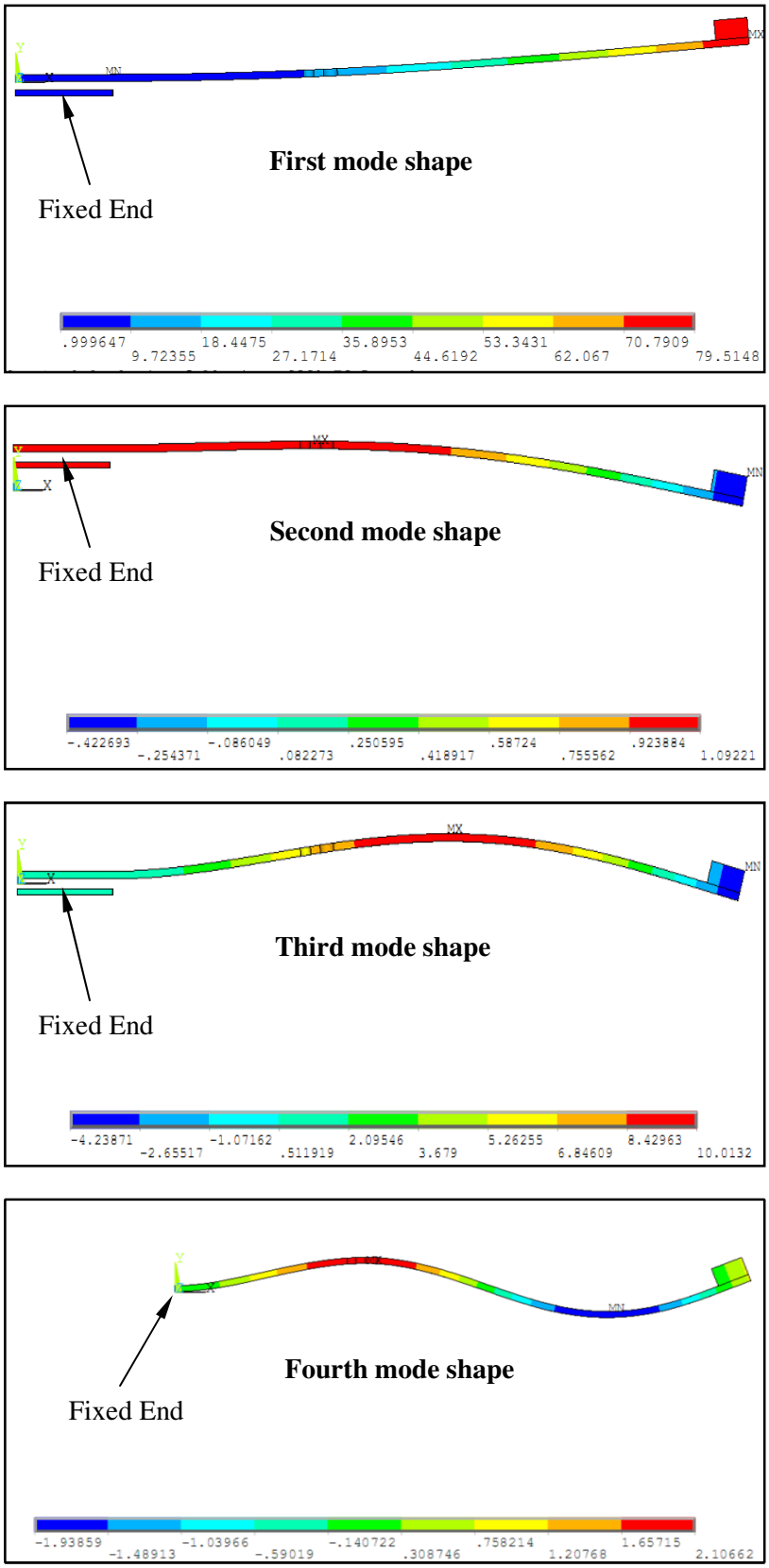

Figure 19: First Four Vibration Modes of the Specimen

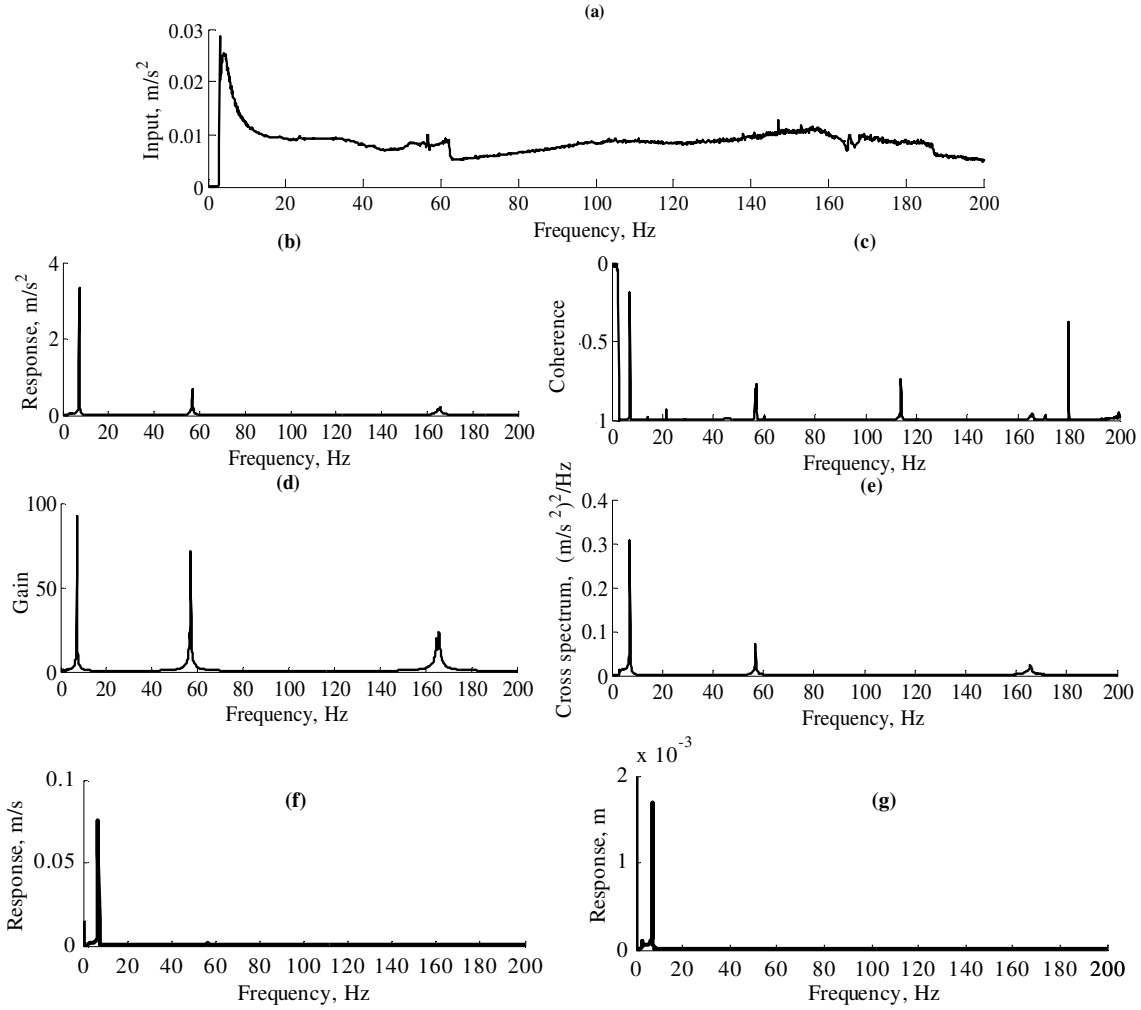

Figure 20: Experimental Sine Sweep FRF spectra

Figure 21 shows the maximum Von Mises strain distribution in the first four vibration modes of the test-piece. The locations of the maximum strain of the FE model in those vibration modes have been encircled in the following figure. In these contour plots, red and blue color represents the maximum and the minimum of the considered parameter, respectively. Hence the bar colors blue to red follow the increasing manner of the contoured parameter. Combining the information of Figure 19 and Figure 21, the possible location of maximum Von Mises stress in the durability tests can be determined. In this

problem, it has already been shown that the first mode is most dominant vibration mode in the bandwidth of 0-60 Hz. Thus for this mode the maximum strain developed at the location A which is the most possible maximum stress location in the durability tests in this frequency band.

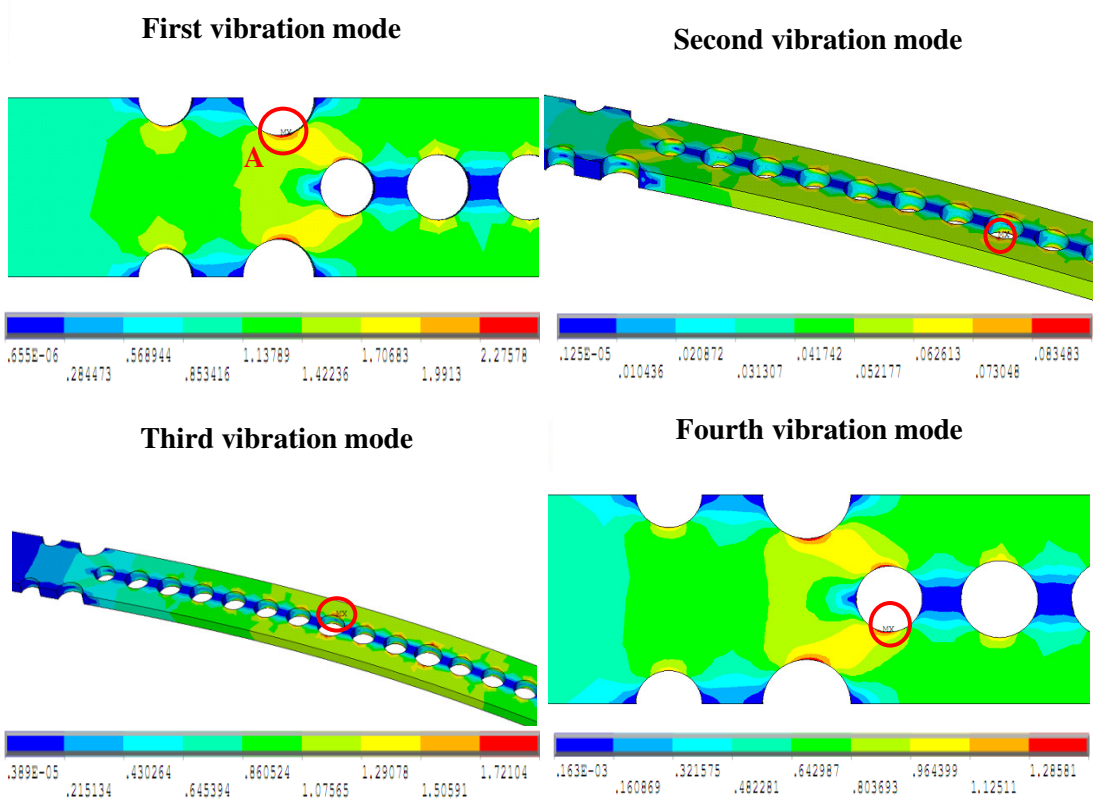

Figure 21: Von Mises Strains at First Four Natural Frequencies of the Specimen

Von Mises stress is one of the most popular stress invariant to perform the stress analysis for the ductile materials. A Von Mises stress contours over the CAM for the 2-hour AD loading profile has been presented in Figure 22. In this figure the location of maximum stress in the FE model is shown at the location A, which is consistent with the location presented in Figure 21. As the stress distributions are qualitatively similar for all AD loading profiles, only one of them has been presented.

As the geometry of the structure and the loading is symmetric about the plane of symmetry along the longitudinal axis (mid-plane), the stress distribution is also symmetric about the mid-plane. Hence, location A and location B or similar points (equally distant) to the mid-plane should be ideally symmetric regarding the stress distribution. So most likely the locations A and B are the two most vulnerable locations to fatigue failure as well.

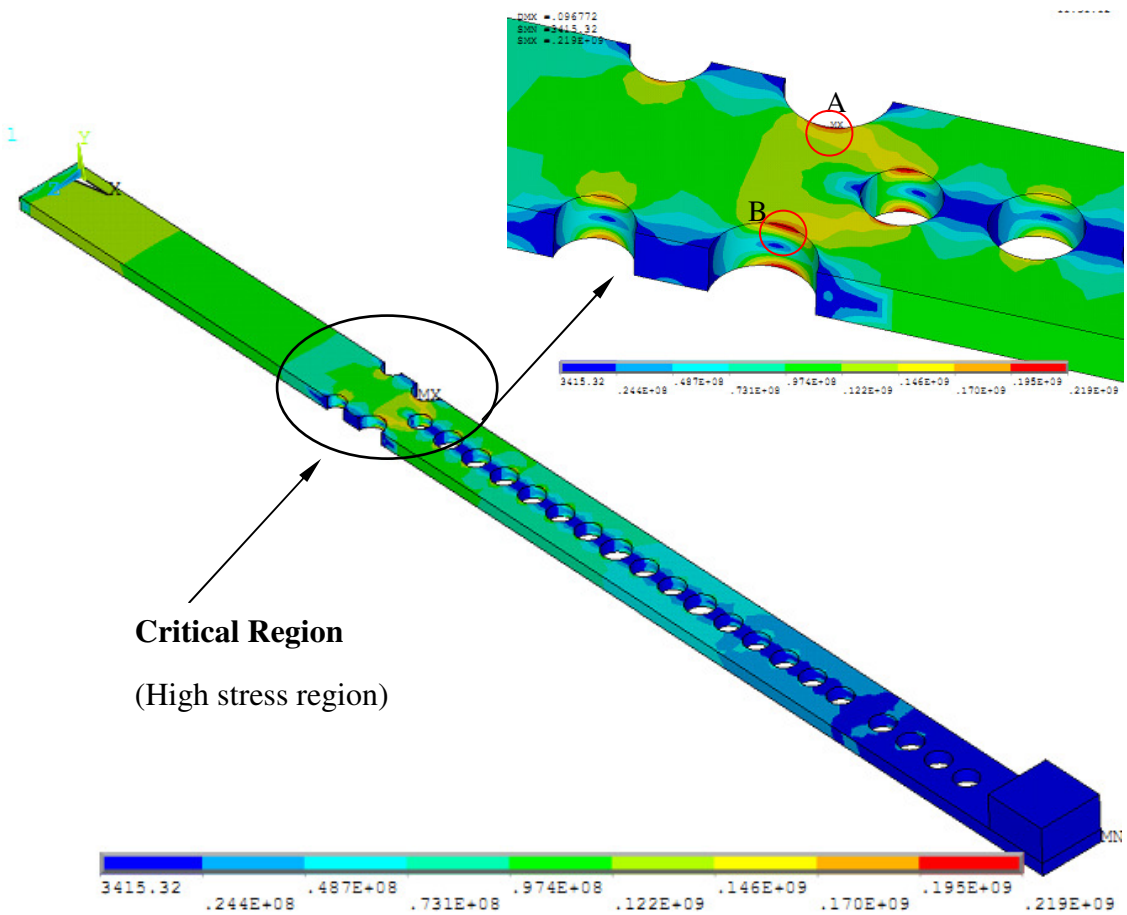

Figure 22: Von Mises Stress Distribution over the Model

Table 5 shows a comparison among the different stresses developed in the FE model of the test-piece. The AD loading profiles of 24, 20, 15, 8, 4 and 1-hour are applied to the

FE model (CAM) and the 1-sigma stresses, i.e., Von Mises, longitudinal, maximum principal and the maximum shear stress are determined.

Table 6: Comparisons of the RMS Stresses (1-Sigma) Over the CAM

Duration of the PSD (Hours)	Maximum Von Mises Stress (MPa)	Longitudinal Stress (MPa)	Maximum (First) Principal Stress (MPa)	Maximum Shear Stress (X-Z plane) (MPa)
24	41.0	41.2	41.2	15.0
20	48.7	48.7	48.9	17.7
15	51.1	51.1	51.3	18.6
8	56.7	56.7	56.9	20.7
4	63.7	63.6	63.9	23.2
1	80.2	80.2	80.5	29.3
Modified 01	142	142	142	51.8

Among them, based on their maximum values, the first three stresses are quantitatively equivalent, which implies that the bending stress is very dominant. The shear stress is the least dominated stress among the other four, which can overestimate the fatigue life of the structure if it is used as the stress invariant in the fatigue analysis. As the yield stress of the material of the test-piece is around 270MPa, there is a strong possibility of attaining the plasticity for the 'modified 01' hour loading as the 2-sigma and 3-sigma stress is much higher than the elastic limit of the material. The 'modified 01' hours loading is obtained by linear scaling of the RMS of the 1 hour loading with a factor of 1.67.

Figure 23 presents a detailed stress and strain distributions of the FE model (CAM) for the 4-hour PSD. From these distributions, the Von Mises (Figure 23(a)), maximum principal (Figure 23(c)) and the longitudinal (Figure 23(e)) stress have been found to be qualitatively equivalent.

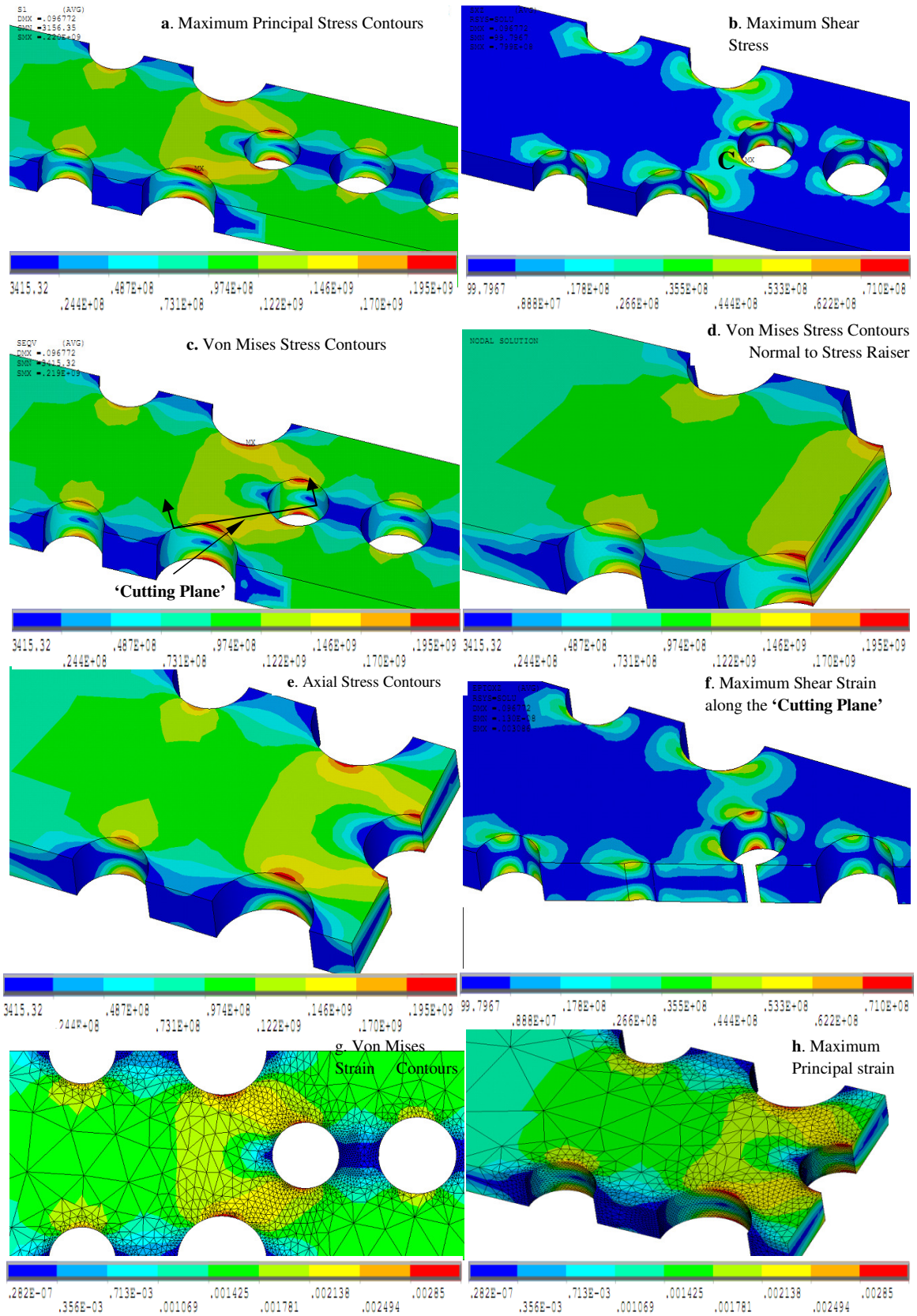

Figure 23: Stress/Strain Distributions for the 4 Hours PSD over the Critical Region

The maximum shear stress distribution has been found different than the other three above mentioned stress distributions. In maximum shear stress distribution, (Figure 23(b)) the maximum stress has been found in location C, which is different than the other three distributions. From the 'Cutting Plane' shown in Figure 23 (d, e and f) it has become prominent that the maximum stress is only locally found on the notch roots and its vicinity. The Von Mises and the maximum principal stress distributions (elemental) shown in Figure 23 (g and h) have been found as continuous which means that the well meshed zone is capable enough of convergence of the results around the discontinuity. In Figure 24, the peak of the stress PSD spectra at the first natural frequency has also found dominating for which is consistent with the strain distribution shown in Figure 21 and Figure 22. The peak of the stress PSD spectra at the second natural frequency has been found lower than that of the first one.

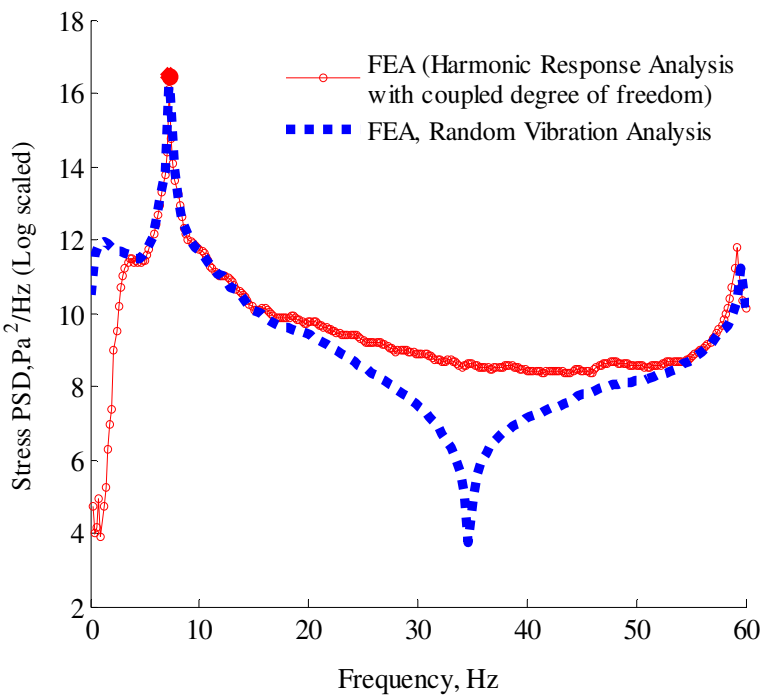

Figure 24: The Stress PSD Determined from the FEA

3.2.5. Stress Relation With Fatigue Life

The development of this relationship is a part of the iterative design technique. It relates the estimated fatigue life with the tress (the absolute maximum principal stress under unit excitation) which is related to the notch orientation, tip mass, geometry, material and the boundary conditions of the test piece. In this case, only the combinations among the five notch sizes and tip masses are used keeping the geometry, material and the boundary conditions fixed. As the stress distribution considered in this relationship is due to the unit base excitation, this stress is termed as the stress transfer function (Pa/m). To synthesize the best fit relation of the data (the stress transfer function vs. estimated fatigue life) presented in Figure 25, the exponential fit is used where the estimated fatigue lives are determined via FE based fatigue analysis. This relationship is presented in Eqn. (10)

$$S = K\,N^{-0.202} \tag{10}$$

where, *'S'* is the absolute maximum principal stress transfer function (Pa/m) ,*'N'* is the fatigue life in hours and '*K'*=5x10^{11} (SI unit). It has been determined from the above relation (Eqn. 10) that under the reference loading (the 24-hour loading), to obtain the desired fatigue life for the designed test-piece, the maximum absolute principal stress transfer function should be 2.61x10^{11}Pa/m. Afterwards, the test-piece has been designed via an iterative technique satisfying both the stress transfer function and the specific fatigue life.

In this iterative technique different combinations of notch orientations and tip masses have been considered. There were a total of 48 combinations considered (6 tip masses x 8 notch orientations) for this technique. For every combination the stress transfer function

and corresponding fatigue life has been determined for the 24 hours loading. The relation between the maximum principle stress transfer function for the different notch orientations and tip masses has been presented in Figure 26 and Figure 27 respectively. For the selected combinations from this set, Eqn. (10) has been developed. Using Eqn. (10), for the desired life the stress transfer function has been determined and for that value the combination of the tip masses and notch orientations has been obtained.

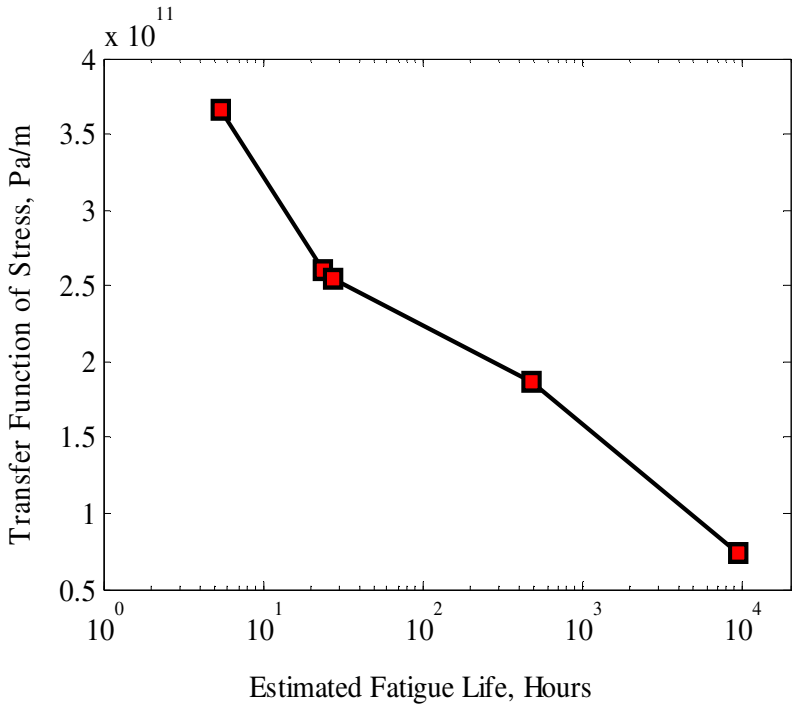

Figure 25: Relation between the Absolute Maximum Principal Stress and the Durability Life

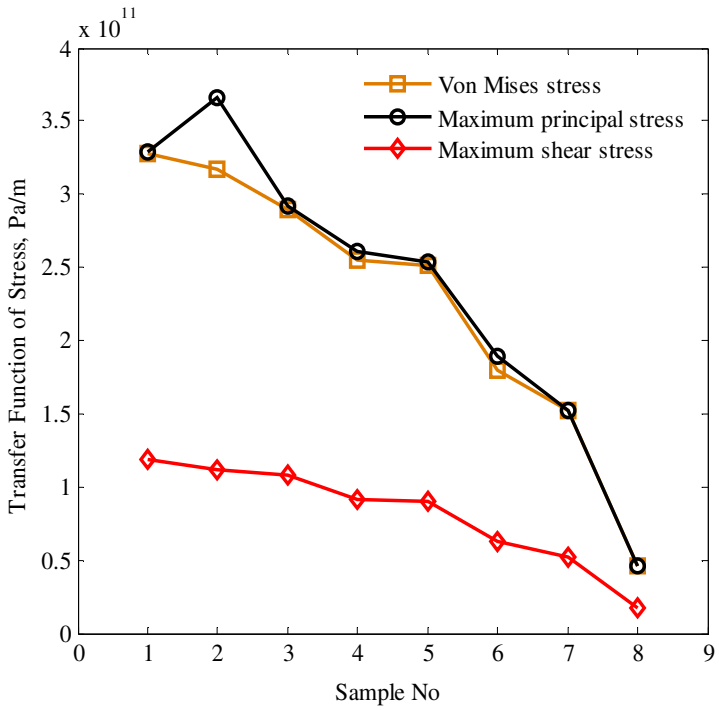

Figure 26: Effect of the Notch Orientations to the Different Stress Transfer Functions

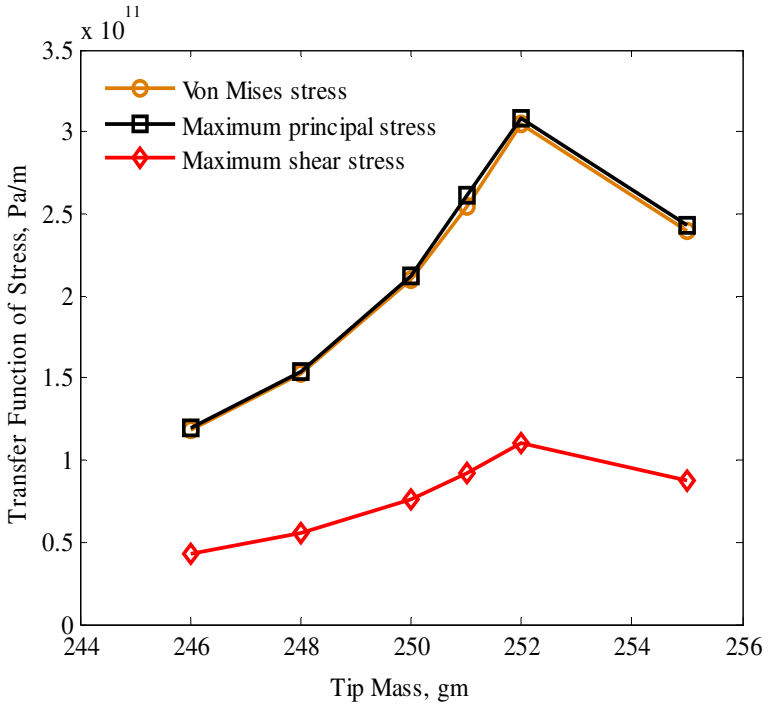

Figure 27: Effect of the End Masses to the Different Stress Transfer Functions

3.3. Verification of the AF of the Developed AD Tests

The validation of the 'modified test tailoring approach' has been discussed in this part. Both numerical and experimental method has been applied to perform this validation.

3.3.1. Numerical Fatigue test and Validation

In this section, the synthesized AD loading profiles have been validated via numerical fatigue tests. The test-piece has been designed to have a fatigue life of 24 hours under the reference 24 hours accelerated PSD and its FLR should be the same as the AF for other accelerated loading profile. Table 6 shows the comparison of the expected and estimated fatigue lives of the designed specimen for all of the synthesized AD loading profiles. In this table, the numerical fatigue test results for the loading profiles, having an AF up to 330 as compared to the field tests have been presented with an average deviation of 4.3% between the determined and expected fatigue life of the test-piece. From the same table, the minimum and maximum deviation has been found as 0.84% for the 24 hours and 12.3% for the 6 hours loading profile respectively. The low errors between the expected and estimated fatigue lives shown in Table 6 indicate the generated AD loading profiles are effective in accelerating the durability tests with the desired AF.

Figure 28 shows the fatigue life distribution over the CAM based on the FE results. It has been found that the fatigue life distribution is consistent with the stress distributions. The minimum fatigue life has been found in point B, which is the second semi-circular notch root from the fixed end.

Moreover, in Figure 29, the fatigue life distribution over the CAM has been presented for various accelerated PSDs. It has been observed in Figure 29 that the fatigue life distributions are similar for all of the accelerated PSD. Importantly, this location has been

found the same for all the applied AD loading profiles. Therefore, location A and B (due to symmetry) are the most probable crack initiation locations in the model.

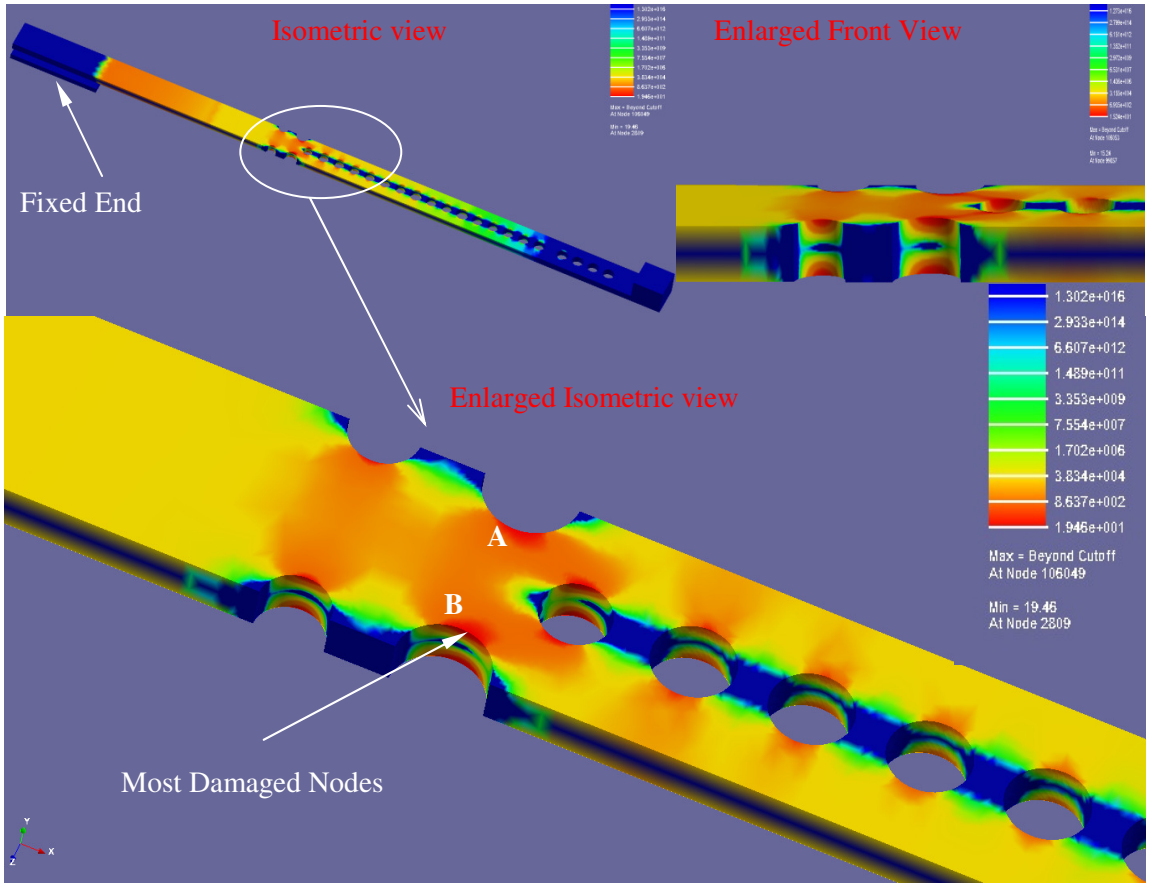

Figure 28: Fatigue Life Distributions over the CAM for 20 Hours PSD

Table 7: Verification of the Synthesized AD Tests (b=6)

Parameters of AD Loading Profiles	AD Validation Method	Expected Fatigue Life of the Specimen	Fatigue Life Determined Through FE based Fatigue Model	Absolute Percentage (%) of Deviation
b=6 & TD=24hours	SRS & FDS	24 hours	23.80 hours	0.84%
b=6 & TD=20hours	SRS & FDS	20 hours	19.46 hours	2.77%
b=6 & TD=15hours	SRS & FDS	15 hours	15.24 hours	1.60%
b=6 & TD=10hours	SRS & FDS	10 hours	9.420 hours	5.80%
b=6 & TD=6 hours	SRS & FDS	6 hours	6.740 hours	12.3%

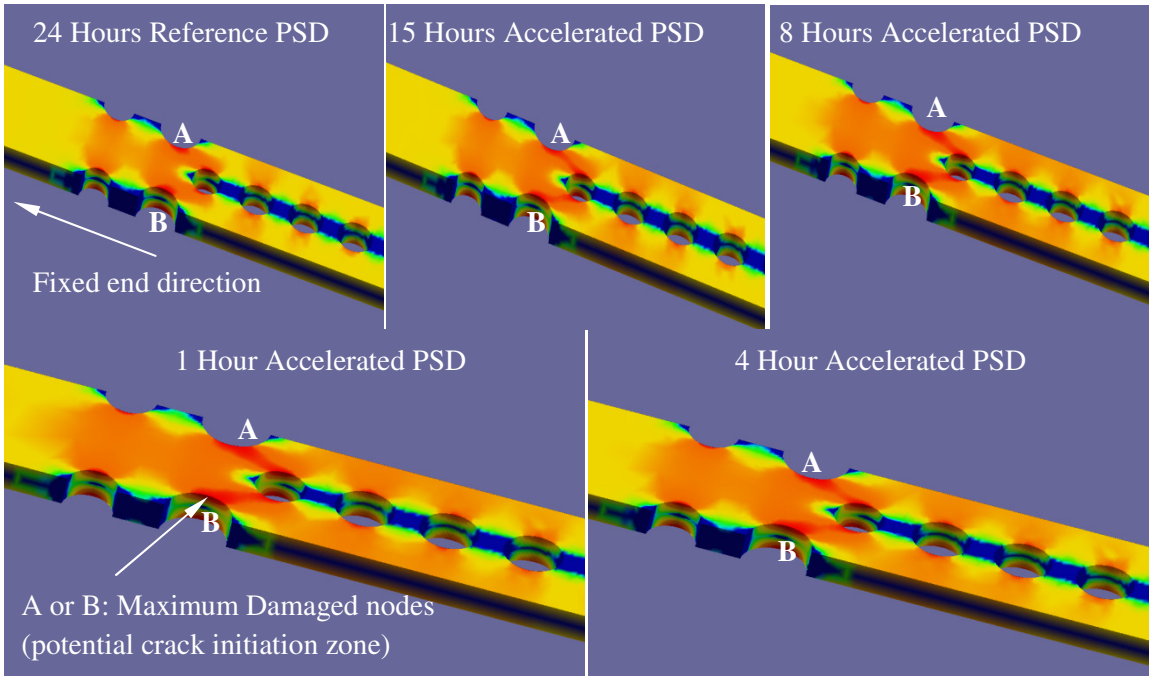

Figure 29: Fatigue Life Distributions over the CAM for Different Accelerated PSD

3.3.2. Experimental Durability Tests and Fractography

Experimental fatigue tests have also been performed on four of the newly fabricated test-pieces (test-set 2) under a selected loading profile (modified 1 hour PSD) to compare the failure phenomenon (the crack initiation location and the failure mechanism) between the numerical and experimental fatigue tests. In Figure 30 the durability results for the designed test-piece have been presented. In Figure 30(a) one of the fracture surfaces of the failed beams has been presented. The beach marks on the surface indicate the presence of the fatigue failure. In Figure 30(b) it has been demonstrated that the cracks have been initiated from the predicted notch roots (Location A or B in Figure 28). The crack has propagated through the width of the test-piece from both sides toward the final rapture shown in Figure 30 (c).

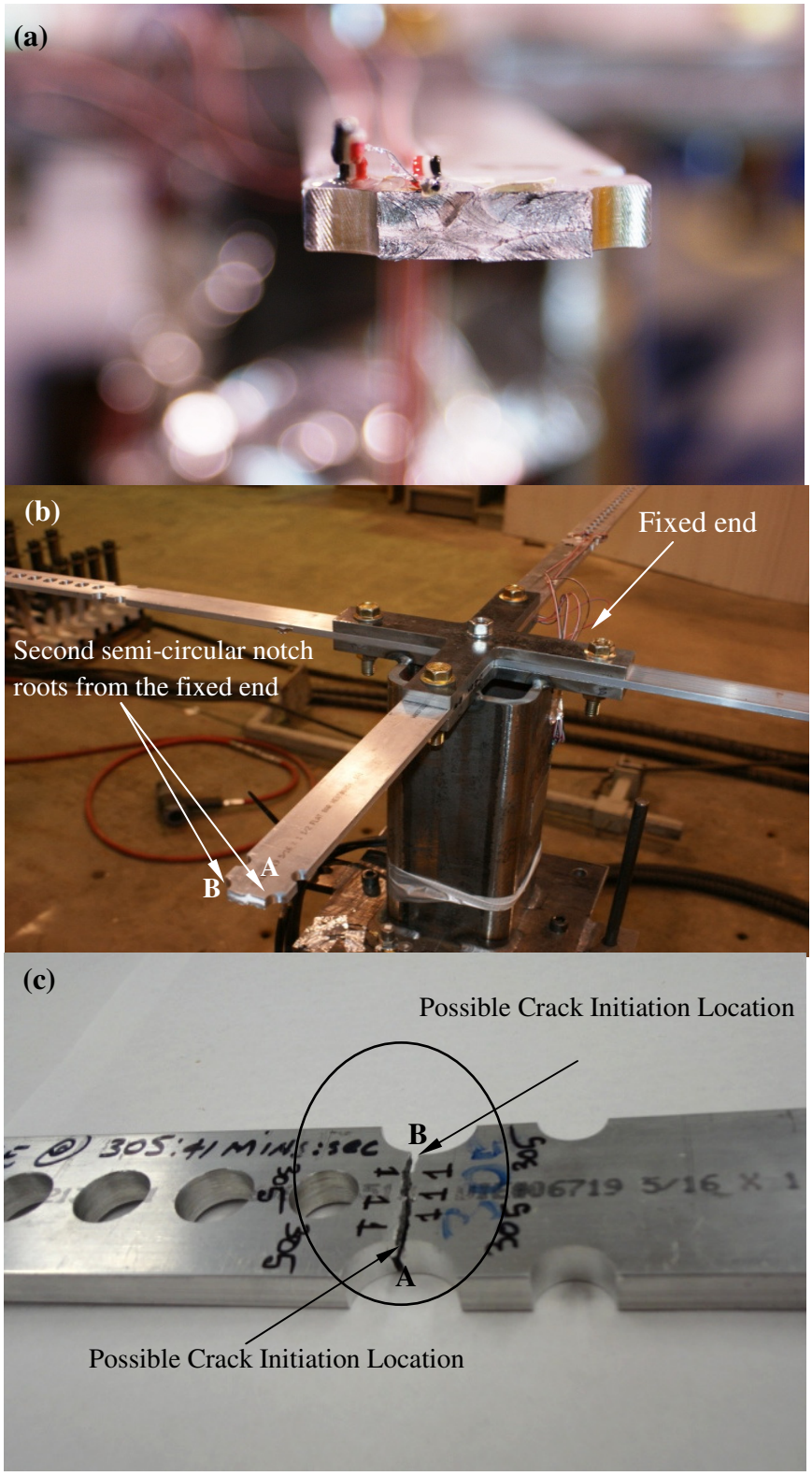

Figure 30: Failure of the Designed Test-Piece (Experimental)

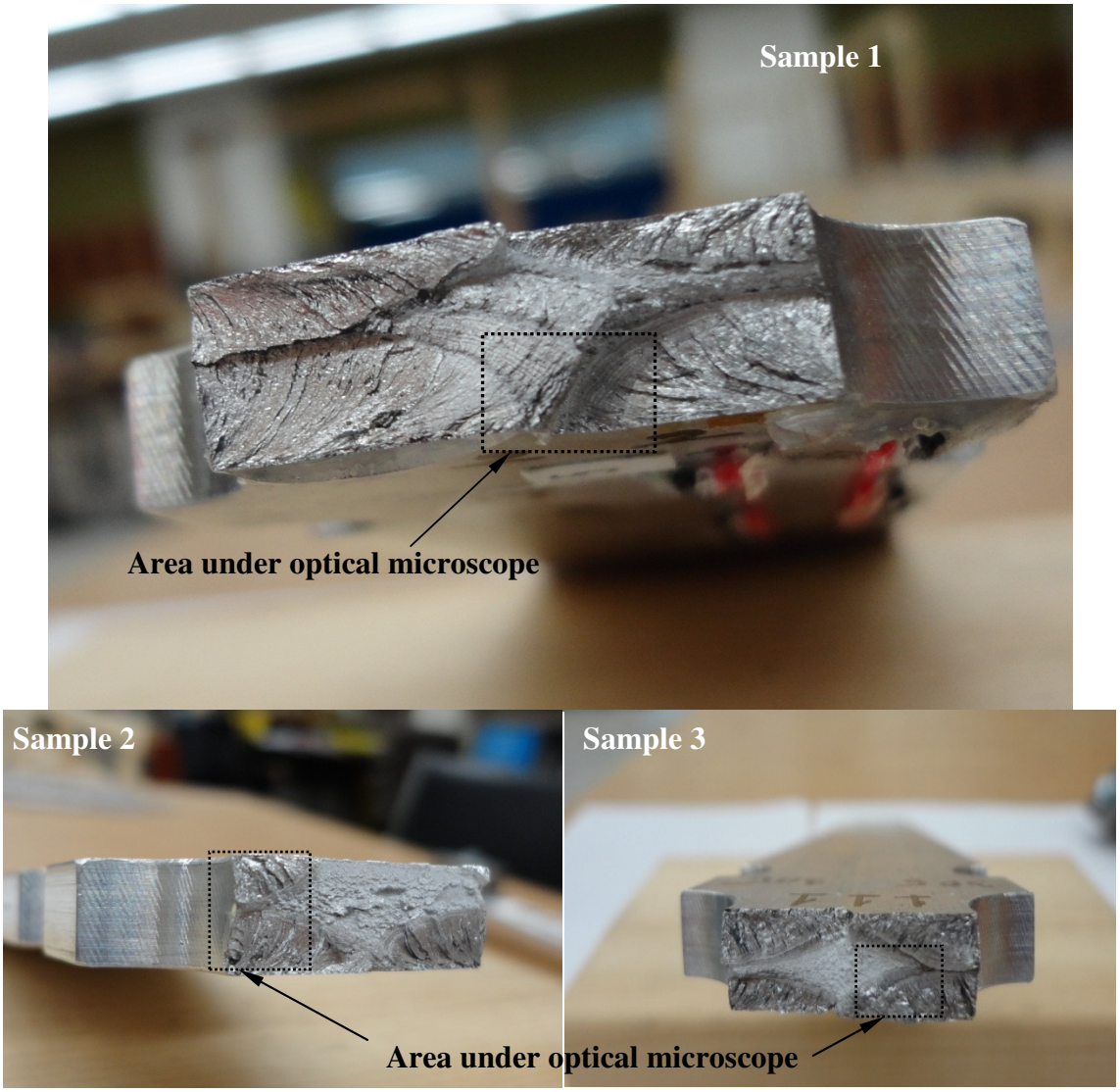

Figure 31(a): Fracture Surfaces of the Failed Test-Pieces

Fractographic examination has also been carried out to confirm the failure mechanism in all of the fracture surfaces. These fracture surfaces (Sample 1, Sample 2 and Sample 3) shown in Figure 31(a) have been examined under the optical electron microscope. Optical microscope images of the fracture surfaces have been presented in the Figure 31(b) to show the features on the surfaces failed by fatigue testing. The beach marks in every failure surface confirm the presence of fatigue as a consistent failure mechanism in

this case. The shiny surface of those figures refers to the region of stable crack growth and the dull surface refers to the unstable crack growth towards final rupture.

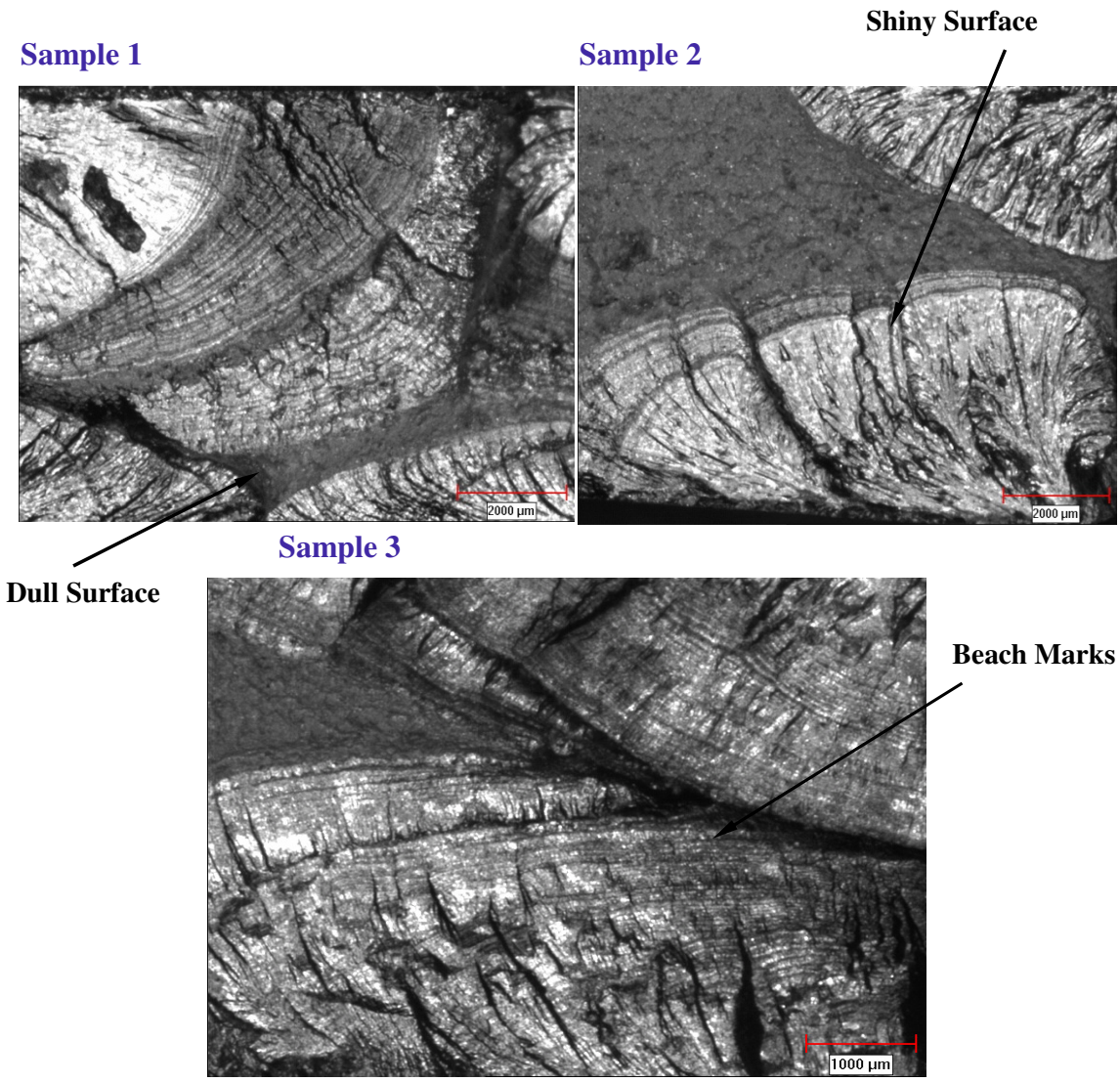

Figure 31(b): Fracture Surfaces of the Failed Test-Pieces under the Optical Microscope

The cracks normal to the beach marks leading towards the notch roots (sample 2) indicate these cracks initiate from the notch roots. Thus the failure mechanism (crack initiation location and the failure type) has been verified by the experimental durability test and fractography.

3.3.3. Effect of Plasticity and S-N Curve Slope in Durability Life

After the numerical durability analysis the experimental durability test has been performed on the newly fabricated beam set 2. The partial test loading profile corresponding to the 1-hour PSD has been used to carry out this test. However, the test was not successful (failure time did not mach) due to the inaccuracy of the manufacturing of the beam. Hence the 1-hour loading profile (Modified 1 hour loading profile) has been modified to obtain desired dynamic response (natural frequencies, stresses and mode shapes) in the preliminary tests.

To verify claimed inaccuracy of manufacturing, a sine sweep test with amplitude of 0.2 g (peak-peak) in a frequency bandwidth of 3-65 Hz and 5-minute trial durability tests with the 20-hour, 4-hour and 1-hour loading have been performed. The results from these discussed tests have been compared with those from numerical analysis. In Table 7, the natural frequency and the damping ratio have been compared between two test-sets of the fabricated beams.

Table 8: Natural Frequencies and Damping Ratios for the First Two Bending Vibration Modes for the Different Specimens

Test sets	Natural Frequency of the 1st Mode (Hz)	Damping Ratio of the 1st Mode (%)	Natural Frequency of the 3rd Mode (Hz)	Damping Ratio of the 3rd Mode (%)	Gain Ratio of the 1st and 3rd Mode
1	7.114	0.2054	56.91	0.6857	3.190
2	6.856	0.3794	59.60	0.5546	3.120
Deviation	3.634%	84.76%	4.728%	19.11%	2.190

It is found that for the second set of beams the deviation from the expected value in the natural frequency and damping ratio are 3.634% and 84.74% respectively. For the second mode the deviation of these parameters has found as 19.11% and 2.190%. This deviation of the damping ratio and the natural frequencies have significantly affected to the strain distribution in the newly fabricated test-piece as well.

In Table 8, the experimental strain RMS from the location R_1, A_1 and A_2 shown in Figure 16(a) have been compared with that of the FEA. The experimental strains have been collected from the 5-minute trial durability test with the 20-hour, 4-hour and 1-hour loading profiles. With this set of beams (set 2) the average deviation found for location R_1 as 12.68%, A_1 as 13.01% and A_2 as 13.09% for different loading profiles which is much higher than the previous set of beams.

Table 9: Comparison of Strains between the FE and the Experiment for Beam Set 2

Loading Profiles	Beam Set-Strain Gauges or Rosettes	Area Averaged FE Strains ($\mu\varepsilon$) RMS (1-Sigma)	Experimental Strains($\mu\varepsilon$) RMS	Absolute Deviation in Strains (%)
20 hours PSD	2-A_1	492.8	580.9	17.88
	2-A_2	473.0	575.3	21.56
	2-R_1	512.5	617.9	20.50
04 hours PSD	2-A_1	643.8	630.8	2.014
	2-A_2	618.0	624.6	1.061
	2-R_1	669.5	670.9	0.217
Modified 01 hours PSD	2-A_1	809.0	654.0	19.15
	2-A_2	777.0	647.7	16.64
	2-R_1	841.5	695.4	17.33

Thus the new fabricated beam is not supposed to fail within the prescribed time for which it has been designed. Hence, the existing loading needs to be modified according to the

new test-piece. The average experimental durability life of the newly designed cantilever beams (test set-2) which have been subjected to the modified 1-hour durability test has been as 11.77 hours.

From Table 9, it has been found that the experimental fatigue life for the specimen is 11.77 hours which has been predicted as 0.706 hours for the modified 1 hour loading using the standard S-N analysis. The possible reasons behind this deviation can be (1) the involvement of plasticity, (2) inaccurate estimation of the slope of the S-N curve, b, in the 'test synthesis' process. Hence, the effect of these two probable causes has been investigated.

In the experiment, the strains have been found exceeding the elastic limit ($\sim 3855\mu\varepsilon$), where the stress-strain relation is nonlinear which can underestimate the fatigue life. The Von Mises, absolute maximum principal and maximum shear strain histories from location R_1 and the sample bending strain histories from the location A_1 and A_2 have been shown in Figure 32. From these strain histories, it has been observed that the developed strains in these locations are exceeding the elastic limit of the considered material. Therefore numerical strain life analyses using the experimental strains have been used to accommodate the plasticity in the fatigue analysis and the fatigue life was determined as 13.12 hours.

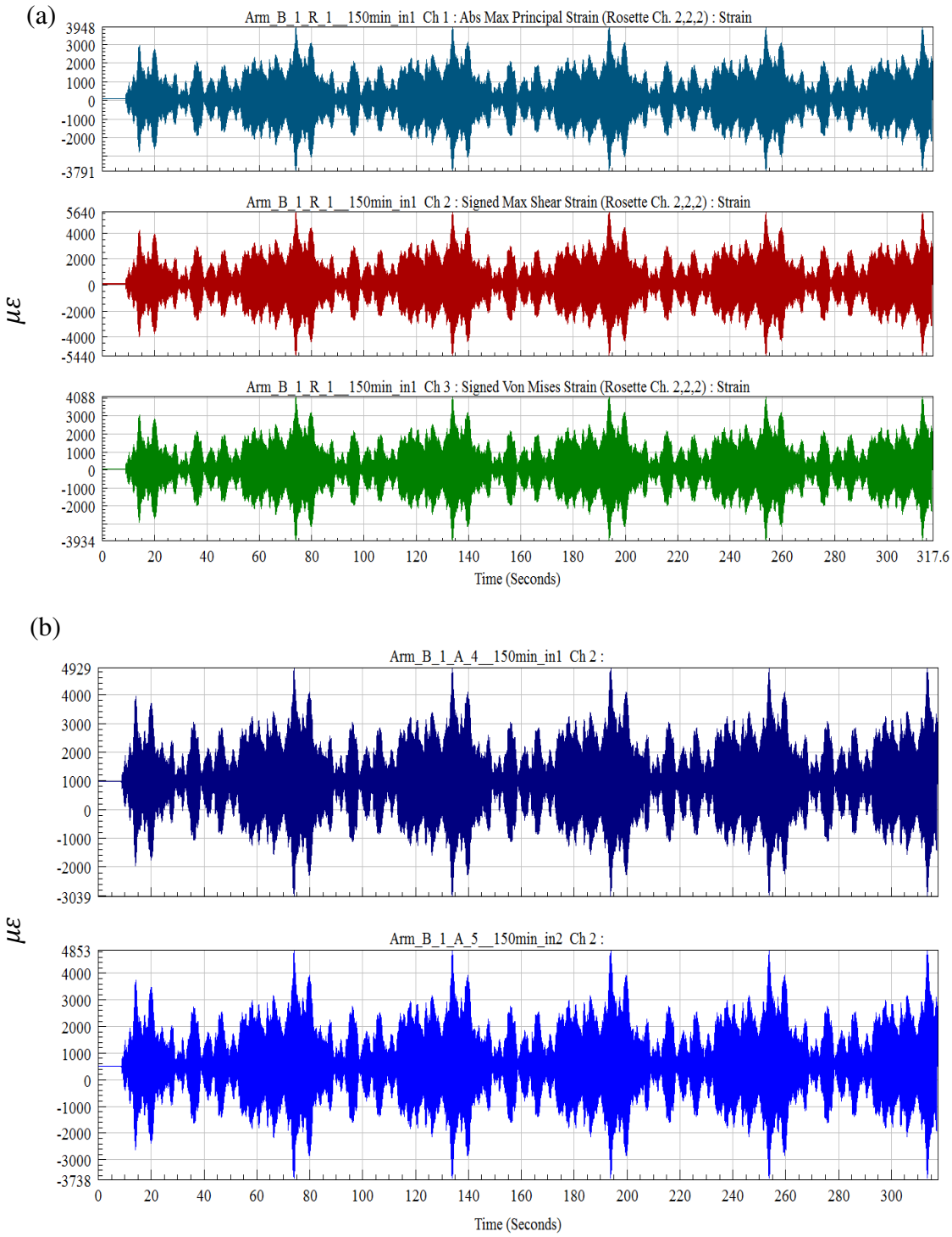

Figure 32: The Strain History of an Overly Compressed Durability Loading Profile

Moreover, in the 'test synthesis' process, the S-N curve slope, *b*, has been taken as 6. This value is suggested in the previous work [43] which may be inadequate for this

specific material. Hence in this section the effect of the S-N curve slope has been explored. To observe the effect of changing this parameter, *b*=5.5 [29] has been used with the results shown in Table 10.

Table 10: Verification of the Synthesized AD Tests (*b*=5.5)

Parameters of AD Loading Profiles	AD Validation Method	Expected Fatigue Life of the Specimen	Fatigue Life Determined Through FE based Fatigue Model	Absolute Percentage (%) of Deviation
b=5.5 & TD=24 hours	SRS & FDS	106.0 hours	106.0	Reference
b=5.5 & TD=20 hours	SRS & FDS	88.33 hours	87.79	0.6113%
b=5.5 & TD=15 hours	SRS & FDS	66.25 hours	72.32	8.3930%
b=5.5 & TD=12 hours	SRS & FDS	53.00 hours	54.53	2.8870%
b=5.5 & TD=10 hours	SRS & FDS	44.16 hours	46.43	4.4610%
b=5.5 & TD=08 hours	SRS & FDS	35.33 hours	35.85	1.4720%
b=5.5 & TD=6 hours	SRS & FDS	26.50 hours	27.02	1.9620%
b=5.5 & TD=4 hours	SRS & FDS	17.66 hours	15.43	12.620%
b=5.5 & TD=2 hours	SRS & FDS	8.833 hours	7.179	13.510%

It has been found from Table 10 that with the same AF, the expected and estimated fatigue lives increase significantly as *b* decreases from 6 to 5.5. As discussed in the Section 2.1, a lower value of b results in a lower magnitude of the generated PSD, which allows a longer fatigue life, i.e., the inverse Basquin's exponent *b* has a significant effect on the generated durability testing loading profiles. Therefore using an improper S-N curve exponent can be one of the causes for the discrepancy between the numerical and experimental fatigue lives. As for generating a better AD testing profile, the effect of b has been found crucial; so the material specific S-N curve can be used.

In contrary, Figure 33 has been plotted using the data set of Table 10 to show how the estimated fatigue life deviates from the expected fatigue life for different time compression ratios. The time compression (TC) ratio here is referred to the AF. The standard deviation of the results found for different AF plotted in Figure 34 provides a simple statistical evaluation of the estimated fatigue lives for b=5.5. So it is prominent that the durability loading profiles are very effective for b=5.5 as well.

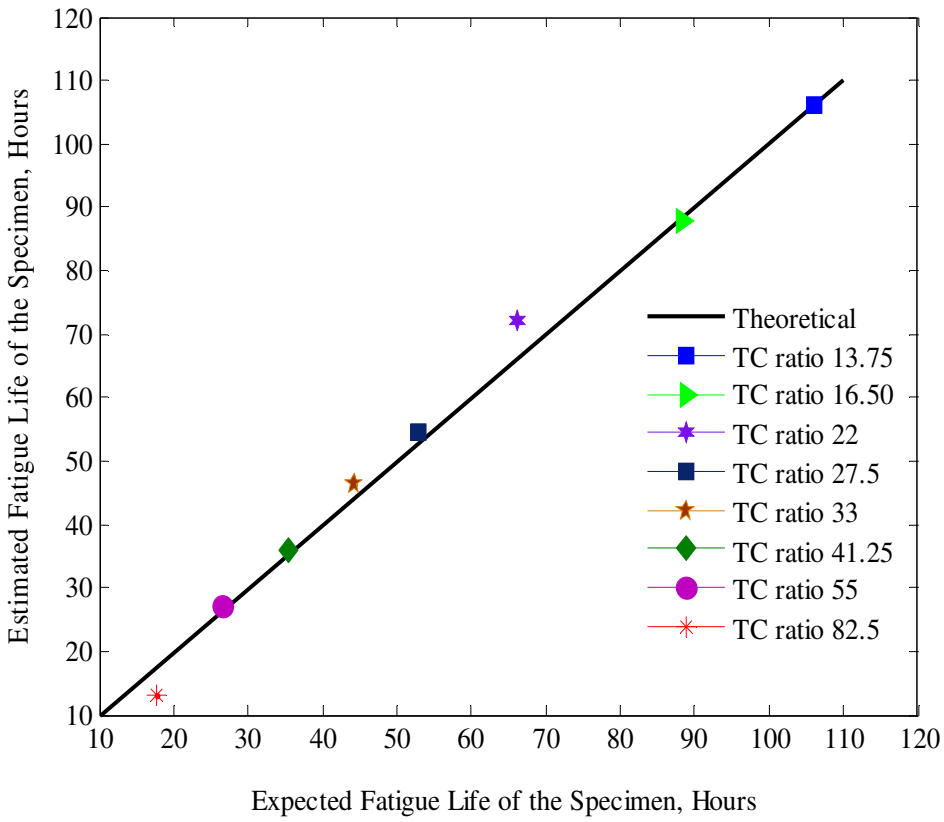

Figure 33: Comparison of the TC Ratio of Different AD Profiles With the Theoretical One

Although the fatigue life increases with the decrease in b, the AF of the generated loading profiles remains the same as the FLR, which indicates the 'modified test tailoring approach' is equally efficient in different S-N curve exponent. Hence, the effectiveness

of the AD profiles of different AF synthesized via 'modified test tailoring approach' has been validated using a newly designed test-piece.

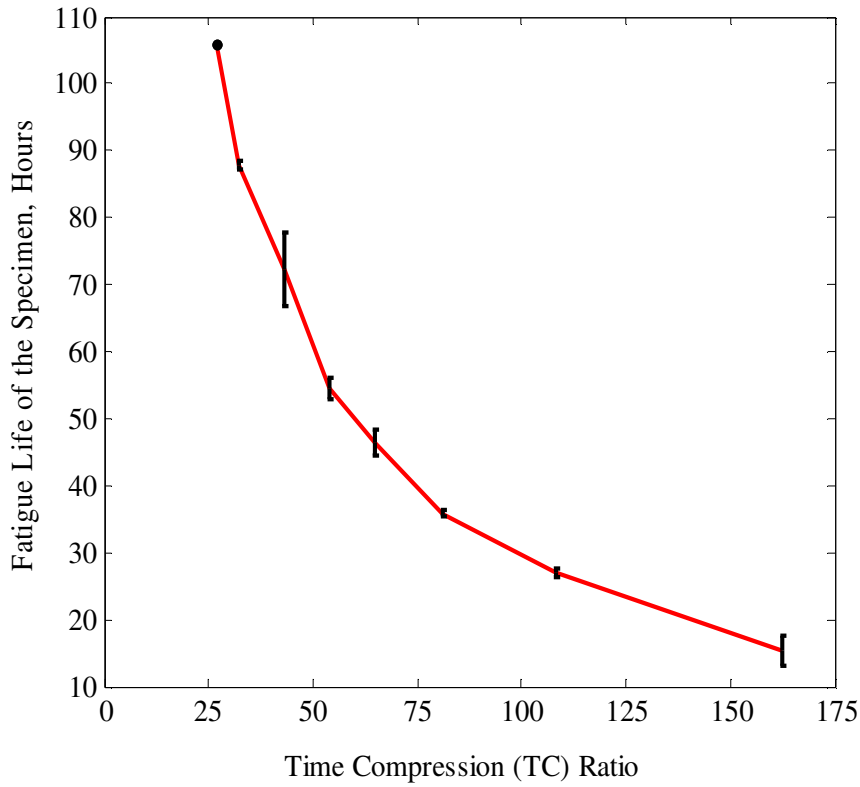

Figure 34: Deviation in the Determined Fatigue Life for Different TC Ratios

The following issues should also be considered into the 'modified test tailoring approach':

(1) The 'test tailoring approach' is based on linear SDOF system which is limited to the elastic limit for the material.

(2) If the generic *b* is used to synthesis the AD loading profiles, it is necessary to check the developed stress level (plastic/elastic) in the test-piece for the synthesized AD loads.

(3) To account the plasticity in the fatigue analysis the strain life method should be adopted to predict the structural life with over-compressed AD loading profile.

An over -compressed loading profile has an ERS higher than the SRS of the field test and has the FDS same as the FDS of the same as the field test. Though generation of this kind of loading profile is not encouraged in the ‘test tailoring approach’, strain life analysis can be used as a remedy.

Chapter 4

Conclusions and Future Works

A computer-aided AD test has been performed to validate the 'modified test tailoring approach' of generating highly AD loading profiles for ground vehicle components. This approach has been previously proposed in [43]-[44] due to the limitations of testing implementation and the requirement of high AF in the durability tests of heavy ground vehicle components. In the modified approach, the full period of accelerated PSD can be represented by an equivalent 60s time series multiples, keeping the same amount of damage. This new modified approach needs to be validated. Hence in this work, the 330-hour field test has been accelerated up to a 1-hour durability test using the modified approach and the corresponding fatigue analysis has been performed on a newly designed test-piece to verify those AD loading profiles, hence the 'partial test approach'.

In this work, the test-piece has been designed via a conjugative approach involving FEA and fatigue analysis for a specific 24 hours of durability life. To justify the design, it has been satisfactorily tested against the experiment. Good agreements have been found between the numerical results from the CAM and the experimental result of the test-piece. Hence the developed CAM properly represents the physical system used in the experiment.

Numerical fatigue tests have been performed on the verified CAM using the generated AD loading profiles and a sound agreement has also been found on the estimated and the expected fatigue lives. The effectiveness of the synthesized AD loading profiles has also been observed almost insensitive to the S-N curve; hence the modified approach can be used for a wide range of materials. From the simulation results, the estimated crack initiation locations are the same for different AD loading profiles. In addition, these initiation locations have been found identical in the experiment and the simulations. Moreover, fractography shows the beach marks on the failure surfaces which indicate the presence of fatigue failure of the specimen. Although in this study the experimental and the numerical fatigue lives have not matched for the designed test-piece, the failure mechanism has been found to be consistent between the experimental and numerical analyses. The probable reasons behind the discrepancy in the fatigue lives under 1-hour loading profile has been investigated and outlined in the previous Section 3.3. Thus, the AD profiles synthesized based on the modified approach have also successfully passed the computer-aided fatigue tests.

The modified approach is very promising to produce the driving files for the test rig to perform highly AD tests of the ground vehicle components. As future work, aaccelerated labs tests can be performed with the generated durability loading profiles validate the durability life of the test-piece. Furthermore, the use of the 'Transmission Electron Microscopy' to examine the effect of local plasticity can be a very good addition to the current work. Importantly, caution should also be taken to the fact that the modified approach is valid up to the elastic limit of the material when accelerating the field test with high an AF.

References

[1]. Pennsylvania Transportation Institute – Vehicle System and Safety Group. (2007, Nov. "Bus Research and Testing Facility ("Test Track") [Online] Available: http://www.vss.psu.edu/BTRC/btrc_test_track_htm.

[2]. Xu Ke, Development of Vibration Loading Profiles for Accelerated Durability Tests of Ground Vehicles, MSc thesis, University of Manitoba, (2011).

[3]. K. Dressler, M. Speckert, and G. Bitsch. "Virtual durability test rigs for automotive engineering", Vehicle System Dynamics. vol. 47 (4) April 2009, 387-401.

[4]. Steve S., "An introduction to Mutli-Axes Simulation Tables (MAST)", Slides from WESTEST, 2010.

[5]. Nelson, W., 1990, Accelerated Testing, Statistical Models, Test Plans and Data Analyses, John Wiley & Sons, New York.

[6]. Caruso H and Dasgupta A.," A Fundamental Overview of Accelerated Testing Analytical Models", Reliability and Maintainability Symposium (RAMS) Proceedings, IEEE, 1998, pp. 389 – 393.

[7]. Meeker, W.Q. & Escobar, L.A. (1993). A Review of Recent Research and Current Issues in Accelerated Testing, International Statistical Review 61, 1, pp. 147-168.

[8]. Ashmore C., Piersol A. G., Witte J. J., 1992, "Accelerated Service Life Testing of Automotive Vehicles in a Test Course", Vehicle Systems Dynamics , Vol. 21, pp.89–108.

[9]. Abdullah S, Nizwan C K E, Nauwi M Z, 2009, A Study of Fatigue Data Editing Using the Short-Time Fourier Transform (STFT), American Journal of Applied Science 6(4): 565-575.

[10]. Kadhim N A, Abdullah S, Ariffin A K. Effect of the fatigue data editing technique associated with finite element analysis on the component fatigue design period. Materials and Design, 2011: 32 1020-1030.

[11]. Stephens et. al., Fatigue Damage editing for accelerated durability testing using strain range and SWT parameter criteria, Int. J. of Fatigue Vol. 19, Nos 8-9, pp. 599606, 1997.

[12]. Yay, K., Ereke, I. M., Bilir, M., Cataltepe, V. , 2009, Fatigue strength of an urban type midi bus vehicle chassis by using FEM analysis and accelerated fatigue life test, Society of Automotive Engineers World Congress, ISSN 0148-7191, Detroit, USA.

[13]. Ziong J.J., Shenoi R.A., A load history generation approach for full-scale accelerated fatigue tests, Engineering Fracture Mechanics 75 (2008) 3226–3243.

[14]. Lin, K-Y, Hwang, J-W and Chang, J-M, Accelerated durability assessment of motor cycle components in real life simulation testing, Proc. IMechE Vol. 224 Part D: J. Automobile Engineering, 2009.

[15]. Abdullah, S, Giacomin, J A, and Yates, J R, A mission synthesis algorithm for fatigue damage analysis, Proc. IMechE Vol. 218 Part D: J. Automobile Engineering, 2004.

[16]. Chinnaraj K , Sathya P M, Lakshmana R C. Dynamic Response Analysis of a Heavy Commercial Vehicle Subjected to Extreme Road Operating Conditions. Journal of Physics: Conference Series 181 (2009) 012070, doi:10.1088/1742-6596/181/1/012070.

[17]. Haiba M., Barton D.C., Brooks P.C. and Levesley M.C., Review of life assessment techniques applied to dynamically loaded automotive components, Computers and Structures 80 (2002) 481–494.

[18]. N.W.M. Bishop, The use of frequency domain parameters to predict structural fatigue, PhD thesis, Warwick University, (1988).

[19]. Jhung D.H. and Bae S.I., Automotive Component Fatigue Life Estimation by Frequency Domain Approach, Key Engineering Materials, Vols. 297-300 (2005), pp. 1776-1786.

[20]. N.W.M.Bishop, Vibration Fatigue Analysis in the Finite Element Environment, XVI ENCUENTRO DEL GRUPO ESPAÑOL DE FRACTURA, (1999).

[21]. Halfpenny A., A Frequency Domain Approach for Fatigue Life Estimation from Finite Element Analysis, Key Engineering Materials, Vols. 167-168 (1999), pp. 401-410.

[22]. A. Al-Yafawi, S. Patil, D. Yu, S. Park, J. Pitarresi, Random Vibration Test for Electronic Assemblies Fatigue Life Estimation, Thermal and Thermomechanical Phenomena in Electronic System (ITherm), IEEE, 2010, pp. 1-7.

[23]. S. Patil, D. Yu, S. Park, S. Chung, Finite Element Based Fatigue Life Prediction for Electronic Components under Random Vibration Loading, Electronic Components and Technology Conference (ECTC), IEEE, 2010, pp. 188-193.

[24]. Ma C.H., Study of Acoustic Fatigue Life Estimation for Composite Structure Based on Power Spectral Density, Materials Research Innovations, Vols. 15 (2011), pp. 118-121.

[25]. Li R. S., 2001, ‘‘A Methodology for Fatigue Prediction of Electronic Components under Random Vibration Load,’’ ASME J. Electron. Packag. 123(4), Dec., pp. 394–400.

[26]. Hyun D.H., Automotive Component Fatigue Life Estimation by Frequency Domain Approach, Key Engineering Materials, Vols. 297-300(2005), pp. 1776-1783.

[27]. Moon S-I, Chao I-J and Youn D, Fatigue Life Evaluation of Mechanical Components Using Vibration Fatigue Analysis Technique, Journal of Mechanical Science and Technology 25 (3) (2011) 631-637.

[28]. C-J. Kin, Y. J. Kang, B-H. Lee, Experimental spectral damage prediction of a linear elastic system using acceleration response, Mechanical Systems and Signal Processing 25 (2011) 2538–2548.

[29]. Pothula A, Gupta A and Kathawate Guru R (2011) Fatigue failure in random vibration and accelerated testing, Journal of vibration and control 0(0), 1-8.

[30]. Pace, L., Jayat, F., Konieczny, R., Forster, M. et al., "Accelerated Durability Test for Metallic Substrates Tailored for Motorcycle Application," SAE Technical Paper 2011-32-0512, 2011, doi:10.4271/2011-32-0512.

[31]. Wala MKBG and Gupta, A, “Accelerated testing and Damping”, Proceedings of International Modal Analysis Conference XXVII: Conference & Exposition on Structural Dynamics, 2009.

[32]. Nagulapalli VK, Gupta, A, and Fan S. "Estimation of Fatigue Life of Aluminum Beams subjected to Random Vibration", Proceedings of International Modal Analysis Conference XXV, 2007.

[33]. J. Pulido, Practical Reliability of Structure under Road Loading, Reliability and Maintainability Symposium (RAMS) Proceedings, IEEE, 2011, pp. 1-7.

[34]. Allegri G, Zhang X., On the inverse power laws for accelerated random fatigue testing, International Journal of Fatigue, 30 (2008): 967-977.

[35]. Sun FQ, Li XY, Zhang ZR and Jiang TM, 2010, Step-stress Accelerated Random Vibration Life Testing, Advanced Material Research, Vol. 118-120, pp.606–610.

[36]. Lee Y-L, Polehna D and Kang H-T, 2010, "Fatigue Damage Severity Calculation for Vibration Test", Journal of Testing and Evaluation, Vol. 38(6), pp.1–10.

[37]. Halfpenny A. (2006). Mission Profiling and Test Synthesis based on fatigue damage spectrum. Ref. FT342, 9th Int. Fatigue Cong. Atlanta, USA. Elsevier, Oxford, UK. Available: www.hbm.com/ncode.

[38]. Pompetzki, M., Dabel B,, Lin X., (2010), Advancement in Automotive Durability Process, Structural Durability and Health Monitoring, Vol. 5, No. 2, pp.69–76.

[39]. Halfpenny A and Kihm F. Environmental Accelerated Testing. Use of Virtual test to extend physical Approach, White Paper (2008). Available: www.hbm.com/ncode.

[40]. Jung D-H. Reliability achievement of the driving systems parts through development of vibration-fatigue evaluation method. Engineering Procedia 10 (2011) 1906-1916.

[41]. Özsoy S, Celik M, Kadioglu F S. An accelerated life test approach for aerospace structural components, Eng Fail Anal 2008; 15(7): 956-957.

[42]. M. Aykan, M. Celik , Vibration fatigue analysis and multi-axial effect in testing of aerospace structures, Mechanical Systems and Signal Processing 23(2009) 897-907.

[43]. Xu K., Wu Y. and Wu C. Q., 2011 Development of Vibration Loading Profiles for Accelerated Durability Tests of Ground Vehicles, 4th Annual Dynamic Systems and Control Conference, Arlington, VA, USA.

[44]. S. Cull, C. Yang, and C. Wu, "Generation and verification of accelerated durability tests", Department of Mechanical and Manufacturing Engineering, University of Manitoba, Internal Report, 2010.

[45]. GlyphWorks Theory [Electronic], Available with nCode GlyphWorks software, nCode, 2010.

[46]. ANSYS13.0 Software ANSYS Inc., Canonsburg, PA, USA.

[47]. DesignLife Worked-out Examples [Electronic], Available with nCode GlyphWorks software, nCode, 2010.

[48]. Piersol A. G., "ACCELERATED VIBRATION TESTING- proceed with caution," Tustin Training News, January 1993. Available at: http://www.ttiedu.com.

[49]. NATO AECTP 200 (2003). Validation of mechanical environmental test methods and severities. NATO AECTP 200, Ed. 3, Section 2410. Final Draft Sept 2003.

[50]. Wannenburg, J. and Heyns, P.S. (2010) 'An overview of numerical methodologies for durability assessment of vehicle and transport structures', Int. J. Vehicle Systems Modeling and Testing, Vol. 5, No. 1, pp.72–101.

[51]. Zalaznik A and Nagode M. Frequency Based Fatigue Analysis and Temperature Effect. Materials and Design 32 (2011) 4794–4802.

[52]. Palsma E.S. and Vidal F.A.C., (2002), Fatigue Damage Analysis of on Body Shell Of A Passenger Vehicle, Journal of Materials Engineering and Performance, Vol. 11, No. 4, pp.450-460.

[53]. J. Gilbert Kaufman, 2008, "Properties of Aluminum Alloys-Fatigue data and the effects of temperature, Product Form and Processing", ASM international, ISBN-10:0-871170-839-7.

[54]. Multi-axial Fatigue Theory, MSC software [online], Available at: http: // www. mscsoftware.com/training_videos/patran/Reverb_help/index.html#page/Fatigue%20Users%20Guide/fat_mulitaxial.07.5.html.

[55]. P. M. Hall, On Using Strain Gauges in Electronic Assemblies When Temperature Is Not Constant, IEEE Transactions On Components, Hybrids And Manufacturing Technology, Vol .Chmt-9,No.4,December 1986.

[56]. Han S. and Chung J.W., A, "Retrieving Displacement Signal from Measured Acceleration Signal", Proceedings of International Modal Analysis Conference

XX: Conference & Exposition on Structural Dynamics, 2002.

[57]. Shafiullah, A.K.M., Wu, C.Q., 2012, "Validation of Loading Profiles for Accelerated Durability Testing of Ground Vehicle Components", Proceedings of CSME. (Submitted).

[58]. Heiber G., "Test Time Exaggeration Factor," Tustin Training News, 1994. Available: http://www.ttiedu.com.

[59]. Paulus M. and Doughty K. (2010) 'Effect of Resonant Frequency Shifting on Time to Failure of a Cantilevered Beam under Vibration , Journal of IEST, Vol. 53, No. 1, pp.59–68.

[69]. Petracconi et. al., Fatigue life simulation of a rear tow hook assembly of a passenger car, Engineering Failure Analysis 17 (2010) 455–463.

[61]. Oman S, Fazdiga M, Nagode M. Estimation of air-spring life based on accelerated experiments. Materials and Design, 2011: 32 1020-1030.

[62]. "Theoretical and Experimental Researches Using Accelerated Life Testing in Aerospace", International Journal for Engineering and Information Sciences ,Vol. 4, No. 2, pp. 117–122 (2009).

[63]. Brown G.W. and Ikegami R.," The Fatigue of Aluminium Alloys Subjected to Random Loading", Experimental Mechanics. 1970, pp. 321-327.

[64]. D. Benasciutti, R. Tovo, "Spectral methods for lifetime prediction under wide-band stationary random processes", International Journal of Fatigue, vol.27, pp. 867-877, 2005.

[65]. S. Srikantan, S. Yerrapalli, H. Keshtkar, "Durability design process for truck body structure", International Journal of Vehicle Design, vol.23, pp. 94-108, 2000.

[66]. Specification Development using ERS and FDS, Available at: http: // christian.lalanne. free.fr/Home/Home_ E.htm, 2009.

[67]. Western Canada testing Inc. (Feb, 2008). "WESTEST MAST Table" [Online]. Available: http://www.westest.ca /mast.htm [August 16, 2009].

Appendices

Appendix A- Details of the all Considered Test-Pieces and their Comparison with the Selected One

Three other test-pieces has also been modeled and fabricated to verify the adopted numerical method in this work. These three models have different fatigue life than 24 hours under the reference loading. The fatigue lives of all the four different models/specimens are presented in Table 1A.

Table 1A: Fatigue Lives of Different Test-Pieces under the 24 Hours Loading

Test Duration	Fatigue Lives in Hours			
	Specimen 1 (selected)	Specimen 2	Specimen 3	Specimen 4
24 hour	23.80	5.436	131.2	9385

Other than the fatigue life, the criterions presented in Section 2.2 have been maintained mentioned, while modeling those specimens. The dynamic features of all of the 4 specimens have been compared in this section. Among the specimens the selected one shows the 'best fit' with the experiments.

Table 2A shows that all of the considered specimens have two bending modes in the frequency range of 0-60 Hz. The lateral modes have not been extracted from the experiment as only the vertical excitation has been applied. Table 3A demonstrates the dominancy of the bending mode in the considered frequency range (0-60 Hz). It is

prominent from the results tabulated in Table 3A that the first bending mode is much more dominant than the second bending mode. Therefore this mode can be responsible for the damage and response of the structure.

Table 2A: The Natural Frequencies and the Damping Ratios for the First Vibration Mode for Different Specimens (Experimental)

Beams/ Arms	Natural Frequency of the 1st Mode, (Hz)	Damping Ratio of the 1st Mode, (%)	Natural Frequency of the 3rd Mode, (Hz)	Damping Ratio of the 3rd Mode (%)
Selected	7.114	0.2053	56.90	0.6856
1	7.172	0.2248	57.01	0.9345
2	7.114	0.2353	56.34	0.5424
3	6.990	0.2701	57.00	1.103

Table 3A: Gain Ratios of the First Two Bending Modes (Experimental)

Beams/ Arms	Gain in the 1st Bending Mode	Gain in the 2nd Bending Mode	Ratio Between the Gains
Selected	284.0	88.87	3.190
2	261.0	78.91	3.300
3	246.6	116.7	2.113
4	213.4	47.01	4.539

The RMS strains (the longitudinal, Von Mises, maximum shear and the maximum principal strains) developed usnig the FE model (CAM) under the 24-hours loading have been tabulated in Table 4A. Three type of strain RMS has been presented in the Table 4A according to the normal distribution. They are (1) (1- σ) where 68.3% of the time the maximum strain will be less than the 1-σ RMS value, (2) (2- σ) where 95.6% of the time

the maximum strain will be less than the 2-σ RMS value and (3) (3- σ) where 99.7% of the time the maximum strain will be less than the 3-σ RMS value.

Table 4A: Strains Developed in the 24 Hours Durability Test in the FE Models

Beams/ Arms/ Specimens	Type of the Strain Result	Maximum Strain in the X direction (Longitudinal axis of the beam) (μE)	Maximum Von Mises Strain (μE)	Maximum Shear Strain (XZ Plane) (μE)	Maximum Principal Strain (μE)
Selected (Set 1)	(1-σ)	802.3	814.6	769.5	835.6
	(2-σ)	1604	1629	1539	1707
	(3-σ)	2407	2443	2308	2506
1	(1-σ)	756.4	756.1	623.3	756.4
	(2-σ)	1512	1512	1246	1512
	(3-σ)	2269	2268	1870	2269
2	(1-σ)	741.7	741.8	609.7	743.2
	(2-σ)	1483	1483	1219	1486
	(3-σ)	2225	2225	1818	2230
3	(1-σ)	710.4	709.1	590.6	712.9
	(2-σ)	1420	1418	1181	1426
	(3-σ)	2131	2127	1772	2138

Table 5A shows the comparison of the natural frequencies between the experiment and the FEA results for considered specimens. First four modes have been taken for the comparison. The lateral vibration mode (second mode) has not been compared as only vertical excitation has been considered. From the results, for the first vibration mode the least deviation has been observed in 'Specimen 2' as 1.723% and the most one as 2.702% in specimen 3. Overall the maximum deviation in the natural frequency has been found in 'Specimen 2' as 5.090% in the fourth mode. The maximum deviations in the natural

frequencies (of the specimens) between the FEA and experimental results have also been presented in Figure 1A with bar diagrams. Through this figure a comparison of the 'good of fit' of the specimen's analytical (FEA) natural frequency with the experiments have been demonstrated.

Table 5A: Comparison of the Natural Frequencies between the FE and the Experimental model

Beams/ Arms/ Specimens	Vibration Modes	Experimental Natural Frequencies (Hz)	Analytical Natural Frequencies (Hz)	Absolute Percentage (%) of Deviation
Selected	First (bending)	7.114	7.273	2.163
	Second (transverse)	N/A	33.82	----------
	Third (bending)	56.91	59.66	4.616
	Fourth (bending)	165.8	174.7	5.090
1	First (bending)	7.171	7.297	1.723
	Second (transverse)	N/A	35.441	---------
	Third (bending)	57.01	59.57	4.288
	Fourth (bending)	167.40	175.5	4.654
2	First (bending)	7.114	7.308	2.661
	Second (transverse)	N/A	34.718	----------
	Third (bending)	56.34	59.13	4.728
	Fourth (bending)	164.8	173.4	4.941
3	First (bending)	6.989	7.184	2.702
	Second (transverse)	N/A	32.987	---------
	Third (bending)	57.00	59.82	4.723
	Fourth (bending)	166.6	175.4	5.056

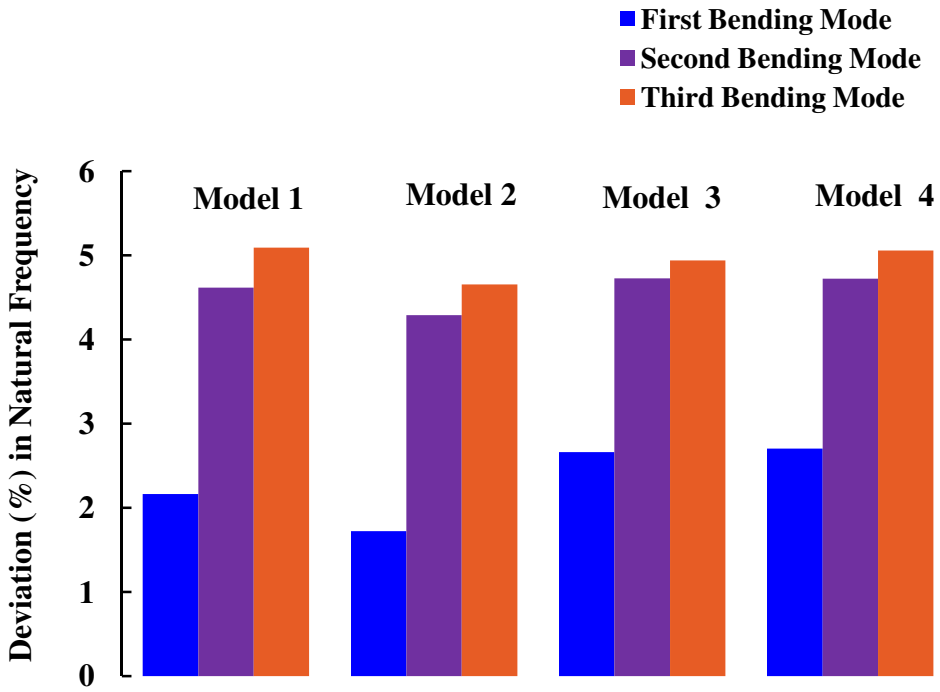

Figure 1A: Comparison of Natural Frequencies between the FE and the Experiment

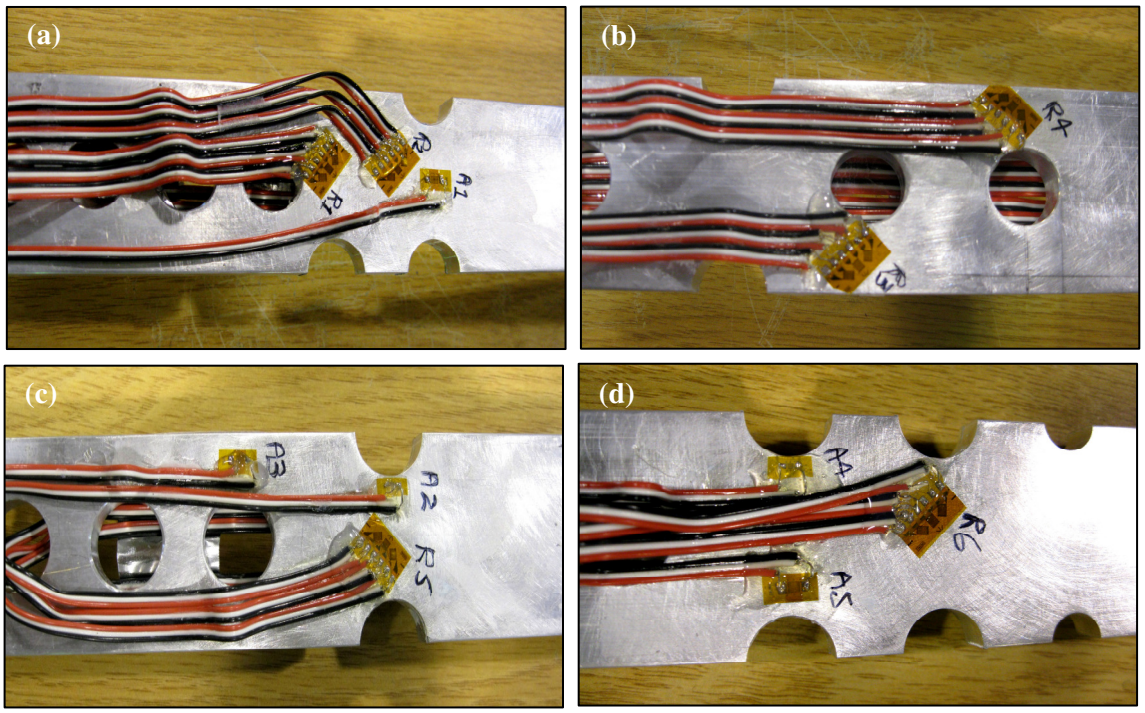

Figure 2A: Attached Strain Gauges in Differently Designed Specimens

According to this 'good of fit' the specimens can be arranged in the following order: Specimen 2, Specimen 1, Specimen 3 and Specimen 4. Table 6A presents a comparison of maximum Von Mises strain results at different locations of the considered specimens determined via FEA and experiments. In these locations, presented in Figure 2A, the strain gauges have been attached to the beams to collect the experimental strains. In this figure R1, R2, R3, R4, R5, R6 are strain rosettes and A1, A2, A3, A4 and A5 are the axial strain gauges.

Table 6A: Comparison of Strains between the FEA and the Experiment

Strain Gauges/ Rosettes	Attached with the Arm No	Area Averaged FE Strains (μE)	Experimental Strains (μE)	Absolute Deviation in Strains (%)
A1	Selected	1416	1454	2.610
R1	Selected	984.0	990.5	0.660
R2	Selected	1266	1271	0.390
R3	1	1639	1880	12.79
R4	1	1500	1725	13.04
A2	2	1635	1695	3.540
A3	2	1318	1317	0.114
R5	2	1359	1290	5.349
A4	3	1624	1583	2.620
A5	3	1336	1305	2.414
R6	3	1329	1272	4.481

The strains have been collected from 24-hours trial durability test. From this table, the least average (of location A1, R1 and R2) deviation in the strain results has been found as 1.22% in the selected specimen and the maximum average (of R1 and R2) deviation is

listed as 12.92% in specimen 2. The average strain deviation is 3% (considering location A2, R3 and R5) and 3.17% (considering location A4, A5 and R6) in specimen 3 and specimen 4respectively.

In Figure 3A, the average deviations (%) in the maximum Von Mises strain results for the considered specimens have been presented via bar diagrams. From Figure 3A it is prominent that the experimental strain in specimen 1 is the least deviated from the FEA with the applied assumptions.

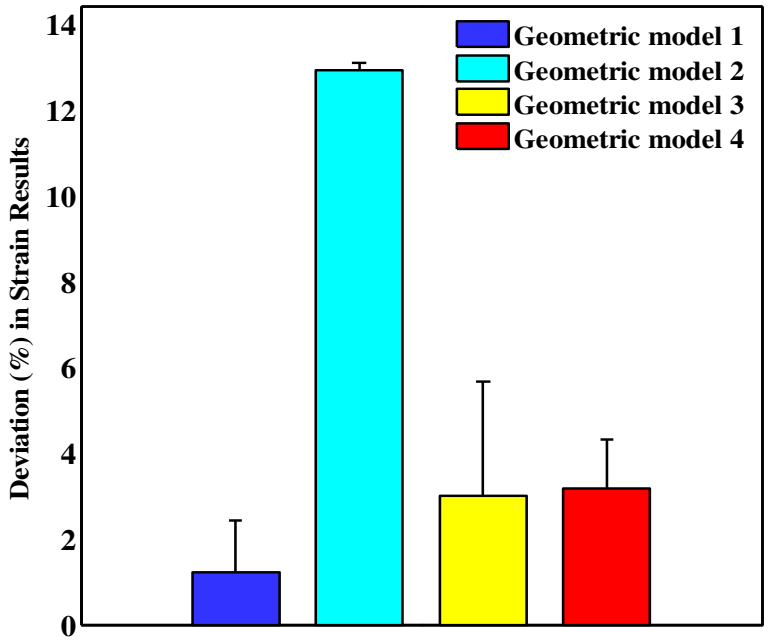

Figure 3A: Comparison of the Strain Results between the FE and the Experiment

Table 7A presents the strain ratio of two different location of the same specimen determined from both FEA and experiments. In this case the deviations of strain ratios have been found significantly lower, which further indicates that the FE model is good enough to predict the strains. The maximum deviation in this ratio between the FEA and

experiment has been found as 2.070% among all the considered pairs of gauges presented in Table 7A.

Table 7A: Comparison of Strain Distributions between the FE and the Experiment

Strain Gauges/ Positions	Ratios of Strains from FEA	Ratios of strain from Experiments	Absolute Deviation
A_5, A_4	1.216	1.213	0.2467 %
A_4, R_6	1.222	1.244	1.807 %
R_2, R_1	1.286	1.283	0.272 %
A_1, R_1	1.439	1.469	2.070 %
R_3, R_4	1.093	1.089	0.283 %
A_2, A_3	1.240	1.287	1.240 %

Appendix B- Other Fatigue Results

The fatigue life using the experimental strains collected from different locations presented in Figure 2A has been demonstrated in the Table 8A.

Table 8A: Fatigue Lives in Different Locations of the Specimens Based on Experiments

Beams/ Arms/ Specimens	Locations	Approaches	Fatigue Lives (hours)
1	A1	SN Method with Goodman correction	208.0
1	R1	SN Method with Goodman correction	7613.0
1	R2	SN Method with Goodman correction	773.6
2	R3	SN Method with Goodman correction	58.89
2	R4	SN Method with Goodman correction	26.60
3	A2	SN Method with Goodman correction	63.00
3	A3	SN Method with Goodman correction	680.9
3	R5	SN Method with Goodman correction	736.9
4	A4	SN Method with Goodman correction	153.2
4	A5	SN Method with Goodman correction	931.1
4	R6	SN Method with Goodman correction	1145

In this case, the fatigue lives have been determined in the time domain using the stress life (S-N) technique. Goodman criterion has been used to correct the mean stress effect. These results can be used with the results from Table 5A to deduce a relationship between the strain RMS value and the expected fatigue life. This relationship can be used

as a preliminary tool to find out the fatigue life of critical locations based on the developed stress.

Furthermore, in the *frequency-domain-based* S-N method for fatigue life estimation depends on the different of cycle counting algorithms. It has previously been found that Dirlik algorithm in the *frequency-domain-based* techniques has the best match with the 'rainflow cycle counting algorithm' in the time based domain techniques. In this case, effect of other different cycle counting algorithms like Narrowband, Steinberg and Lalanne on the fatigue life of the specimens have also been explored. It has been found that the Narrowband algorithm yields a conservative value of fatigue life and Lalanne algorithm overestimate the fatigue life than the other two algorithms. In this work, Specimen 1 has been designed for 23.8 hours under the reference 24 hours AD loading profile using Dirlik's algorithm. Table 9A represents the fatigue life of four selected specimens using different cycle counting algorithms in frequency domain.

Table 9A: Estimated Fatigue Life of the Four Selected Specimens Using Different Cycle Counting Algorithms in the Frequency Domain

Loading Duration	Cycle Counting Algorithm	Fatigue Life in Hours			
		Specimen 1 (Selected)	Specimen 2	Specimen 3	Specimen 4
24 hours	Dirlik	23.80	5.436	131.2	9385
	Narrowband	8.416	5.424	130.7	2482
	Steinberg	10.30	6.979	159.4	3206
	Lalanne	38.48	5.428	130.9	1.223×10^4
20 hours	Dirlik	19.46	4.044	105.5	6548
	Narrowband	7.037	4.035	105.1	1659
	Steinberg	8.630	5.479	128.2	2204

Table 9A (Cond.)					
Loading Duration	Cycle Counting Algorithm	Fatigue Life in Hours			
		Specimen 1 (Selected)	Specimen 2	Specimen 3	Specimen 4
20 hours	Lannane	31.50	4.038	105.2	7827
15 hours	Dirlik	15.24	2.331	67.26	5606
	Narrowband	7.876	2.326	67.06	1483
	Steinberg	9.740	3.760	81.98	1970
	Lannane	25.17	2.327	67.12	5573
10 hours	Dirlik	9.419	0.880	31.18	2484
	Narrowband	2.927	0.878	31.07	593.4
	Steinberg	3.744	1.771	38.41	708.1
	Lannane	10.92	0.878	31.11	2468
8 hours	Dirlik	8.391	0.721	26.66	2155
	Narrowband	2.055	0.719	26.57	472.9
	Steinberg	2.658	1.480	32.98	564.4
	Lannane	8.540	0.720	26.60	2142
4 hours	Dirlik	4.091	0.421	17.26	1468
	Narrowband	1.258	0.420	17.20	319.2
	Steinberg	1.695	0.986	21.72	384.4
	Lannane	5.336	0.421	17.22	1497
2 hours	Dirlik	1.901	0.223	10.63	821.4
	Narrowband	0.709	0.223	10.59	193.1
	Steinberg	1.023	0.597	13.80	232.2
	Lannane	3.098	0.222	10.60	915.4
1 hours	Dirlik	1.045	0.062	3.557	352.6
	Narrowband	0.244	0.062	3.543	77.50
	Steinberg	0.442	0.148	5.298	94.16
	Lalanne	1.017	0.062	3.547	350.3

Appendix C- Miscellaneous Findings While Generating the AD Test

Figure 4A presents the ERS of the partial tests of different duration. These partial tests has been synthesized using inverse Basquin's exponent, b=6. It has been observed that the ERS of the synthesized profiles exceeds the SRS of the field test in a good manner when the duration of the partial tests is 10 hours or less. All the synthesized loading profiles are equivalent to 330 hours of field test.

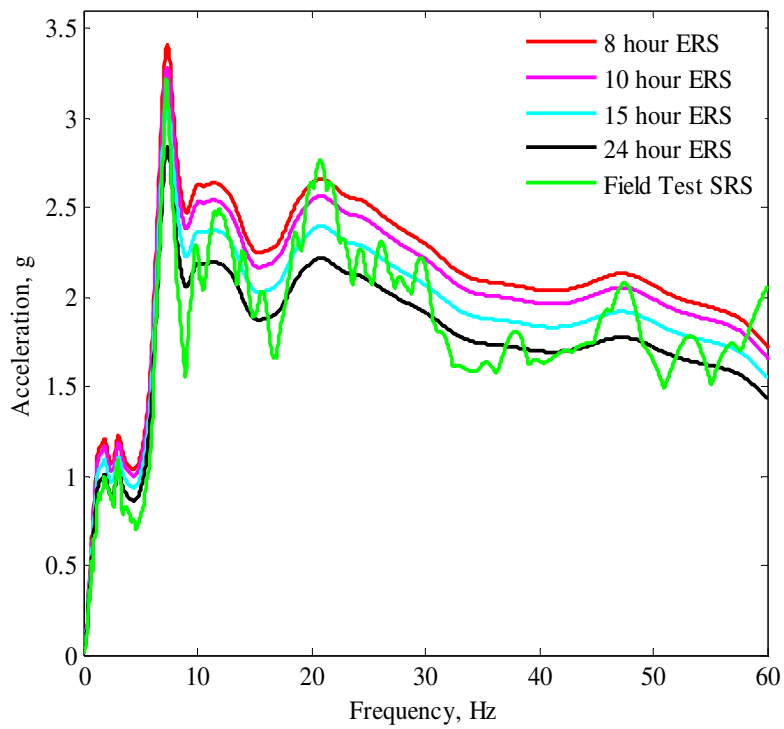

Figure 4A: Response Spectra of Different AD Tests for Constant FDS (b=6)

Therefore it is necessary to conclude that using suggested b=6 by Xu [2], the accelerated loading profiles should not be generated for 12 hours or less. Hence to generate loading profiles up to 1 hour a different S-N curve slope, b=5.5 has been used in this work.

There are different algorithms to calculate the FDS from the input acceleration data. The Rayleigh and Lalanne are two of these algorithms which produce the FDS with slightly different damage content. It has been observed from the comparison of Figure 5A and Figure 14 that for the Lalanne algorithm, FDS of the partial tests fit better with the FDS of the field test than the Rayleigh algorithm.

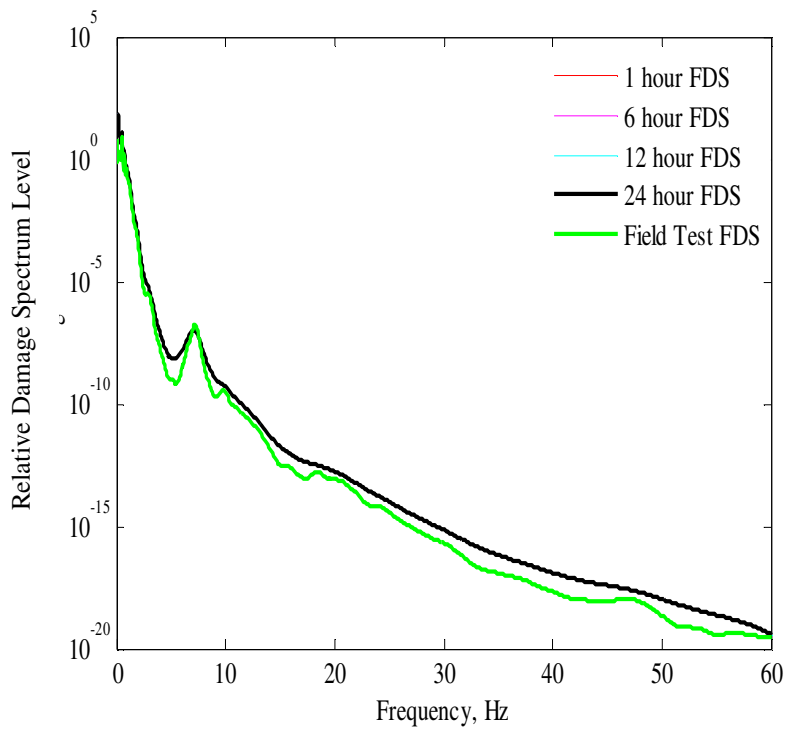

Figure 5A: Damage Spectra of Different AD Tests for Constant FDS (b=6)

AD loading profiles also can also be synthesised keeping the ERS constant. In this case the FDS of the AD loading profiles will vary with the change of the duration of the loading profiles. Figure 6A presents the ERS of different AD profiles when SRS of the

field test has been taken as the input to the 'test synthesis' process. This technique enables us to generate the AD profiles with less duration as the ERS of loading profile is insensitive with the attained AF. However, as the FDS does change in this technique, there is a good chance of the alteration of failure mechanism in this case. Hence practically this technique should not be practised.

Figure 7A shows the equivalent FDS of the different AD loading profile which has been synthesized keeping the ERS constant. This figure demonstrates that equivalent FDS of the AD loading profile changes when the duration of the AD test changes for a constant ERS. Thus in this approach the response of the system can be controlled by sacrificing the damage content which is not recommended.

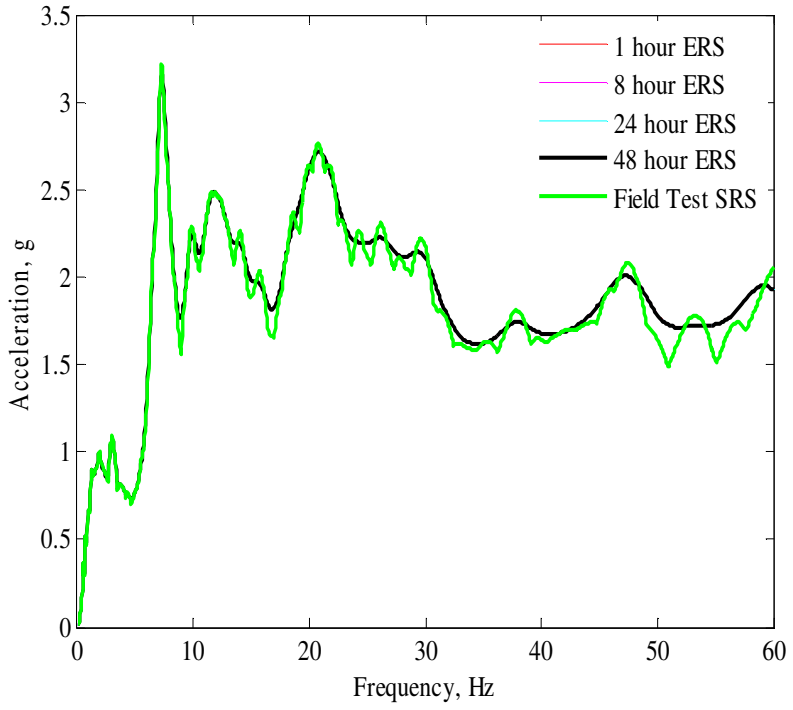

Figure 6A: Response Spectra for Different AD Tests (Full) for Constant ERS (b=6)

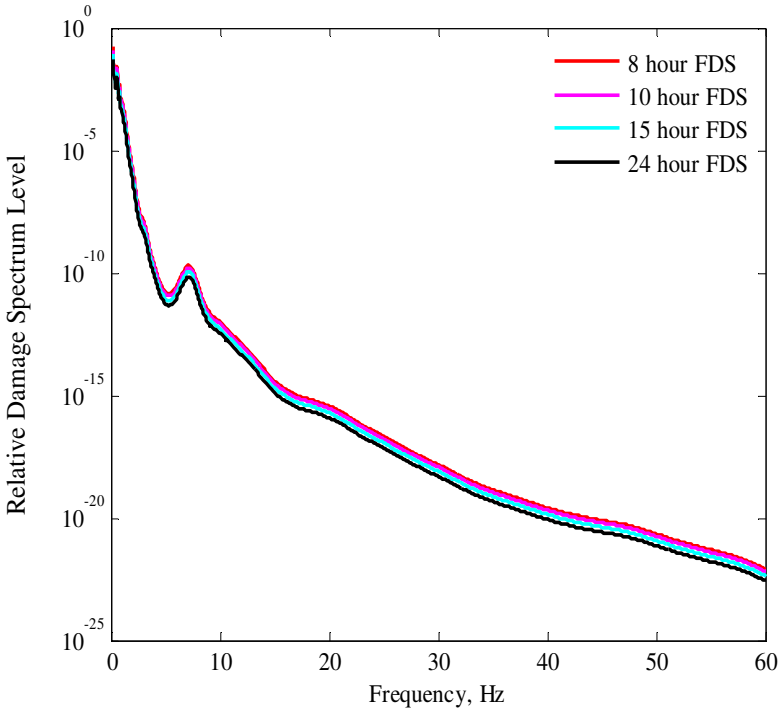

Figure 7A: FDS for Different AD Tests (Full) For Constant ERS (b=6)